Technical University of Crete
School of Electrical and Computer Engineering

Energy Management and Real-Time Operation of Microgrids of Large Building Complexes

MASTER THESIS

Dimitra G. Kyriakou

EXAMINING COMMITTEE

Professor Kanellos Fotios (Supervisor)

Professor Koutroulis Eftychios

Professor Stavrakakis Georgios

Chania, Crete, February 2023

Acknowledgements

First and foremost, I would like to express my sincere thanks to my supervisor, Professor Kanellos Fotios, for his valuable assistance, continuous support and guidance throughout my master thesis. His extensive research experience and activity, as well as, his vast knowledge have inspired and encouraged me during my academic research.

I would also like to thank my committee members, Professor Stavrakakis Georgios and Professor Koutroulis Eftychios, for their helpful comments and time.

Moreover, I am genuinely grateful to *Pancretan Endowment Fund* for the *"Pancretan Scholarship of Excellence"*, providing me the financial support to fulfill my graduate studies and research at Technical University of Crete.

Last, but not least, I would like to express my deepest gratitude and appreciation to my family and close friends for their unconditional love, support, encouragement and trust, thus drawing strength to chase my dreams and complete my studies. This endeavor would not have been possible without them.

Chania, February 2023
Dimitra G. Kyriakou

Abstract

The present and future conditions in the energy market impose extremely high standards to the operation of building energy systems. Moreover, distribution networks face new operational and technical challenges as a result of the rapid penetration of renewable energy sources (RES) and other forms of distributed generation. Consequently, Active Distribution Networks (ADNs) will play a crucial role in the exploitation of smart building prosumers, smart grids and RES.

In this work, advanced, fully parametric systems for the optimal energy management and real-time joint operation of large building complex microgrids and the hosting active distribution network is developed. The examined energy systems include buildings scaling from simple residential ones up to mega office or commercial buildings, single Plug-in Electric Vehicles (PEVs) up to large PEV parking lots, local power generators, PVs and wind turbines. The modeling of the examined system's components is performed, including those of the thermal and electrical loads of the buildings with the latter being divided in critical and non-critical loads that can be shifted in time. Moreover, a dynamic equivalent aggregate battery model for the cluster of PEVs hosted by the parking lots of the microgrid is developed. Finally, building local power generation units modeling is carried out and suitable optimal power flow algorithms are applied to ADNs hosting microgrids of building prosumers. The ADN-microgrid joint operation scheduling is executed with the purpose of minimizing microgrid's total energy cost on the assumption of the operation under variable electricity price. Specifically, it provides the optimal total electric power demand of the HVAC systems and optimally shifts building non-critical electrical loads. Moreover, the charging of the hosted PEVs and the operation of the local power generation units are optimally scheduled. Efficient optimization techniques are first applied at microgrid scale to facilitate the optimization process and sub-optimization problems are then solved in order to optimally dispatch the total power demand of microgrid to its components. To this end, suitable flexibility indices are developed for each type of microgrid component. At the same time, a large number of constraints including all the operation and technical constraints of the components of the microgrid and the active distribution network it is connected to, are satisfied. Moreover, the microgrid is able to provide frequency support. Frequency support is enhanced and optimized by suitably exploiting the flexibility of building prosumers and PEVs. Frequency is also supported by adjusting the power of the building local generation units and by suitably adjust their non-critical loads in an optimal way according to their flexibility. In addition, the reactive power is optimally regulated in order to maintain the local voltages of the microgrid and the hosting distribution network within the permissible limits. All the developed models at different microgrid integration levels and algorithms are verified through the simulation of realistic case studies.

Περίληψη

Οι σημερινές και μελλοντικές συνθήκες στην αγορά ενέργειας επιβάλλουν εξαιρετικά υψηλές προδιαγραφές στη λειτουργία των ενεργειακών συστημάτων των κτιρίων. Επιπλέον, τα δίκτυα διανομής αντιμετωπίζουν νέες λειτουργικές και τεχνικές προκλήσεις ως αποτέλεσμα της ταχείας διείσδυσης των ανανεώσιμων πηγών ενέργειας (ΑΠΕ) και άλλων μορφών κατανεμημένης παραγωγής. Συνεπώς, τα Ενεργά Δίκτυα Διανομής θα διαδραματίσουν κρίσιμο ρόλο στην εκμετάλλευση των έξυπνων καταναλωτών-παραγωγών κτιρίων, των έξυπνων δικτύων και των ΑΠΕ.

Στην παρούσα διατριβή αναπτύσσονται προηγμένα, πλήρως παραμετρικά συστήματα για τη βέλτιστη διαχείριση ενέργειας και την κοινή λειτουργία σε πραγματικό χρόνο του ενεργού δικτύου διανομής και των μεγάλων κτιριακών μικροδικτύων που φιλοξενούν. Τα ενεργειακά συστήματα που εξετάζονται περιλαμβάνουν κτίρια που κλιμακώνονται από απλές κατοικίες μέχρι πολύ μεγάλα κτίρια που στεγάζουν γραφεία ή εμπορικά κτίρια, μεμονωμένα ηλεκτρικά οχήματα μέχρι μεγάλους χώρους στάθμευσης ηλεκτρικών οχημάτων, τοπικές γεννήτριες, φωτοβολταϊκά και ανεμογεννήτριες. Πραγματοποιείται η μοντελοποίηση των στοιχείων του εξεταζόμενου συστήματος, συμπεριλαμβανομένων αυτών των θερμικών και ηλεκτρικών φορτίων των κτιρίων με τα τελευταία να χωρίζονται σε κρίσιμα και μη κρίσιμα ηλεκτρικά φορτία που μπορούν να μετατοπιστούν χρονικά. Επιπλέον, αναπτύσσεται ένα δυναμικό ισοδύναμο μοντέλο μπαταρίας για την ομάδα των ηλεκτρικών οχημάτων που φιλοξενούνται στους χώρους στάθμευσης του μικροδικτύου. Τέλος, πραγματοποιείται η μοντελοποίηση των κτιριακών τοπικών μονάδων παραγωγής ηλεκτρικής ενέργειας και εφαρμόζονται κατάλληλοι αλγόριθμοι βέλτιστης ροής ισχύος σε ενεργά δίκτυα διανομής που φιλοξενούν μικροδίκτυα καταναλωτών-παραγωγών κτιρίων. Ο προγραμματισμός της κοινής λειτουργίας ενεργού δικτύου διανομής-μικροδικτύου εκτελείται με σκοπό την ελαχιστοποίηση του συνολικού ενεργειακού κόστους του μικροδικτύου με την παραδοχή της λειτουργίας υπό μεταβλητή τιμή ηλεκτρικής ενέργειας. Συγκεκριμένα, παρέχει τη βέλτιστη συνολική ζήτηση ηλεκτρικής ισχύος των HVAC συστημάτων και μετατοπίζει βέλτιστα τα μη κρίσιμα ηλεκτρικά φορτία των κτιρίων. Επιπλέον, η φόρτιση των ηλεκτρικών οχημάτων, καθώς και η λειτουργία των τοπικών μονάδων ηλεκτροπαραγωγής προγραμματίζονται βέλτιστα. Εφαρμόζονται αρχικά αποτελεσματικές τεχνικές βελτιστοποίησης σε κλίμακα μικροδικτύου για να διευκολυνθεί η διαδικασία βελτιστοποίησης και στη συνέχεια επιλύονται υποπροβλήματα βελτιστοποίησης προκειμένου να κατανεμηθεί βέλτιστα η συνολική ζήτηση ισχύος του μικροδικτύου. Για το σκοπό αυτό, αναπτύσσονται κατάλληλοι δείκτες ευελιξίας για κάθε στοιχείο μικροδικτύου. Ταυτόχρονα, ικανοποιείται ένας μεγάλος αριθμός περιορισμών, συμπεριλαμβανομένων όλων των λειτουργικών και τεχνικών περιορισμών των στοιχείων του μικροδικτύου και του ενεργού δικτύου διανομής στο οποίο είναι συνδεδεμένο. Επιπλέον, το μικροδίκτυο έχει τη δυνατότητα στήριξης της συχνότητας. Η στήριξη συχνότητας ενισχύεται και βελτιστοποιείται με την κατάλληλη αξιοποίηση της ευελιξίας των κτιριακών συγκροτημάτων και των ηλεκτρικών οχημάτων. Η συχνότητα στηρίζεται επίσης με τη ρύθμιση της ισχύος των τοπικών μονάδων παραγωγής, καθώς και με την κατάλληλη προσαρμογή των μη κρίσιμων ηλεκτρικών φορτίων των κτιρίων με βέλτιστο τρόπο ανάλογα με την ευελιξία τους. Επιπλέον, η άεργος ισχύς ρυθμίζεται βέλτιστα ώστε να διατηρούνται οι τοπικές τάσεις του μικροδικτύου και του ενεργού δικτύου διανομής εντός των επιτρεπτών ορίων. Όλα τα μοντέλα που αναπτύχθηκαν σε διάφορα επίπεδα του μικροδικτύου και οι προτεινόμενοι αλγόριθμοι επαληθεύονται μέσω προσομοίωσης ρεαλιστικών σεναρίων λειτουργίας.

Contents

Nomenclature

Abbreviations

ADN	Active Distribution Network
DER	Distribution Energy Resources
EC	Electric Chiller
EMS	Energy Management System
ESS	Energy Storage System
HVAC	Heating, Ventilation and Air Conditioning
MAS	Multi-Agent System
m.u.	monetary unit
OPF	Optimal Power Flow
PB	Parking equivalent Battery
PEV	Plug-in Electric Vehicle
RES	Renewable Energy Sources
SoC	State of Charge
V2G	Vehicle to Grid

Sets and indices

$\mathcal{B}$, b	buildings' set, building's number index
CB	cluster of buildings number index
CEV	cluster of PEVs number index
$\mathcal{E}$	external walls set
$\mathcal{G}$, g	Auxiliary generators' set, generator's number index
$\mathcal{I}$	internal walls set
$\mathcal{N}$	neighboring thermal zones set
x	xth internal wall index
y	yth external wall/window index
z	zth thermal zone index

Parameters, constants and variables

β_z	surface slop
θ, θ_z	incidence angle, zenith angle
τ_{win}	window glass transmission coefficient
a_{0g}, a_{1g}, a_{2g}	gth generator FC coefficients
a_w	the external wall absorbance coefficient
C_z	specific heat capacity
COP	coefficient of EC performance
EP	Variable price of electricity (m.u./kWh)
F_{wall}, F_{win}	wall/window surface area
FC	fuel cost function
$FL_b^{\uparrow}$	flexibility of a building to increase its power demand
$FL_b^{\downarrow}$	flexibility of a building to decrease its power demand
$FL_{CB}^{\uparrow}$	flexibility of a cluster of buildings to increase its power demand
$FL_{CB}^{\downarrow}$	flexibility of a cluster of buildings to decrease its power demand
I_b, I_d, I	beam, diffuse and total radiation on horizontal surface, respectively
$I_{T,z}$	total solar radiation
n_{ch}, n_{disch}	PEVs' charging (discharging) efficiency coefficients
n_{shift}	optimal load shifting coefficient
N_g	diesel generators' total number
N_z	thermal zones total number
p_g	ground reflectance
p_z	the density of the zth thermal zone
$P_{CEV,max}, P_{CEV,min}$	active power boundaries of CPEV/As (MW)
P_{DNload}	Distribution Network Load (kW)
$P_{EC,total,b}$	Electric power consumption for cooling (kW)
$P_{EC,total,min}, P_{EC,total,max}$	electric cooling power consumption boundaries (kW)
$P_{EL,total,max}, P_{EL,total,min}$	Total electrical loads power consumption boundaries (MW)
$P_{EL,CB,max}, P_{EL,CB,min}$	CBEL/As electrical loads power consumption boundaries (MW)
$P_{EL,b,max}, P_{EL,b,min}$	Each building's HVAC power consumption boundaries (MW)
$P_{HVAC,total,max}, P_{HVAC,total,min}$	Buildings' total HVAC power consumption boundaries (MW)
$P_{HVAC,CB,max}, P_{HVAC,CB,min}$	CBTL/As HVAC power consumption boundaries (MW)
$P_{HVAC,b,max}, P_{HVAC,b,min}$	Each building's HVAC power consumption boundaries (MW)
P_{max}, P_{min}	active power boundaries of each PEV (MW)
P_g	gth generator's power generation
$P_{g,min}, P_{g,max}$	diesel generators' power boundaries
$P_{non\_cr}^*$	optimal shiftable loads' power consumption of all buildings
$P_{PB,max}, P_{PB,min}$	power boundaries of PEVs' aggregate battery
P_{PV}	Photovoltaic power production (kW)
P_{WT}	WT power production of the (kW)
P_{grid}	Power of the main electric grid (kW)
$P_{grid,max}, P_{grid,min}$	Power boundaries of the main electric grid (MW)
$Q_{EC,total}$	total buildings' cooling power (kW)
$Q_{EC,z}$	thermal zone's power production for cooling (kW)
$\dot{Q}_{ex,wall,z}$	external walls heat exchange (kW)
$Q_{g,max}, Q_{g,min}$	Boundaries of the gth generator reactive reactive power
$\dot{Q}_{in,wall,z}$	internal walls heat exchange (kW)
$Q_{in,z}$	internal heat gains f (kW)
$Q_{PEV,max}, Q_{PEV,min}$	boundaries of the PEV's reactive power
$\dot{Q}_{sg,z}$	solar radiation through the windows (kW)
$\dot{Q}_{sw,z}$	heat gain of external walls' solar radiation (kW)
$\dot{Q}_{win,z}$	heat transfer across the windows (kW)
R_{se}	heat resistance of the external surface
SC	the shading coefficient of the windows
SoC_{high}, SoC_{low}	max/min stored energy (MWh) of each hosted PEV
$SoC_{CEV,high}, SoC_{CEV,low}$	max/min stored energy (MWh) of CPEV/As
$SoC_{PB,high}, SoC_{PB,low}$	max/min stored energy (MWh) of

PEVs' aggregate battery

$SoC_{PB,max}, SoC_{PB,min}$ max/min stored energy (kWh) of PEVs' aggregate battery

SoC_0 level of energy (MWh) of an individual PEV at the beginning

$SoC_{0,PB}$ level of energy (kWh) of the of PEVs' aggregate battery at the beginning

SoC_{target} target level of energy (MWh) of an individual PEV

$SoC_{t,PB}$ target level of energy (kWh) PEVs' aggregate battery

$T_{auto,0}, T_{auto,f}$ period of microgrid's islanded operation

T_{D1}, T_{D2}, T_{D3} the equivalent time constants of the speed governor

T_{D4} the time constant of diesel power generation

$T_{DN\_sh,0}$ $T_{DN\_sh,f}$ the beginning and the end of the time period where the where the distribution network flexible loads can be shifted in time

$T_{in,b}$ building's temperature (°C)

$T_{in,nz}$ indoor temperature of the neighbor thermal zone

$T_{in,z}$ thermal zone's temperature (°C)

$T_{max,z}, T_{min,z}$ thermal zone's temperature boundaries (°C)

$t_{ON,g}, t_{OFF,g}$ time when diesel generator begins/ends running

$T_{ON\_min,g}, T_{OFF\_min,g}$ gth diesel generator's minimum permissible duration of operation or inactivity

T_{out} outdoor temperature (°C)

$T_{shift,0}, T_{shift,f}$ Allowed time frame for the shiftable loads

SC the shading coefficient of the windows

SoC_{PB} Total energy of the PEVs' aggregate battery (kWh)

U_{wall}, U_{win} factor of the heat exchange of the external wall/window

V_b volume of the air of the bth building

$\boldsymbol{V}_{\max\,(\min)}$ a vector comprising the upper(lower) bounds of the amplitude of node voltages

V_z volume of the air of the zth thermal zone

Chapter 1

Introduction

1.1. General

In recent years, the rapid increase in energy consumption by buildings has accelerated negative impacts to the environment. As a result, innovative technologies are needed for the development of smart building energy management energy saving systems. Microgrid is a small electric power system consisting of usually small power generation units, local loads and storage devices. The microgrid concept has shown to be quite effective in applications of various types of building complexes. Except from the grid-connected mode of operation, microgrids can also operate autonomously i.e., island mode. This means that local generation units should be able to serve the local load on their own. Therefore, microgrids should exploit appropriate algorithms for the control and operation scheduling of these units.

Electric Vehicles (EVs) have been experiencing considerable development in recent years. Their increasing penetration promises a challenging future full of new opportunities for microgrid energy management systems. Furthermore, the use of EVs in microgrids may improve their resilience during grid outages without having to spend more money for extra local power generation capacity. In the event of a contingency, they have the ability under specific conditions to supply energy to islanded microgrids provided that the used charging facilities allow for Vehicle to Grid (V2G) operation.

Future electric power systems will be characterized by the increased penetration of renewable energy sources (RES). Distributed generation will pave the way to this end; however, it will increase the current level of operational complexity and pose several technical problems and challenges. Active distribution networks are a characteristic network paradigm that is suitable to host distributed generation, RES and flexible loads providing demand response capacity to the power grid. Moreover, the organization of parts of active distribution networks in microgrids will provide reliable solutions to problems resulting from the increased complexity of these networks while also provide more degrees of freedom in their control and optimal operation.

High penetration of RES poses several challenges in electric power operation with the power system stability being among the most significant. Systems frequency provides information about the balance between power system generation and consumption and can be used as a regulating parameter to achieve overall power system stability. If power balance is not maintained, the grid will suffer from power outages. When a significant power imbalance occurs, the frequency will suffer significant deviations from its nominal value. This requires advanced frequency control and support methodologies to overcome such challenges, especially in microgrids operating in isolated mode. Commercial buildings offer the potential for frequency support as they are among the largest energy consumers and comprise several loads that can be adjusted or shed. Frequency support can be provided by buildings by appropriately changing their power consumption in order to help the power system to achieve power balance. In this way, buildings contribute to the improvement of the overall reliability of the electric power system. Moreover, PEVs can be employed as distributed energy storages and controllable loads based on V2G technology exploitation, thereby, they provide significant potential for rapid frequency regulation.

Chapter 2

Background

2.1. Microgrid Operational Configurations

2.1.1. Conceptual Configuration for Distribution Systems

Electrical utility distribution systems can be categorized into three types: centralized, decentralized, and distributed. A simple connection of nodes to a central source of electricity production defines a centralized system. This is prevalent in utility configurations where the electricity produced by central power plants is delivered directly to individual users via transmission lines. Multiple generator units in the central power plants ensure that power is available at all times e.g., the reliability of the system is increased. However, if the configuration at the central station fails, the entire system may fail.

In a decentralized design, multiple spatially dispersed points of electrical generation are connected to their loads a number of remote stations. Decentralized systems offer a higher level of robustness than centralized systems.

In a web-like structure, distributed configurations provide both generation and loads at each node and are linked to all other generation and load points. Because a failure at any station or link may be handled by rerouting transmission to assure reliability, distributed networks are the most resilient. Decentralized or distributed network architectures are common in microgrids. When single transmission pathways or specific nodes are compromised, distributed configurations are the most resilient.

2.1.2. Distributed Generation

The "distributed generation" (DG) term generally refers to the production of electricity near the consumption. Combined heat and power or cogeneration (CHP) units and renewable energy sources (RES) are among the most widespread distributed generation resources Renewable energy is energy produced from natural resources such as wind, sunlight, tides, waves, geothermal heat and biomass. DGs can be used in an isolated way, supplying the consumer’s local demand, or integrated into the grid supplying energy to the electric power system, or a combination of these. These generating units are generally connected to the power systems at the low voltage distribution level.

Distributed generation is characterized by some features which are not present in centralized systems:

- the power generated is relatively small and has variations dependent on the availability and variability of primary energy source
- the power flow is bidirectional, in comparison with the central generation system where the power flow is unidirectional
- location in the network area dependent of the presence of the primary energy source.

Distributed generation is the key to meet growing power demand, provide benefits to consumer by improving the quality of life, relieves utility to supply additional loads and opens the opportunities for power trading in a competitive environment. They can play an important role in:

- reducing the transmission losses
- improving the power quality
- improving the reliability of the grid
- providing better voltage support
- reducing the greenhouse emissions

The major obstacle for the distributed generation has been the need to control a large number of dispersed energy sources and loads. This problem is mainly solved through microgrids and advanced control techniques and supervisory systems.

The centralized and the distributed generation are presented in the following figure and some additional information is provided in the following paragraph.

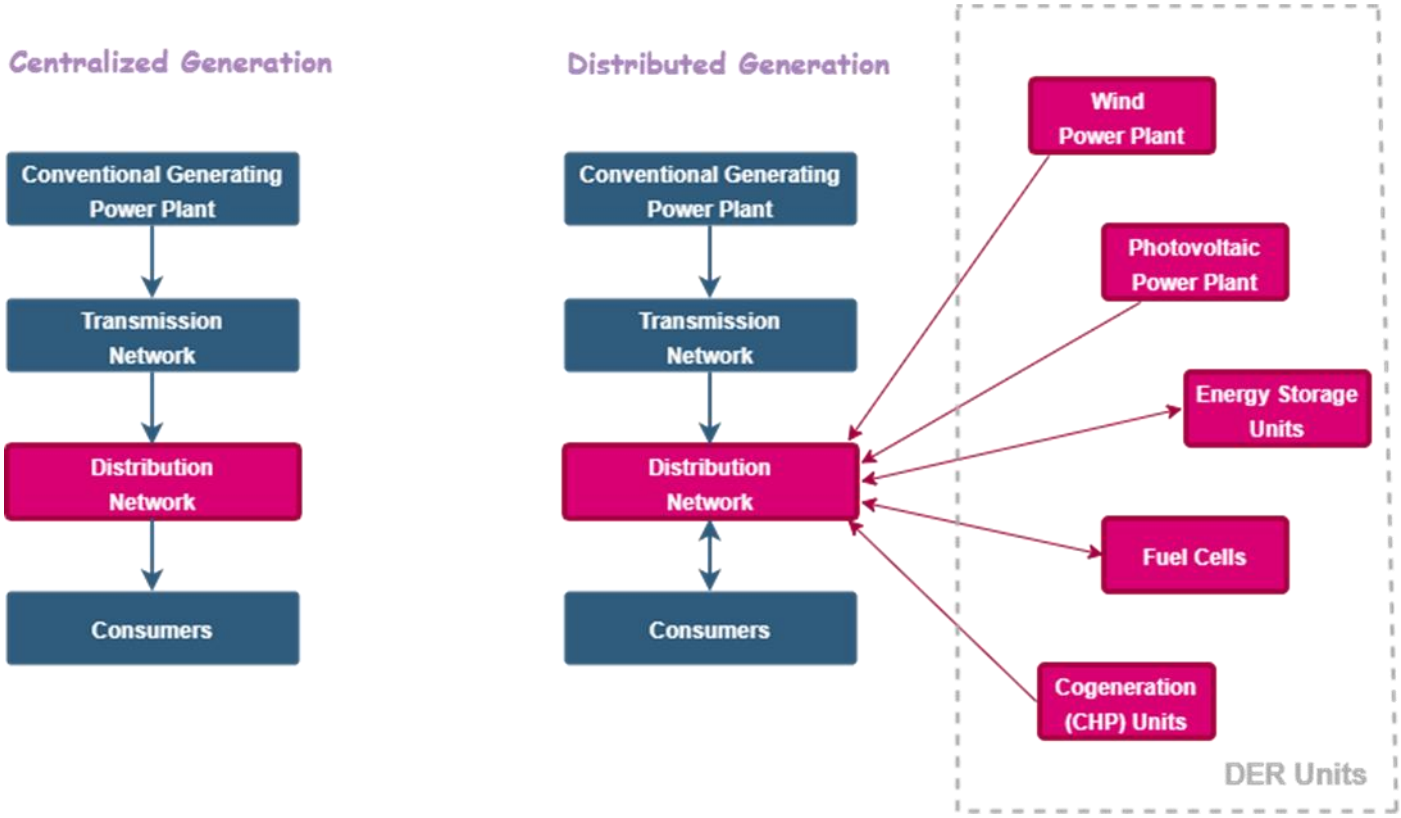

Fig. 1. A unidirectional centralized (left) and a bidirectional distributed (right) generation system

2.2. Benefits of Microgrids

Microgrids are a continuously growing sector of the energy industry, representing a paradigm shift from remote central station power plants toward more localized, distributed generation—especially in cities, communities and campuses. Their capability to isolate from the larger grid makes microgrids resilient while their ability to conduct flexible, parallel operations makes the grid more competitive.

By "islanding" from the grid in emergencies, a microgrid can both continue serving its load when the grid is down and serve its surrounding community by providing a platform to support critical services-allowing safe and reliable operation in a wide extend of activities and services.

Microgrids have several benefits to the environment, to utility operators, and to customers [1].

- Microgrids offer the opportunity to deploy more zero-emission electricity sources, thereby reducing greenhouse gas emissions. The microgrid manager (e.g., local energy management system) can balance generation from non-controllable renewable power sources, such as solar, with distributed, controllable generation, such as natural gas-fueled combustion turbines. They can also use energy storage and the batteries of electric vehicles to balance power production and consumption within the microgrid.

- Microgrids can make use of on-site energy that would otherwise be lost through transmission lines and heat that would otherwise be lost on pipes. When power has to travel long distances (e.g., from a centralized power station), electrical line losses occur, requiring additional generation to ensure that the distant demand is met. Since microgrid electricity is generated next to where it will be used (also known as distributed generation), line losses are minimized and less power is required to meet the same level of demand while system stability is enhanced. Also, when electricity is generated from certain centralized power sources (e.g., fossil fuels and nuclear power) a great amount of heat energy is created and typically released – unused – into the atmosphere. When power is generated close to the end users, it becomes economically feasible to use this heat energy productively, such as heating water or space in nearby homes and businesses, reducing greenhouse gas emissions.

- Microgrids can improve local management of power supply and demand, which can help defer costly investments by utilities in new power generation. When sited strategically within the electricity system, microgrids help reduce or manage electricity demand and alleviate grid congestion, thereby lowering electricity prices and reducing peak power requirements. In this manner, microgrids may support system reliability, improve system efficiency, and help delay or avoid investment in new electric capacity (e.g., "peaker" plants, substations, transmission lines, energy storage or other infrastructure). When connected to the local distribution network or transmission system, microgrids can also export excess electricity or import imbalances from the surrounding system from a single node.
- Microgrids can enhance grid resilience to more extreme weather or cyber-attacks. Microgrids can continuously power individual buildings, neighborhoods, or entire cities, even if the surrounding macrogrid suffers an outage. This concept of a microgrid functioning independently from the surrounding system is known as islanding. Microgrids can also help the macrogrid recover from a system outage, either indirectly, by sustaining services needed by restoration crews, or directly, by helping to re-energize the grid.

2.3. Challenges of Microgrids

Irrespective of their numerous advantages, implementing microgrids faces serious challenges not only on a federal and state level, but also on a technological level. On a federal level, we have microgrids contributing to distributed systems that provide power on a wholesale basis. Microgrids have the ability to provide multiple benefits like load abating and resource provision. However, market regulations do not allow for such multiple utilities [2]. Technological challenges faced in the operation and deployment of microgrids are mentioned below.

- The fault current in microgrids can be much higher than those faced in distributed systems. It can severely affect protection methods and damage safety devices. This is a major concern during island operation. Blindly implementing microgrids on feeders without careful analysis of the various protective measures can lead to serious damages to the grid.
- Issues during start-up of island mode- During the initial stages of island mode start-up can cause a sudden intake of current which can affect the frequency of the system and voltages. This can cause the generators to trip and go offline during the initial phase. In order to combat this, an analysis is needed on energy generation control methods during island mode and specialized controls need to be developed.
- Balancing between generation and load in island mode- This is one of the most common challenges faced by microgrids. The balance between load and power generation needs to be constantly maintained. Sudden or large change in loads can introduce instability into the island system.

2.4. Microgrid Energy Production

Microgrids generate electricity using distributed energy resources. Electrical generation and storage systems are combined in DERs, which can be deployed in a large number of units. Distributed fossil-fuel generators, batteries, and renewable resources such as solar panels and wind turbine generators can all be used to power microgrids. It's worth noting that when batteries are discharging, the system perceives them as a source of power generation.

Microgeneration is the local distribution of power generated by residences and small businesses. Despite the granularity of the generation, the contribution from microgeneration sources has a significant impact. The option to choose from a variety of generation sources, usually in complementing combinations, is a benefit of microgrid architecture. The aim is to maximize electricity generation depending on available resources, efficiency, and costs.

In a microgrid, it is essential to maintain the power supply-demand balance because the generation of the intermittent distributed sources such as photovoltaic and wind turbines is difficult to be predicted and their generation may fluctuate significantly depending on the availability of the primary sources (solar irradiation and wind). The supply-demand balancing problem becomes even more important when the microgrid is operating in island mode where only limited supply is available to balance the demand [3].

2.5. Microgrid Energy Storage

Storage units have a very important role in microgrids, especially in their autonomous operation, since they can substitute the generation units or regulate the loads. Energy can be stored either directly or indirectly, as shown in the following diagram. Energy storage technologies that are suitable for microgrids are batteries, flywheels and hydrogen storage technologies.

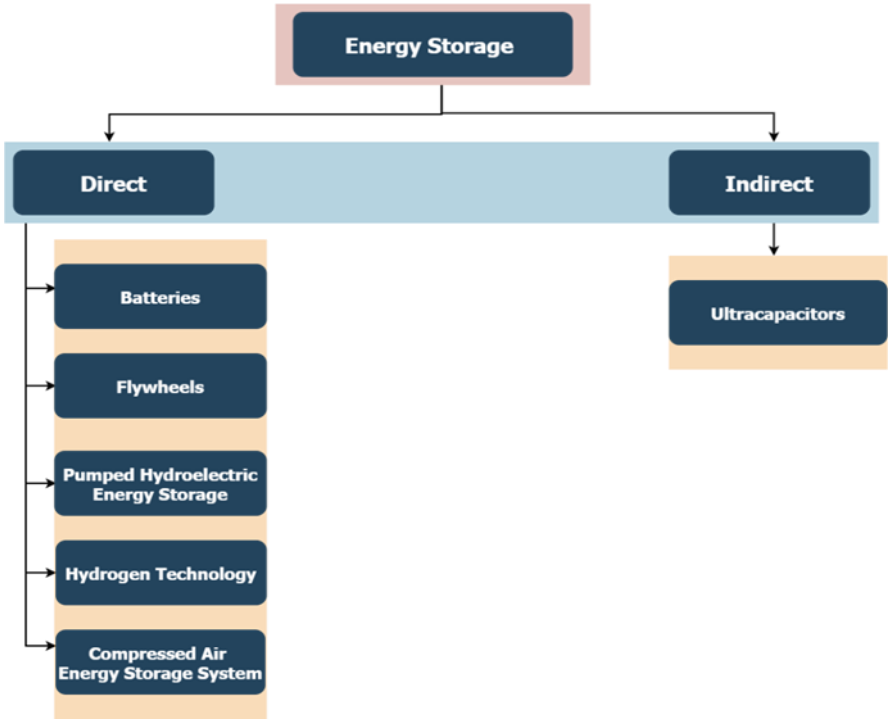

Fig. 2. Classification of Storage Units

2.5.1. Batteries

Batteries are devices that store electricity in electrochemical form. Nowadays, there is a wide variety of rechargeable batteries available commercially and many more under design. The most prominent types are mentioned below.

- ***Lithium-Ion***

A Lithium-Ion (Li-Ion) battery is an advanced battery technology that uses lithium ions as a key component of its electrochemistry. These batteries have one of the highest energy densities of any battery technology today. Li-ion batteries have no memory effect, a detrimental process where repeated partial discharge/charge cycles can cause a battery to 'remember' a lower capacity. Li-Ion batteries have displaced Ni-Cd batteries as the market leader in portable electronic devices, such as smartphones and laptops [4].

- ***Lead-Acid***

Lead-Acid batteries have the distinct benefit of being the most widely utilized type of battery for the most rechargeable battery application, such as starting vehicle engines. Despite their low energy density, moderate efficiency and high maintenance requirements, lead-acid batteries have a long lifetime and low costs when compared to other battery types [5].

- ***Flow Batteries***

A flow battery is a rechargeable battery in which electrolyte flows through one or more electrochemical cells from one or more tanks. With a simple flow battery, it is straightforward to increase the energy storage capacity by increasing the quantity of electrolyte stored in the tanks. Flow batteries have been installed in several places for a wide range of applications. They are a reliable, low cost and an environmentally friendly method for electrical energy storage [6].

2.5.2. Flywheels

They are rapidly rotating disks or cylinders used to store kinetic energy, which is easily converted into electrical energy by coupling them to a generator. It is an expensive, very efficient and flexible technology.

2.5.3. Pumped Hydroelectric Energy Storage

It is a widespread large-scale energy storage technique. It consists of two large tanks, which are located at points with a significant difference in altitude, and a pump and hydro turbine arrangement. During the period of low electricity consumption, water is pumped from the lower to the upper tank, where it is stored until needed. During periods of high demand, water from the upper tank is released through the pipes and flows into the hydro turbine, so that it works like a classic hydroelectric project, generating energy.

2.5.4. Fuel Cells – Hydrogen Energy Storage

A fuel cell uses the chemical energy of hydrogen to cleanly and efficiently produce electricity. Fuel cells can be used in a wide range of applications, providing power for applications across multiple sectors, including transportation, industrial/commercial/residential buildings, and long-term energy storage for the grid in reversible systems. Fuel cells have several benefits over conventional combustion-based technologies currently used in many power plants and vehicles. Fuel cells can operate at higher efficiencies than combustion engines and can convert the chemical energy in the fuel directly to electrical energy with efficiencies capable of exceeding 60%. Fuel cells have lower or zero emissions compared to combustion engines [7].

2.5.5. Compressed Air Energy Storage System

Energy is stored with the form of compressed air. Compressed air is used to rotate turbines that are the prime movers of electric generators.

2.5.6. Ultracapacitors

Ultracapacitors, or supercapacitors as they are also known, are an energy storage technology that offers high power density, almost instant charging and discharging, high reliability, and very long lifetimes. Ultracapacitors are now delivering significant economic benefits across a wide range of markets including automotive, grid and renewables, transportation and industrial applications [8].

2.6. Electric Vehicles

In recent times, Electric Vehicles (EVs) are rapidly increasing around the world, mainly, due to the fact that they have significant advantages in environmental protection. Therefore, electric vehicles present new opportunities and challenges to the operation of the electric power systems.

2.6.1. Benefits of Electric Vehicles

The most significant advantages of EVs are the following [9],[10]:

- Reduce car emissions to help the environment: Carbone dioxide emissions from traditional vehicles contribute to greenhouse gases in the atmosphere and accelerate climate change. All electric vehicles do not release carbon dioxide into the atmosphere and hybrid electric cars use their battery to greatly improve the maximum covered distance with a gasoline-powered engine ensuring higher efficiency and lower emissions than conventional vehicles. Electric Vehicles can be fueled by electricity from renewable sources, such as wind, hydropower and solar. They are also built to be more environmentally friendly than conventional vehicles, as the large battery inside the electric car can be recycled.
- Lower operating and maintenance costs: Any type of fully electrically powered vehicle has a significant difference on the consumption cost compared to the cost of any gasoline or diesel car. Not only electricity is less expensive than gasoline but it is also much more, meaning that rapid fuel price swings are all but eliminated by going electric. Moreover, conventional engines require expensive maintenance over their lifetimes, while electric vehicles do not.
- Electric motors are more efficient and have a much better response than conventional motors.
- Reduction of noise caused by the traffic, since the electric vehicles' motor running is significantly quieter, thanks to the missing exhaust.

2.6.2. Types of Electric Vehicles

The term “electric vehicle” actually includes three types of electric cars. Each type of vehicle has its advantages and disadvantages regarding range, emissions and affordability [11]. The types of EVs are:

1. *Hybrid Electric Vehicles (HEVs)*

They are powered by both gasoline/diesel and electricity. The vehicle alternates between the two to maximize efficiency. They contain a fuel tank and a classic engine along with an electric battery and motor. The battery is only recharged by the conventional engine and by the energy generated when decelerating and braking (regenerative braking).

2. *Plug-In Hybrid Electric Vehicles (PHEVs)*

Versatile hybrids in which the electric battery can be recharged both by the electricity grid and by the combustion engine. They are similar to HEVs with the difference being that they are mostly powered by electricity instead of classic fuel. Like hybrids, PHEVs offer greater range than fully electric vehicles.

3. *Battery Electric Vehicles (BEVs)*

Also known as “plug-in” electric vehicles, they exclusively use battery power, which needs to be recharged by connecting to the electricity grid or by a process known as regenerative braking in which the car’s motor slows down the vehicle to recover energy. They do not emit pollutants and are ideal for short urban journeys.

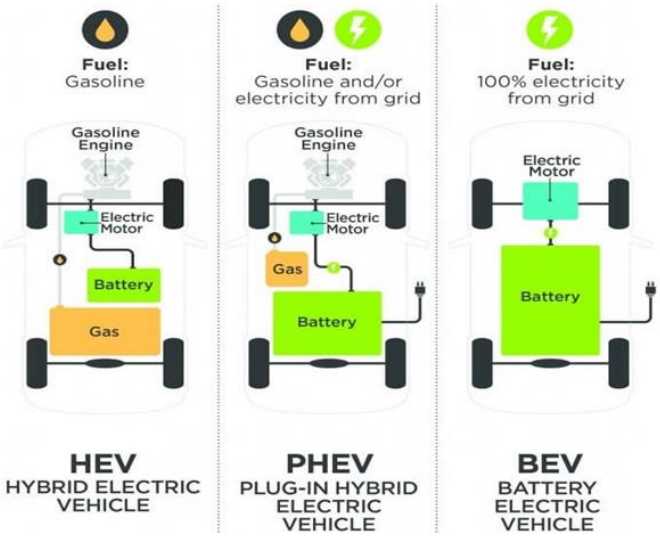

Fig. 3. The three types of Electric Vehicles [7]

2.6.3. Operation Mode of Electric Vehicles

The charging points of the parking lot considered in this study are able to provide bidirectional power flow which comprises two operation modes.

- Grid to Vehicle (G2V) operation mode

PEV draws power from the network and charges its battery packs. The power drawn from the network can be appropriately adjusted according to electricity price and loading of the network.

- Vehicle to Grid (V2G) operation mode

PEV injects power to the network. Hence, the electricity can be transferred from the PEV batteries back to the grid at periods that transmission system is overloaded or electricity price is high.

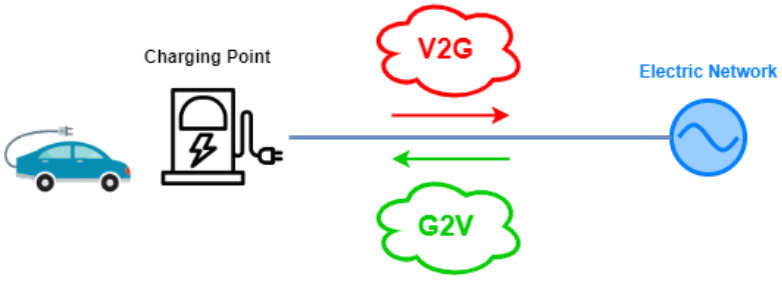

Fig. 4. V2G and G2V operation mode of Electric Vehicles

2.7. Load Management

Depending on the amount of electricity required and their operation characteristics and constraints, loads can be classified into groups. Sensitive, adjustable and shedable are the most typical classifications.

a) Sensitive Loads

Sensitive loads consist of all devices that must operate continuously without fail, hence the nominal power has always to be guaranteed. These might include elevators, emergency lighting, computers and TVs. It is assumed that the algorithm does not have any control on these loads.

b) Adjustable Loads

Adjustable loads can operate at lower power levels than their nominal power. These loads can reduce their power consumption during peak periods due to high energy prices. Examples include mainly Heating, Ventilation and Air Conditioning (HVAC).

c) Shedable / Shiftable Loads

Shedable and shiftable loads are those whose power consumption can be shed or shifted to a different time slot so that they can use electricity in the appropriate electricity price time period. The microgrid can shift this load from the peak period of power consumption to another period, thereby reducing the operation cost. This type of loads might include kitchen equipment, interior lighting, washing machines etc.

2.8. Microgrid Control

Energy management in Microgrid systems must be done properly in order to improve the system's overall efficiency, reduce the cost of the electricity, and lengthen the life of its components (e.g., converters, batteries, fuel cells). The exploited control strategies can be classified into three main categories: Centralized, decentralized, and hierarchal control. These control strategies are presented in the rest of this paragraph [12].

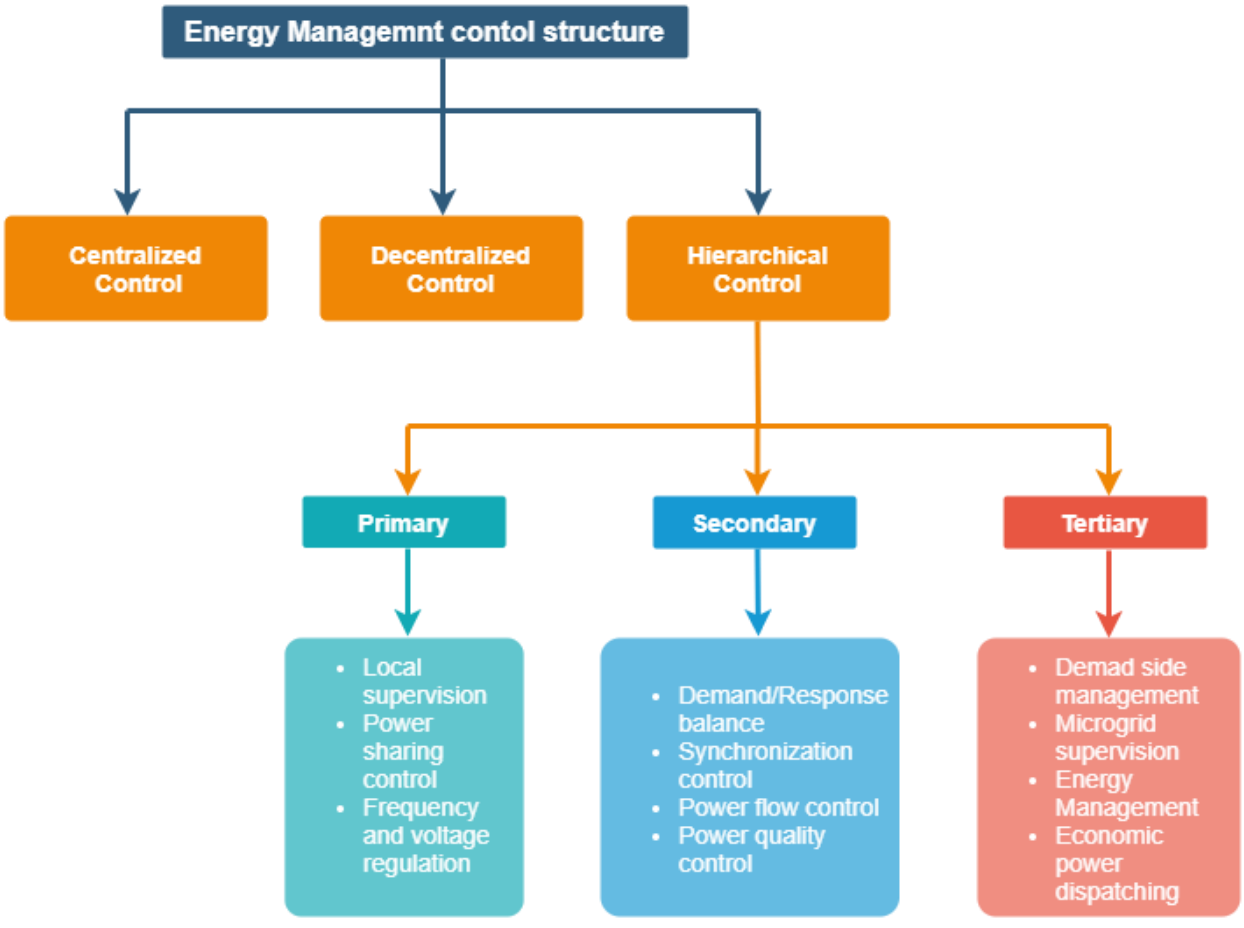

Fig. 5. Control structure for energy management in microgrid systems

2.8.1. Centralized Control

In order to manage different entities of the system, centralized control approaches use a single central controller, which is characterized by a high-performance processing unit and a secure communication architecture. To communicate and interact directly with the central controller, each entity needs a local controller. Furthermore, the central control may monitor, gather and analyze real-time data using contemporary communication and computing technologies. This enables all entities to collaborate with the central controller while maintaining microgrid's operation flexibility in both grid-connected and island mode. The central controller gathers data such as RES energy production, energy consumption patterns, market operator energy prices, and weather conditions, and then implements the most optimal and efficient system control.

2.8.2. Decentralized Control

Unlike centralized strategies, decentralized control considers each entity autonomous with the use of a local controller. This signifies that a leader is in charge of various groupings of entities. The phrases "decentralized" and "distributed controls" are often used in place of each other in the literature. The distributed control can be considered as a decentralized control in which local controllers use local measurements, such as frequency and voltage values. They are also allowed to share information with neighbors. For a distributed control, local controllers do not only use local measurements but also are able to send and receive required information to other local controllers. Limited local connections are necessary in decentralized control approaches, and control decisions are based only on local measurements.

2.8.3. Hierarchical Control

A compromise between the fully centralized and decentralized control structures is realized by providing hierarchical control structures according to three control levels: Primary, secondary, and tertiary.

1) Primary Control

The primary control level stabilizes the voltage and frequency generated from each source in order to satisfy the limits required by the standards. Moreover, the active and reactive power is divided. In addition, the primary control level detects the operating mode of the microgrid, offering the ability to operate in grid-connected and island modes.

2) Secondary Control

In secondary control level, the microgrid voltage and frequency are restored after system's load variation and the changes introduced by renewable energy sources are offset. The aim is to ensure and enhance the power quality within the limits required by the standards, allowing the synchronization between the microgrid systems and the main electrical network.

3) Tertiary Control

In tertiary control, optimal operation scheduling of the operation of the microgrid over a given time horizon takes place. In addition, the cost of operating the system is minimized, taking into account load forecasts, renewable energy production and the price of electricity.

Chapter 3

State of the Art and Innovation

3.1. State of the Art

Buildings' energy management systems (EMS) often place more emphasis on the optimization and control of individual buildings [13],[14] instead of the control of microgrids of building complexes. Energy management algorithms have focused more heavily on residential buildings [15],[16] or residential microgrids [17] than commercial buildings and microgrids, which are more complicated and difficult to optimize. An effective energy management strategy for a microgrid in both grid-connected and islanded modes is presented in [18]-[20], in contrast to [21],[22] wherein the autonomous operation of the microgrid is not taken into consideration. Specifically, as is featured in [20], when the microgrid is connected with the main electric grid, the grid regulates the system frequency and voltage. In the case of a significant load variation in the island mode operation of the microgrid, a diesel generator controls the system frequency and voltage. An optimal energy management method for HVAC systems' control of commercial buildings is proposed in [23]-[25]. Thermal zones are used to describe the building's thermal system, ensuring that the occupants have a comfortable indoor environment. Additionally, the EMS that is suggested in [26] divides the electrical loads into dispatchable and non-dispatchable categories and takes into account the thermal behavior of a commercial building, in contrast to [27], wherein the various building load types that were employed in this study were not independently modeled. Moreover, the majority of the existing works do not consider the Vehicle-to-Grid (V2G) operation [28],[29] of electric vehicles, in contrast to [30] wherein Plug-in Electric Vehicles (PEVs) were used as an energy storage system by absorbing or injecting active power from or into the electric grid. Even though many studies do not include any distributed power generation or energy storage units, the energy management systems that are proposed in [31]-[33] comprise various RES and energy storage systems. In [34], an integrated buildings and microgrid system with different renewable energy resources and controllable loads that is based on multiagent energy management system was monitored and optimally controlled. The proposed algorithm has the capability to minimize a system's operational cost and meet user demands in a variety of weather-related scenarios and pricing models. In [35], the proposed optimization method was applied in an office building microgrid, comprising EVs and batteries, that was connected to the main electric grid. Batteries were utilized as static energy storage, while EVs were employed as dynamic energy storage in order to maximize the overall profit of the microgrid and balance the fluctuations of demand, electricity price and RES generation. Moreover, the EVs' behavior and driving patterns have been taken into consideration. In [36], a two-level optimization strategy is suggested for the optimally distributed generation planning for active distribution networks taking into account the incorporation of energy storage systems. A method for allocating energy storage systems into active distribution networks is suggested in [37]. The Energy Storage Systems (ESSs) were properly modelled so as to support the electric network in terms of network losses and voltage variations. Moreover, the proposed method takes into consideration of the stochastic behavior of both loads and renewable energy source generation. In [38], a model-based robust control method was developed in order to manage tracking control and to take advantage of statistical identification for learning to model parametric and nonlinear environmental uncertainties. Parameter identification techniques could be applied especially to the building model as its parameters are characterized by their stochastic behavior and constant change.

A thorough review of the literature and state of the art has been done in order to identify opportunities for further research and possible technological improvements in the examined area. A few efforts have been made to evaluate frequency regulation capacity. More focus has been placed on studying the use of HVAC systems in residential buildings for providing ancillary services [39], [40], while very few studies on non-residential buildings can be found [41]. Many similar studies were carried out for a specific building [42], [43] or a group of buildings [44]. A model-based method for assessing commercial building frequency

support capability is presented in [43]. The proposed approach is demonstrated through detailed simulations for medium and large office buildings. In [45], load profiles are categorized according to their sheddability, controllability and frequency support capability of various types of loads is estimated. In [46], [47] the capability of commercial buildings' HVAC systems to support frequency is examined. The power consumption of HVAC system supply fans is considered as the only source of flexibility. Coordination strategies are proposed in [48] to optimally utilize the flexibility of building loads and energy storage in order to provide services to the power system and end-users such as frequency support and energy cost reduction. A framework for fast primary frequency response by a group of flexible building loads and controllable distributed energy resources (DERs) that are organized together in real-time, is developed in [49]. In [50], during microgrid grid-connected operation, the grid regulates the system frequency and voltage while when being in islanded mode operation local diesel generators are in charge. Microgrids deal with challenges arising by DERs' stochastic power production and varying load demand. Power management method for microgrid with distributed energy resources is proposed in [51], [52]. The reactive power is set by a voltage droop characteristic and the real power by a frequency droop characteristic. In order to minimize both frequency and voltage fluctuations in islanded microgrids, a strategy for demand response and DERs coordination is developed in [53]. For this purpose, the set-points for the DERs and the amount of the required power curtailed by adjustable loads are estimated.

Some studies propose ESS control strategies for frequency support in microgrids with high-RES penetration [54], [55]. In [55], a two-level optimized primary and secondary frequency controller, controls the ESS active power response. System stability is enhanced by responding to frequency fluctuations using a conventional droop control approach in combination with a virtual inertia function. Plug-in Electric Vehicles (PEVs) have the potential to provide ancillary services the power systems, such as frequency regulation, due to their fast-regulating characteristics. Many studies have developed V2G control strategies with adaptive droop frequency control in order to achieve primary frequency regulation [56]-[58]. An optimal PEV aggregator that achieves efficient use of the distributed EVs to provide frequency regulation services is designed in [59]-[61]. In [62], an optimal fuzzy controller is employed to support the frequency of a deregulated grid taking into consideration the state of charge of the EV battery and frequency deviation. A method based on multi-agent systems (MAS) for the real-time control of large ports viewed as prosumer microgrids comprising a large number of flexible loads is proposed in [63]. Moreover, this method provides ancillary services to the power system such as frequency support during unpredictable load changes.

3.2. Innovation

According to the findings of the performed literature and state of the art review, the innovative points of the proposed method are listed next. It is noted that the features listed below are rarely found in the available literature and no research work was found to comprise and jointly apply them to microgrids of large-scale building prosumers.

- The innovative edge of the method is that it requires very short computation times (of the order of a few minutes) for extremely complex systems consisting of very large-scale building complexes with a number of decision variables that can reach a few thousand and operational constraints of a multiple of this number. In order to achieve this, a simple way to dispatch the total needs, in terms of thermal power, of a building to its thermal zones is used. The thermal power that is required to be provided to each thermal zone is a function of the total thermal power that is required by the building, its thermal zone volume and its estimated internal temperature together with its upper and lower limits. As a result, the required computation time is kept very low, since the total required thermal power of the building is optimized and then dispatched to the thermal zones. Moreover, an effective aggregation technique is applied to the plug-in electric vehicles that are hosted by the microgrid.
- To the best of the authors' knowledge, there are very few works studying the coordinated optimal operation of active distribution networks and microgrids (and especially microgrids comprising large building prosumers).
- A series of microgrid operations like the operation of building HVAC systems and building non-critical electrical loads, auxiliary diesel generators operation and the operation of the aggregate

battery of the connected electric vehicles are jointly optimized for microgrid grid-connected and autonomous operation.

- Another advantage of the algorithm is that, during time periods of the day when the electric grid is not available, the microgrid is able to meet the electricity demand of the building itself with the interconnected electric vehicles and the integrated RES and this same provision of electricity may also be called upon if there is a need or it is economically optimal by the use of the building's auxiliary generators.
- The developed power management and control methods ensure optimal frequency support for the microgrid and the electric network it is connected to. To this end, suitable flexibility indices are defined for all associated components and exploited for the optimal provision of ancillary services.
- Simple and effective definition of the flexibility of clusters of buildings to change their power by exploiting fuzzy logic is first proposed in this work.
- Smart power dispatch techniques are applied to buildings and PEVs clusters hosted by the active distribution network, as well as to the residential buildings and PEVs.
- Deviations from the day ahead optimal operation scheduling occurring in real operation of the microgrid are optimally compensated by repeating the operation scheduling optimization in apropriate time periods.
- The operation of the active distribution network comprising RES, flexible loads and a hosted microgrid is optimally jointly scheduled without requiring the microgrid and the active distribution network to disclose to each other their respective internal technical characteristics and information.
- At the same time, a large number of operation, technical and environmental constraints of the active distribution network and its components is ensured. Moreover, the proposed algorithm achieves the highest possible minimization of the daily operation cost of the active distribution network.
- The proposed method for the optimal operation of the ADN goes with the increasing need for sustainable development. The examined system includes renewable energy sources that generate clean energy. Moreover, the autonomous operation of the ADN is ensured, mainly through the hosted PEVs and RES, and there is no need for in-vestment to extra auxiliary power generation units of conventional polluting technology. This contributes to the reduction in emission of greenhouse gases and consequently to the environment's protection. Another significant aspect of the suggested method that ensures its sustainable application is the minimization of the daily operation cost of the examined ADN. Another sustainable feature of the method is the qualitative operation of the ADN as it can ensure the maintenance of the ADN voltages within their permissible bounds.

Chapter 4

Structure of the Proposed Energy Management and Control System

Detailed, fully parametric systems for the energy management and real-time operation of microgrids of large building complexes are developed in this work. Specifically, the examined energy systems include buildings scaling from simple residential ones up to mega office or commercial buildings, single PEVs up to large PEV parking lots, local power generators, PVs and wind turbines. The developed models include those of the thermal and electrical loads of the buildings with the latter being divided in critical and non-critical loads that can be shifted in time. Thermal loads also can be shifted in time and adjust their power demand under their operational and technical constraints. The loads of the examined microgrids are supplied from the local power sources and the main electric grid or only by the local power sources if the microgrid is in island mode of operation i.e., RES, hosted PEVs etc. The operations of the microgrid are organized in a hierarchical MAS. MAS have been proved to be very efficient in the control and management of complex systems that might be difficult to attain using classical control methods. Hence, they can be a very effective solution for highly complex microgrids of large-scale building prosumers.

The developed MAS comprises different types of agents placed at different levels of the MAS as shown in Fig.6.

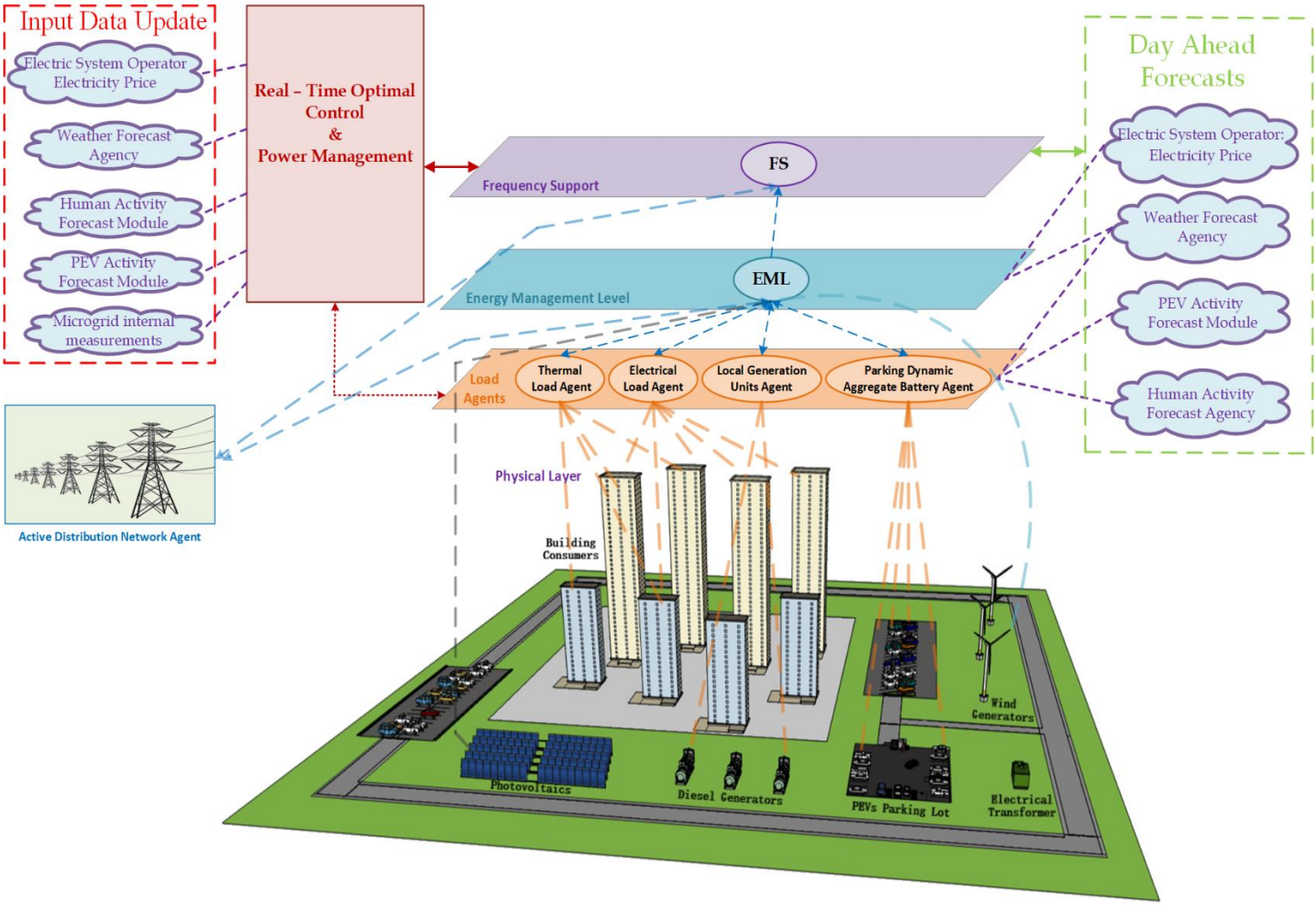

Fig. 6. Structure of the proposed energy management and control system.

The microgrid operation scheduling performed in MAS second level is susceptible to the uncertainties arising from the forecasts of stochastic variables like the price of electricity, the ambient temperature, the production of renewable energy, and the activity of people and electric vehicles. To this end, the setpoints of all microgrid components are optimally readjusted in the real-time operation using updated values of all forecasted quantities in order to cancel out deviations due to prediction errors, as shown in Fig.7.

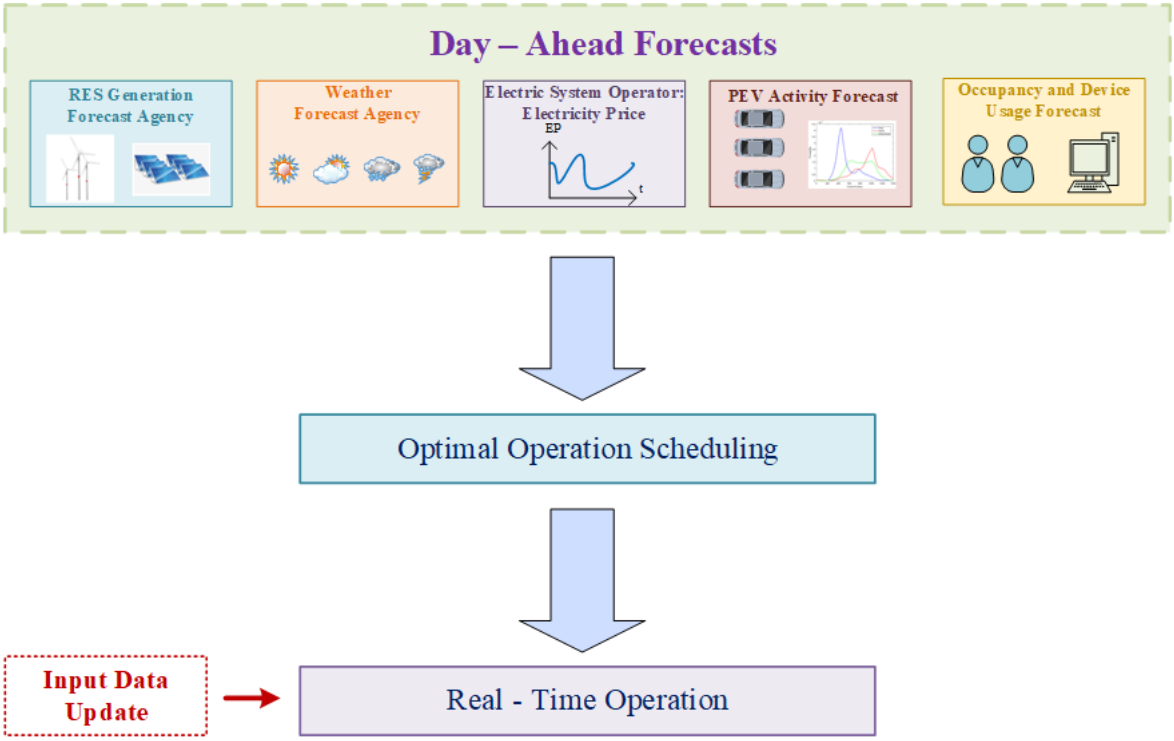

Fig. 7. A generic diagram of optimal operation scheduling and real-time operation

4.1. MAS First Level: Microgrid Load Modelling

Each building is divided into thermal zones. A thermal zone is considered in this work as a section of a building that allows independent control of its internal temperature and has its own characteristic thermal behavior. The agents that are associated with the buildings and placed at the first level of the MAS aim to model the thermal zone loads and building electrical loads according to building technical specifications, occupancy, activity level, various types of used appliances in each thermal zone, conditioned space of each thermal zone, outdoor temperature, solar radiation etc. The same agents, except from the above mentioned, are responsible to receive the setpoints calculated from the higher in the MAS hierarchy level and apply them.

Another type of agent in the lower level of the developed MAS is assigned with the development of a dynamic equivalent battery model for the PEVs hosted by the microgrid. It collects the necessary data from the PEVs, like upper and lower bounds of their stored energy and power, state of charge target at their disconnection time etc. Then it forms the equivalent battery model. PEVs not only absorb power from the network and charge their battery packs, but they also have the ability to operate in V2G mode i.e., PEVs inject power to the grid during specific time periods. This agent is also responsible for the optimal dispatch of the total power to the PEVs it supervises and controls. Finally, agents assigned to the building local power generation units are included in this MAS level.

4.2. MAS Second Level: Microgrid Energy Management

4.2.1. Optimal operation scheduling of active distribution network comprising large office building complexes and plug-in electric vehicles

The proposed energy management system is structured in the five optimization levels that are described next in this section. Before the application of the optimization levels of the method, the forecasts of occupancy, human activity levels, ambient temperature, PEVs' arrival/dwell times, solar radiation, wind speed and electricity price must be performed for the upcoming 24 h.

Optimization Level 1

The main goal of the first optimization level is the minimization of the total daily operation cost of the microgrid on the assumption of operation under variable electricity price. It determines the optimal operation scheduling of the buildings' HVAC and electrical systems, PEV aggregator and local power generation units within a predefined optimization period. Specifically, it provides the optimal total electric power demand of the HVAC systems and optimally shifts building non-critical electrical loads. Moreover, it schedules optimally the output power of the hosted PEVs and the operation of the local power generation units. In addition, the reactive powers of the clusters of PEVs and building local power generators are suitably scheduled to maintain node voltages within their boundaries. At the same time, a large number of constraints including all the operational and technical constraints of the hosted PEVs, diesel generators, distribution network and the building energy systems are satisfied, e.g., an acceptable thermal comfort for the occupants of each thermal zone of the building should be maintained, the electric power demand should not exceed its nominal values etc. Another hard requirement is set according to the PEV aggregate model so as to ensure that each PEV can reach the target of stored energy at its disconnection time without violating any technical constraint. PEVs not only absorb power from the network and charge their battery packs but they also have the ability to operate in V2G mode i.e., PEVs can inject power into the grid during specific time periods.

Optimization Level 2

In the second optimization level, the algorithm aims to minimize the operational cost of the active distribution network by appropriately choosing the adjustment coefficient of the flexible electrical loads of the distribution network at each time interval. Network constraints are not considered in this stage. If the network constraints are not violated then the energy management process stops. Otherwise, time periods wherein the network constraints are violated are identified and sent to the microgrid in order to assess the minimum and maximum possible deviations of its power exchange that will contribute to the elimination of the network constraints' violation.

Optimization Level 3

If the distribution network constraints that result from the second level of optimization are out of their permissible ranges, the third optimization level is performed. In this level, the algorithm determines the maximum feasible variation of the power that is transferred between the microgrid and the active distribution network.

Optimization Level 4

In the fourth optimization level, the algorithm aims to maintain the distribution network's voltages and the currents of the power lines within their permissible limits by suitably shifting the flexible electrical loads in time and regulating the power that is exchanged between the distribution network and the microgrid within the limits that were determined in optimization level 3.

Optimization Level 5

In this optimization level, the algorithm aims to minimize the overall cost of the operation of the microgrid over a 24 h period, taking into consideration the power that the microgrid should exchange with the active distribution network (this was estimated in the fourth optimization level).

4.2.2. Optimal operation scheduling of active distribution network comprising smart residential building prosumers and plug-in electric vehicles

The layout of the examined ADN and the structure of the hierarchical MAS developed work are shown in Fig. 8. In the examined MAS, the agents used are classified into three major types: (1) local agents, (2) cluster agents and (3) active distribution network management agent. Local agents are accountable to model an individual module of the ADN, cluster agents are accountable to gather and properly handle the responses of a cluster of local agents and forward information back to them. All cluster agents are supervised and managed by the Active Distribution Network Management Agent (ADNM/A). ADNM/A is accountable for the optimal coordination of the MAS according to the responses received by cluster agents and possesses the higher place in MAS hierarchy, as depicted in Fig. 8. It can be concluded by Fig.

8 that a bidirectional communication system should be available to each agent. Next, a brief explanation of each type of agent is provided.

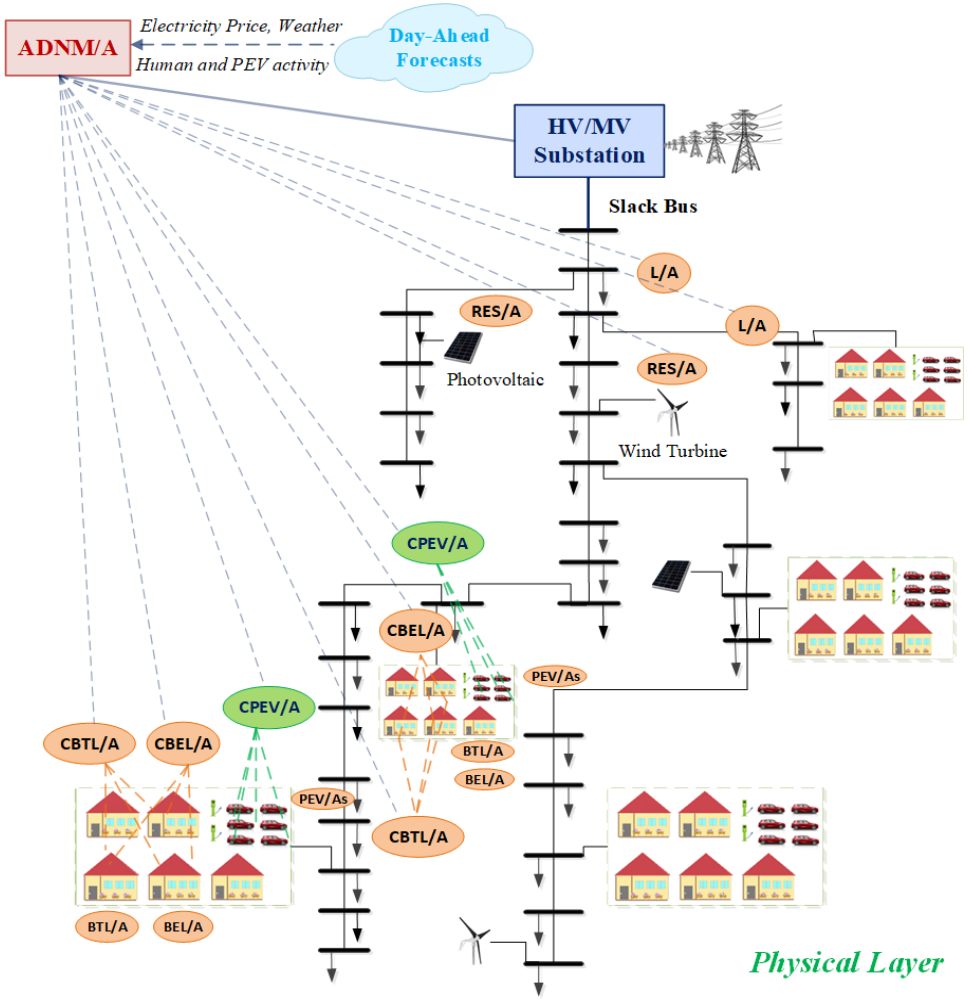

Fig. 8. MAS based power management system structure for active distribution network.

Local Agents

The *Building Thermal Load Agent* (BTL/A), *Building Electrical Load Agent* (BEL/A), *Plug-in Electric Vehicle Agent* (PEV/A), *Renewable Energy Sources Agent* (RES/A) and *Load Agent* (L/A) belong to the type of local agents. Distribution network components' inherent quantities are calculated by local agents. Specifically, BTL/A and BEL/A are assigned to each building of the network and model its thermal and electrical loads, respectively. Additionally, BTL/A calculates the indoor temperature of each building over the optimization horizon. The estimated indoor temperature of the building is used with its upper and lower limits to suitably calculate the flexibility of each building to increase or decrease its thermal power demand. Afterwards, BTL/A and BEL/A send the necessary data to the supervising cluster agents CBTL/A and CBEL/A, respectively. PEV/A calculates the flexibility of each individual PEV to change its power and the bounds of its stored energy and active and reactive power it exchanges with the distribution network. These quantities are forwarded to the CPEV/A that supervises the cluster of PEVs. RES/A executes very short-term forecasts of the power produced by the renewable energy units it is assigned to. L/A is assigned to each node of the distribution network and estimates the active and reactive power demand of the node also by performing very short-term forecasts. RES/A and L/A provide their responses to ADNM/A.

Cluster Agents

Cluster of Building Thermal Loads Agent (CBTL/A), *Cluster of Building Electrical Loads Agent* (CBEL/A) and *Cluster of Plug-in Electric Vehicles Agent* (CPEV/A) belong to the type of cluster agents and they are hierarchically located just above the agents BTL/A, BEL/A and PEV/A, respectively. They are regularly placed on Medium Voltage/Low Voltage (MV/LV) transformers that supply clusters of residential buildings and/or PEVs. Their primary aim is the aggregation of the responses they receive from

the BTL/As, BEL/As and PEV/As being in their control areas. Moreover, CBTL/As and CPEV/As define suitable flexibilities exploiting fuzzy logic based on information regarding the respective node voltage and the flexibility of the supervised BTL/As and PEV/As, respectively. Cluster agents are also responsible for the optimal dispatch of their power to the local agents they supervise and control. Finally, they forward the necessary data to the active distribution network management agent.

Active Distribution Network Management Agent

Active Distribution Network Management Agent (ADNM/A) is at the higher level of the proposed hierarchical MAS. ADNM/A gathers the aggregated responses from the cluster agents and also information for the forecasted price of electricity, the node loads of the network and the power produced by RESs and it exploits an optimization technique for the optimal operation scheduling of the ADN. The proposed method aims to reduce the daily operation cost of the network by shifting the power demand in time periods with low electricity price. At the same time, all the operational constraints of the ADN, building energy systems and hosted PEVs should be satisfied. Constrained optimal power flow algorithm (OPF) is exploited in order to maintain the voltages of the ADN within the permissible limits. Then the active and reactive power set-points resulted from the OPF exploitation are forwarded back to the respective cluster agents so as to be optimally dispatched to the local agents they supervise.

4.3. MAS Third Level: Microgrid Frequency Support (FS)

The microgrid is considered able to provide frequency support to the main power grid. In addition, it is considered able to regulate the reactive power optimally in order to maintain the local voltages of the microgrid and the hosting distribution network within the permissible limits. To this end, constrained optimal power flow algorithms are exploited. A detailed model for the simulation of microgrid frequency deviation due to occurred load changes is developed. The examined system comprises primary and secondary frequency control. In our case, microgrid frequency support can be enhanced by suitably exploiting the flexibility of building prosumers and PEVs and by suitably adjusting the active power of the local power generation units. For instance, in case of frequency drop, the algorithm aims to decrease buildings' power consumption and decrease PEVs' power consumption or increase their power injection to the grid if they are in V2G operation. Moreover, adjustable electrical loads operating at specific energy consumption levels are partially curtailed or increased to support system frequency. Finally, the local building power generation units are suitably controlled to support system frequency. It is noted that all models associated with frequency support are developed in a way that makes them suitable for real-time operation as the time scales involved in the frequency support mode of operation are relatively small in comparison to the operation time scales of microgrid components.

The developed MAS collects from other entities information and data like weather forecast data, electricity price forecast etc. in order to perform optimal operation scheduling and real-time operation of the microgrid, as shown in Fig. 6.

Typical sequence of communications

The communication signals exchanged by the agents of the proposed MAS are shown in Fig. 9. A typical sequence of communications is also depicted in Fig. 9 and briefly described next. Let us assume a 24-hour optimization period.

Initially, the forecasts of work schedule, activity of people, ambient temperature, PEVs' arrival/dwell times, irradiation, wind speed and electricity price are received for the next 24-hour period and they are forwarded to TLA, ELA, PDABA through communication signal SD1.

TLA and ELA take into account the above forecasts to estimate the daily thermal and electrical loads of the microgrid's buildings and PDABA to develop a dynamic equivalent battery model for the cluster of PEVs hosted in the facilities of the microgrid. Moreover, the electric power generation estimation of the WTs and PVs is done taking into account the communication signal SD2.

In addition to the above outcomes, electricity price forecast and diesel generators model parameters are forwarded to EML through communication signals SD4, SD3 and SD5, respectively. EML calculates the most effective operation schedule of the buildings' HVAC and electrical systems, PEV aggregator and local power generation units. In addition, the reactive powers of the PEVs and building local power generators are suitably scheduled to maintain node voltages within their boundaries.

When it is required (during frequency events), the FS level receives the required information from power and energy management system through communication signal SD7. Updated values of all forecasted quantities are also forwarded to FS with signal SD6. The setpoints of all microgrid components are optimally adjusted in real-time in order to provide frequency support. Specifically, frequency support mode of operation is enhanced and optimized by suitably exploiting the flexibility of the building prosumers and PEVs. Frequency is also supported by adjusting the power of local building generation units and by suitably adjust their non-critical loads in an optimal way according to their flexibility.

The obtained results from FS level are forwarded through the communication signal SD9 to Load Agents and smart power dispatch techniques are applied to estimate the power set-points at component level e.g., thermal zones and PEVs. To achieve this, innovative definitions of the flexibility of microgrid components to change their power are exploited and a new sub-optimization problem that maximizes the total flexibility of the system is solved to obtain the optimal power dispatch under all the associated constraints. Then, the resulting setpoints are sent to the Physical Layer through signal SD10 where they are applied to building thermal zones and each PEV of the microgrid. Moreover, the setpoints of diesel generators estimated at FS level are directly forwarded to the Physical Layer through communication signal SD8 and applied to each diesel generator.

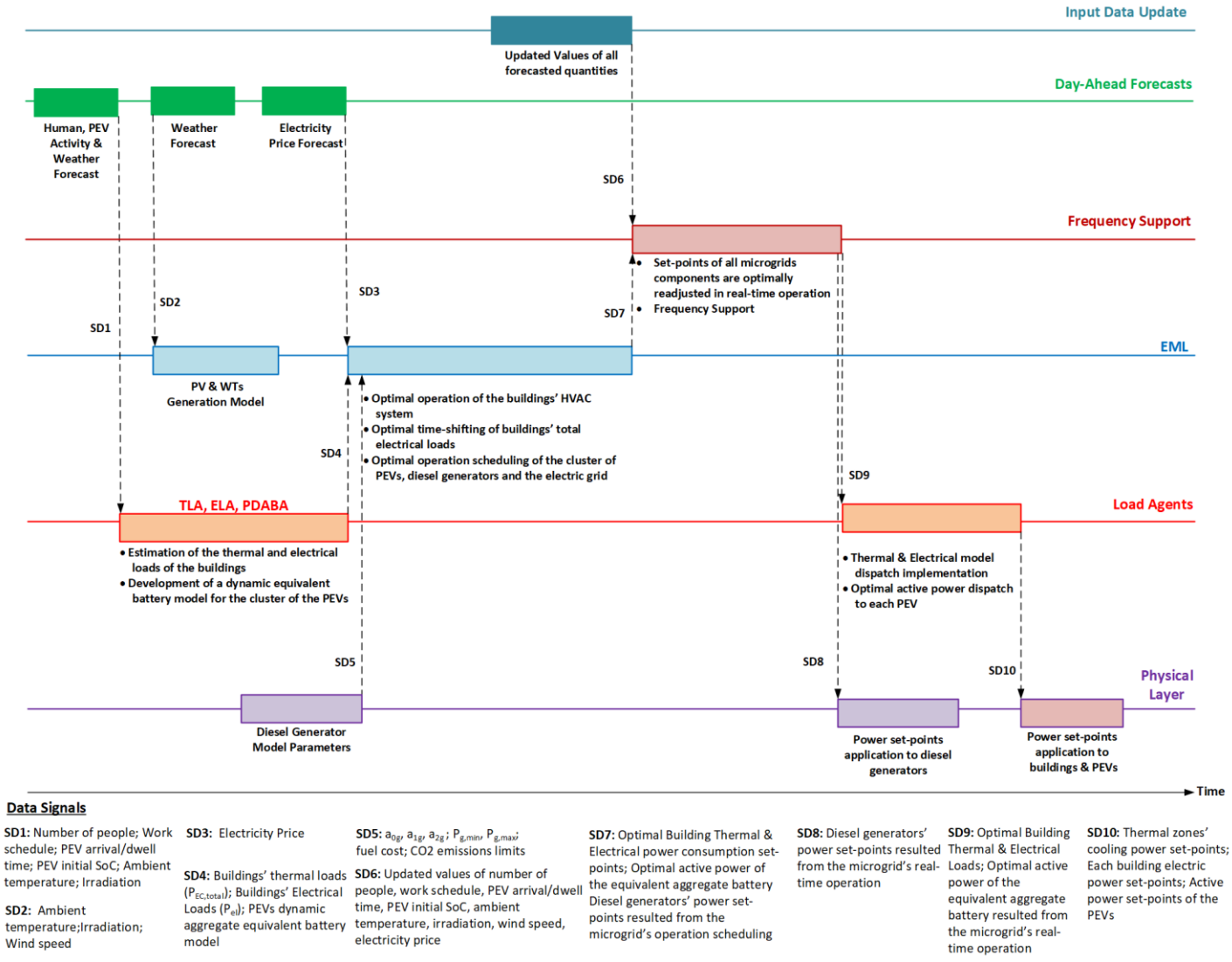

Figure 9. Communication signals sequence.

Chapter 5

Microgrid Components Modelling hosted by the Active Distribution Network

5.1. Model of Building Thermal Load Agent (TLA)

In this work, each building is divided into thermal zones. Using the following thermal equilibrium equation, a mathematical relationship between the internal temperature, thermal gains, thermal loads and ambient temperature can be developed in order to analyze the thermal behavior of each thermal zone [64], [65].

$$p_z \cdot C_z \cdot V_z \cdot \frac{dT_{in,z}}{dt} = \dot{Q}_{ex,wall,z} + \dot{Q}_{in,wall,z} + \dot{Q}_{win,z} + Q_{in,z} + \dot{Q}_{sw,z} + \dot{Q}_{sg,z} - Q_{HVAC,z} \quad (1)$$

The heat exchange between a thermal zone and its outdoor environment is described by Equations (2)-(5), while Equation (6) estimates the heat exchange between a thermal zone and its neighboring zones.

$$\dot{Q}_{ex,wall,z} = \sum_{y \in \mathcal{E}} U_{wall,y} \cdot F_{wall,y} \cdot \left(T_{out} - T_{in,z}\right) \quad (2)$$

$$\dot{Q}_{win,z} = \sum_{y \in \mathcal{E}} U_{win,y} \cdot F_{win,y} \cdot \left(T_{out} - T_{in,z}\right) \quad (3)$$

$$\dot{Q}_{sw,z} = \sum_{y \in \mathcal{E}} a_w \cdot R_{se} \cdot U_{wall,y} \cdot F_{wall,y} \cdot I_{T,z} \quad (4)$$

$$\dot{Q}_{sg,z} = \sum_{y \in \mathcal{E}} \tau_{win} \cdot SC \cdot F_{win,y} \cdot I_{T,z} \quad (5)$$

$$\dot{Q}_{in,wall,z} = \sum_{y \in \mathcal{E}} U_{wall,y} \cdot F_{wall,y} \cdot \left(T_{in,nz} - T_{in,z}\right) \quad (6)$$

By appropriately modifying (1)-(6), the state space system of equations is obtained for each building.

$$\frac{d\boldsymbol{T_{in}}(t)}{dt} = \boldsymbol{A_b} \cdot \boldsymbol{T_{in}}(t) + \boldsymbol{B_b} \cdot \boldsymbol{U} \quad (7)$$

$$\boldsymbol{Y}(t) = \boldsymbol{C_b} \cdot \boldsymbol{T_{in}}(t) + \boldsymbol{D_b} \cdot \boldsymbol{U} \quad (8)$$

The input vector $\boldsymbol{U}$ is of dimension $(2N_Z + 2) \times 1$. It is given in (9).

$$\boldsymbol{U} = \begin{bmatrix} Q_{EC,1}(t) \\ \vdots \\ Q_{EC,N_Z}(t) \\ Q_{in,1}(t) \\ \vdots \\ Q_{in,N_Z}(t) \\ T_{out}(t) \\ I_T(t) \end{bmatrix} \tag{9}$$

with

$$I_{T,z} = I_b \cdot R_b + I_d \cdot \left(\frac{1 + cos\beta_z}{2}\right) + I \cdot p_g \cdot \left(\frac{1 - cos\beta_z}{2}\right) \tag{10}$$

$$R_b = \frac{cos\theta}{cos\theta_z} \tag{11}$$

The elements of the matrix $\boldsymbol{A_b}$ with dimension $(N_Z \times N_Z)$ are calculated in (12)-(13).

$$A_{j,j} = -\sum_{y \in \mathcal{E}} U_{wall,y} \cdot F_{wall,y} - \sum_{x \in \mathcal{J}} U_{wall,x} \cdot F_{wall,x} - \frac{1}{p_z \cdot C_z \cdot V_z} \cdot \sum_{y \in \mathcal{E}} U_{win,y} \cdot F_{win,y} \tag{12}$$

$$A_{j,i} = \begin{cases} \dfrac{1}{p_z \cdot C_z \cdot V_z} \cdot U_{wall,x} \cdot F_{wall,x}, & j,i \in \mathcal{N} \\ 0, & j,i \notin \mathcal{N} \end{cases} \tag{13}$$

The dimension of $\boldsymbol{B_b}$ is $N_Z \times (2N_Z + 2)$ and it is calculated as in the following,

$$\boldsymbol{B_b} = \frac{1}{p_z \cdot C_z \cdot V_z}[-\mathbf{I}_{(N_Z \times N_Z)} \quad \mathbf{I}_{(N_Z \times N_Z)} \quad \boldsymbol{B_{ex,w}} \quad \boldsymbol{B_{rad}}] \tag{14}$$

with

$$\boldsymbol{B_{ex,w}}_{(N_Z \times 1)} = \begin{bmatrix} B_{ex,w,1} \\ \vdots \\ B_{ex,w,N_Z} \end{bmatrix} \tag{15}$$

$$\boldsymbol{B_{rad}}_{(N_Z \times 1)} = \begin{bmatrix} B_{rad,1} \\ \vdots \\ B_{rad,N_Z} \end{bmatrix} \tag{16}$$

The elements of the submatrices $\boldsymbol{B_{ex,w}}$ and $\boldsymbol{B_{rad}}$ of matrix $\boldsymbol{B_b}$ are determined as it follows.

$$B_{ex,w,z} = \sum_{y \in \mathcal{E}} U_{wall,y} \cdot F_{wall,y} + \sum_{y \in \mathcal{E}} U_{win,y} \cdot F_{win,y} \tag{17}$$

$$B_{rad,z} = \sum_{y \in \mathcal{E}} a_w \cdot R_{se} \cdot U_{wall,y} \cdot F_{wall,y} + \sum_{y \in \mathcal{E}} \tau_{win} \cdot SC \cdot F_{win,y} \quad (18)$$

Considering as output the internal temperatures of the thermal zones then the matrices $\boldsymbol{C_b}$ and $\boldsymbol{D_b}$ are defined as in the following,

$$\boldsymbol{C_b}_{(N_Z \times N_Z)} = \mathbf{I}_{(N_Z \times N_Z)} \quad (19)$$

$$\boldsymbol{D_b}_{(N_Z \times 2N_Z+2)} = \mathbf{0}_{(N_Z \times 2N_Z+2)} \quad (20)$$

The system of continuous time equations (7)-(8) is converted to discrete time equations (21)-(22).

$$\boldsymbol{T_{in}}(k+1) = \boldsymbol{A_{b,d}} \cdot \boldsymbol{T_{in}}(k) + \boldsymbol{B_{b,d}} \cdot \boldsymbol{U} \quad (21)$$

$$\boldsymbol{Y}(k) = \boldsymbol{C_{b,d}} \cdot \boldsymbol{T_{in}}(k) + \boldsymbol{D_{b,d}} \cdot \boldsymbol{U} \quad (22)$$

5.2. Model of Electrical Load Agents (ELA)

There are different types of electrical loads in each thermal zone of the building that can be classified to critical and non-critical loads. Critical loads consist of devices, such as lighting, personal computers, TVs, whose power consumption is specific and cannot be changed. Non-critical loads include devices, such as washing machines, that have a certain flexibility to shift their electricity consumption into different time slots of the day.

The power consumed by the electrical loads of the zth building thermal zone, $P_{el\_load,z}$, is calculated taking into account the forecasted number of people and each type of device they use [66]. The total electric power consumption of the building is calculated as in the following:

$$P_{el,b} = \sum_{z} P_{el_{load},z} \quad (23)$$

Where, $P_{el\_load,z}$ is the power consumption of the electrical loads of the zth thermal zone.

In this work, it is considered that the electrical power consumption of the non-critical loads constitutes a percentage (n_{non_cr}) of the total power consumed by the electrical loads of the building.

$$P_{non_{cr}} = \sum_{b} n_{non_{cr}} \cdot P_{el,b} \quad (24)$$

Let us assume that the window of time in which non-critical loads may be shifted is $[T_{shift,0}\ \ T_{shift,f}]$. The optimal load shifting algorithm transfers a specific percentage of the non-critical load of one timeslot to a different one, provided that the energy that is consumed before and after the load shifting remains the same as is formulated in Equation (25).

$$P^*_{non_{cr}}(t) = \begin{cases} n_{shift}(t) \cdot P_{non_{cr}}(t), & \forall t \in [T_{shift,0}\ \ T_{shift,f}] \\ P_{non_{cr}}(t), & otherwise \end{cases} \quad (25)$$

5.3. Parking Dynamic Aggregate Battery Agent (PDABA)

In this paragraph, a dynamic equivalent battery model is developed for the PEVs hosted by microgrid's parking lots. It is based on the forecasts of PEVs' plug-in and dwell times, their initial state of charge and their batteries technical characteristics. The main goal of this model is to obtain the dynamic upper and lower limits of the totally stored energy in their battery packs and the total active power they can exchange with the electric network. The permissible operation area of an individual PEV is shown in Fig. 10.

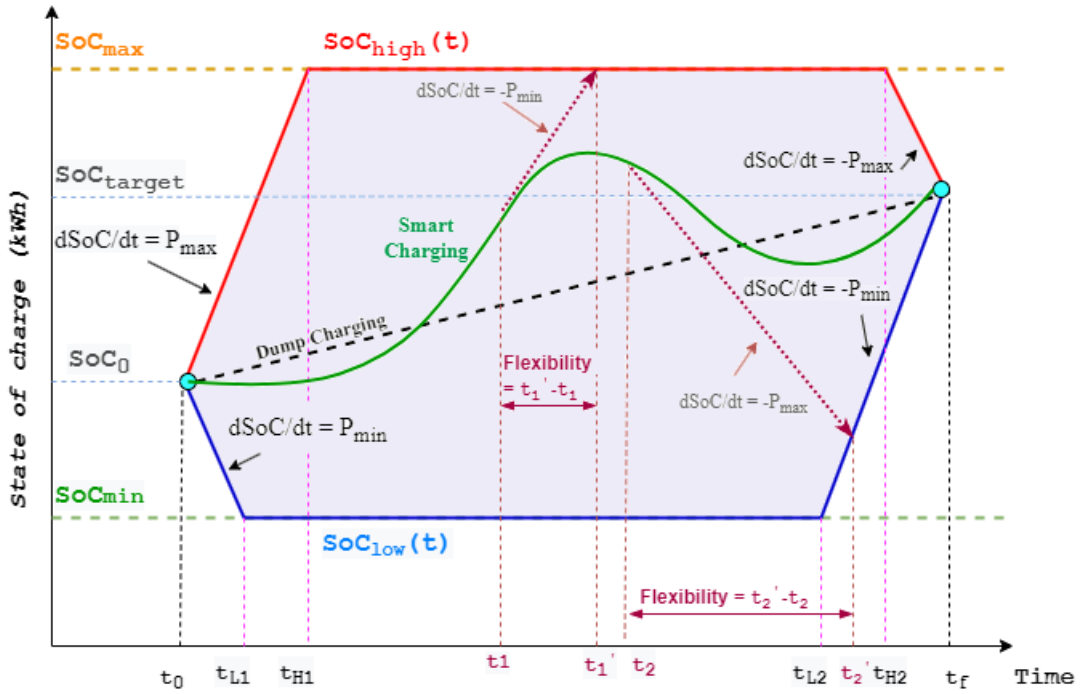

Fig. 10. Bounds of PEV's stored energy

The time that the EV is plugged to the network and unplugged from it is denoted with t_0 and t_f, respectively. SoC_{max} and SoC_{min} are the maximum and the minimum values of PEV's battery state of charge (in kWh). SoC_0 is the initial state of charge (kWh) of each PEV. P_{max} and P_{min} are the maximum and minimum power the PEV's battery can exchange with the network, respectively. SoC_{target} is the stored energy target the driver has defined his PEV should reach at its disconnection time. The dynamic lower and upper bounds of PEV's SoC, SoC_{low} and SoC_{high}, are generally defined by 4 points where they start to decrease or increase with a constant rate of change P_{min} or P_{max}. These points are (t_0, SoC_0), (t_{L_1}, SoC_{min}), (t_{L_2}, SoC_{min}), (t_f, SoC_{target}) for SoC_{low} and (t_0, SoC_0), (t_{H_1}, SoC_{max}), (t_{H_2}, SoC_{max}), (t_f, SoC_{target}) for SoC_{high} and they are shown in Fig. 9.

t_{L_1}, t_{H_1}, t_{L_2} and t_{H_2} are estimated as in the following [67]:

$$t_{L_1}(i) = t_0(i) + \frac{SoC_{min}(i) - SoC_0(i)}{P_{min}(i)} \tag{26}$$

$$t_{H_1}(i) = t_0(i) + \frac{SoC_{max}(i) - SoC_0(i)}{P_{max}(i)} \tag{27}$$

$$t_{L_2}(i) = t_f(i) + \frac{SoC_{target}(i) - SoC_{min}(i)}{P_{min}(i)} \tag{28}$$

$$t_{H_2}(i) = t_f(i) + \frac{SoC_{target}(i) - SoC_{max}(i)}{P_{max}(i)} \tag{29}$$

The time varying technical limits of the equivalent aggregate battery are calculated by the following equations:

$$P_{PB,max}(t) = \sum_{i} P_{max}(i,t) \tag{30}$$

$$P_{PB,min}(t) = \sum_{i} P_{min}(i,t) \tag{31}$$

$$SoC_{PB,max}(t) = \sum_{i} SoC_{high}(i,t) - SoC_{diff}(t) \tag{32}$$

$$SoC_{PB,min}(t) = \sum_{i} SoC_{low}(i,t) - SoC_{diff}(t) \tag{33}$$

The SoC of the parking equivalent battery is dynamically changed due to the continuous plugging and unplugging of EVs. It is denoted by SoC_{diff} and it is calculated in following equation:

$$SoC_{diff}(t) = \sum_{T_0:\Delta t:t} (SoC_{0,PB}(t) - SoC_{t,PB}(t)) \tag{34}$$

$$SoC_{0,PB}(t) = \sum_{\forall ith\ EV\ plugged\ at\ t} SoC_0(i) \tag{35}$$

$$SoC_{t,PB}(t) = \sum_{\forall ith\ EV\ unplugged\ at\ t} SoC_{target}(i) \tag{36}$$

Let us assume that $P_{opt}(t)$ is the optimal active power the equivalent aggregate battery exchanges with the electric network. Adopting generator convention, the resulting SoC (in kWh) at the end of the next time interval is calculated as it follows:

$$SoC_{PB}(t+\Delta t) = \begin{cases} SoC_{PB}(t) - P_{opt}(t) \cdot n_{ch} \cdot \Delta t, & P_{opt}(t) < 0 \\ SoC_{PB}(t) - \dfrac{P_{opt}(t)}{n_{disch}} \cdot \Delta t, & P_{opt}(t) \geq 0 \end{cases} \tag{37}$$

5.4. Operation Scheduling of Diesel Generator Set

The optimal operation scheduling of the diesel generators of the buildings can decrease further the operation cost of the microgrid of building prosumers. Generator fuel cost function FC depends on the produced power P_g and may accurately be approximated by second-order polynomials [68]. Thus, the fuel cost of the gth diesel generator at time t is given as,

$$FC_g\left(P_g(t)\right) = a_{0g} + a_{1g} \cdot P_g(t) + a_{2g} \cdot P_g(t)^2 \tag{38}$$

The fuel consumption function (kgFuel/h) of the *g*th generator is given as:

$$FuelCon\left(P_g(t)\right) = \frac{FC_g\left(P_g(t)\right)}{FuelCost_g} \tag{39}$$

Where, $FuelCost_g$ is the cost of the fuel consumed by the gth generator (m.u./kgFuel).

The mass of the gas emissions of the gth generator produced in time interval Δt is calculated as in the following:

$$m_{em,g}\left(P_g(t)\right) = c_{em,g} \cdot FuelCon\left(P_g(t)\right) \cdot \Delta t \tag{40}$$

where $m_{em,g}$ (in $kgEm_g/h$) is the mass of the gth diesel generator pollutant emission and $c_{em,g}$ (in $kgEm_g/kgFuel$) is the conversion factor of fuel mass to emission mass Em_g.

Chapter 6

Optimal Operation Scheduling of the Microgrid and the hosting Active Distribution Network

In this work, particle swarm optimization (PSO) has been used in order to optimally schedule the operation of the examined system. PSO is one of the most highly efficient heuristic methods and its implementation is remarkably simple. PSO has proved very robust and efficient for application to complex optimization problems as it does not depend on the selected initial point and leads to a global optimum with a high rate of success. It is difficult to find the global optimum for large-dimension optimization problems and formulate extremely complex objective functions using classical methods.

In the examined problem, the building thermal model's differential equations, PEVs aggregated model and distribution network model should be solved within the optimization procedure, making its implementation difficult if classical optimization techniques are applied. However, using PSO algorithm, this problem is overcome since the objective function can be arbitrarily complex and of any form. It can also be easily adjusted in case that new components need to be included.

6.1. First Stage of Optimization Process

The first optimization level uses Particle Swarm Optimization (PSO) and applies it at microgrid scale to facilitate the optimization process. Specifically, it provides the optimal total electric power demand of the HVAC systems and optimally shifts building non-critical electrical loads with the purpose of minimizing building's total daily energy demand and cost. Moreover, the charging of the hosted PEVs, the operation of the local power generation units and the active power that is exchanged by the microgrid and the electric grid are optimally scheduled. The structure of each particle of the swarm with its different parts comprising the respective decision variables associated with the optimization of the aforementioned microgrid subsystems is given in Figure 11.

Some more information about the particle part concerning building generators optimization is provided next. Let us assume that N_g is the number of the diesel generators. Each dimension in this particle part contains a number, S, that takes values from 0 to $2^{N_g} - 1$ and corresponds to the state of operation of the diesel generators set. This number is transformed to binary number containing the state of operation of each diesel generator as described in (41).

$$\left[st_1(t) \dots st_{Ng}(t)\right] = \boldsymbol{dec2bin}(round(S(t)), \quad S \in [0 \quad 2^{Ng} - 1] \tag{41}$$

Where, $\boldsymbol{dec2bin}(round(N(t))$ represents the conversion function of a decimal number to binary.

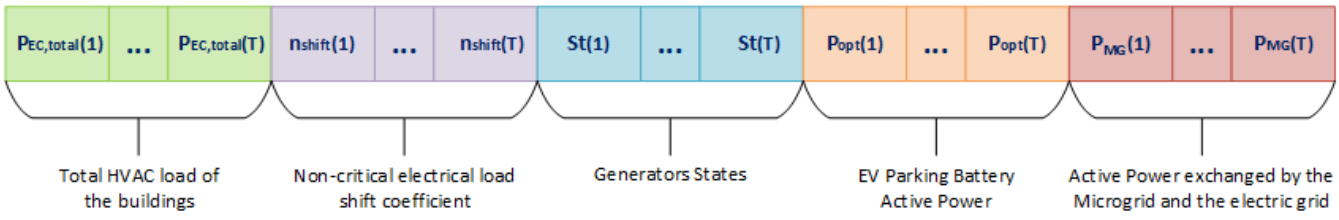

Fig. 11. Particle structure used by first optimization stage

The augmented cost function used by the PSO including the applied constraints, are given in (42). In the first stage of optimization, the algorithm aims to minimize the total operational cost of the microgrid while satisfying all of the associated technical and operation constraints integrated in term (Pen) of the objective function.

$$TC_{MG} = \min_{\substack{st_g, P_{opt}, P_{MG}, \\ P_{EC,total}, n_{shift}}} \left\{ \left(\sum_t P_{MG}(t) \cdot EP(t) + \sum_t \sum_{g \in \mathcal{G}} st_g(t) \cdot FC_g\left(P_g(t)\right) \right) \cdot \Delta t \right\} \quad (42)$$

Sub-optimization problems are solved in order to optimally dispatch: a) the total thermal power to each building of the microgrid b) the total thermal power of each building to its thermal zone, c) the total power consumed by all microgrid building electrical loads to each building and d) the active power consumed/produced by PEVs aggregator to each separate PEV. To this end, suitable flexibility indices are developed for each type of microgrid component.

The estimated indoor temperature of a thermal zone is used with its upper and lower limits to suitably define the flexibility of each building thermal zone to increase or decrease its thermal power demand as in the following equations.

$$FL_z^{\uparrow}(t) = \frac{T_{in,z}(t) - T_{min,z}}{T_{max,z} - T_{min,z}} \quad (43)$$

$$FL_z^{\downarrow}(t) = \frac{T_{max,z} - T_{in,z}(t)}{T_{max,z} - T_{min,z}} \quad (44)$$

The flexibility of a building to increase or decrease its power is the respective weighted average of the flexibilities of the building's thermal zones, as it is described in Equations (45)-(46).

$$FL_b^{\uparrow}(t) = \frac{\sum_z FL_z^{\uparrow}(t) \cdot V_z}{\sum_z V_z} \quad (45)$$

$$FL_b^{\downarrow}(t) = \frac{\sum_z FL_z^{\downarrow}(t) \cdot V_z}{\sum_z V_z} \quad (46)$$

An optimization problem is solved in order to optimally dispatch the total power consumed by the buildings' electrical loads of the microgrid to each individual building, while satisfying all the technical and operational constraints. The augmented objective function is given in (47).

$$\min_{n^*_{shift,b}} \left\{ \sum_t \left(\sum_{b \in B} \left(n^*_{shift,b}(t) - n_{shift}(t) \right)^2 \right) \right\} \quad (47)$$

A last optimization problem is solved to optimally share the active power of the microgrid's parking lot to the PEVs with target to maximize the sum of PEV flexibilities and satisfy all PEVs' constraints.

An innovative definition of the flexibility of a PEV to change its active power at time t, $flex_{PEV}(i,t)$, is proposed in the following equation.

$$flex_{PEV}(i,t) = t'(i,t) - t \quad (48)$$

where $t'(i,t)$ is the time point at which the SoC trajectory crosses SoC_{high} or SoC_{low} limits provided that the i^{th} PEV absorbs or injects active power $P_{min}(i)$ or $P_{max}(i)$, respectively. The measure of PEV flexibility to increase (reduce) its active power at a certain time point is the time required to reach $\text{SoC}_{high(low)}$ limit if it absorbs (injects) the maximum active power, respectively.

If $P(i,t) \geq 0$, then $t'(i,t)$ is calculated in (49).

$$t'(i,t) = min\begin{cases} \dfrac{SoC_{max}(i) - SoC(i,t)}{P_{max}(i) - P_{min}(i)} + \dfrac{P_{max}(i)\cdot t_{H_2}(i) - P_{min}(i)\cdot t}{P_{max}(i) - P_{min}(i)} \\ t + \dfrac{SoC(i,t) - SoC_{max}(i)}{P_{min}(i)} \end{cases} \quad (49)$$

If $P(i,t) < 0$, then $t'(i,t)$ is calculated in (50).

$$t'(i,t) = min\begin{cases} \dfrac{SoC(i,t) - SoC_{min}(i)}{P_{max}(i) - P_{min}(i)} + \dfrac{P_{max}(i)\cdot t - P_{min}(i)\cdot t_{L_2}(i)}{P_{max}(i) - P_{min}(i)} \\ t + \dfrac{SoC(i,t) - SoC_{min}(i)}{P_{max}(i)} \end{cases} \quad (50)$$

Let us assume that $P^*_{PEV}(i,t)$ is the optimal active power of the i^{th} PEV exchanges with the electric network at time t. Adopting generator convention, the resulting SoC (in kWh) of the i^{th} PEV at the end of the next time interval is calculated as it follows:

$$SoC_{PEV}(i,t+\Delta t) = \begin{cases} SoC_{PEV}(i,t) - P^*_{PEV}(i,t)\cdot n_{ch}\cdot \Delta t, & P^*_{PEV}(i,t) < 0 \\ SoC_{PEV}(i,t) - \dfrac{P^*_{PEV}(i,t)}{n_{disch}}\cdot \Delta t, & P^*_{PEV}(i,t) \geq 0 \end{cases} \quad (51)$$

The SoC estimated in (51). is used in Eqs. (48)-(50) to obtain the estimated flexibility of the i^{th} PEV, $flex_{PEV}(i,t+\Delta t)$, at time $t+\Delta t$.

The used augmented objective function is given in (52).

$$\max_{P^*_{PEV}(i,t)} \sum_i flex_{PEV}(i,t+\Delta t) \quad (52)$$

S.t.

- *Power Balance Constraints*

$$\sum_{b\in\mathcal{B}} \left(P_{EC,total,b}(t) + P_{el,b}(t)\right) = st_{MG}(t)\cdot P_{MG}(t) + P_{opt}(t) + P_{PV}(t) + P_{WT}(t) + \sum_{g\in\mathcal{G}} st_g(t)\cdot P_g(t)) \quad (53)$$

with

$$st_{MG}(t) = \begin{cases} 0, & \forall t \in [T_{auto,0}\ T_{auto,f}] \\ 1, & otherwise \end{cases} \quad (54)$$

$$P_{MG,min} \leq P_{MG}(t) \leq P_{MG,max} \quad (55)$$

- *Building Thermal Load Constraints*

$$T_{min,z} \leq T_{in,z}(t) \leq T_{max,z} \quad (56)$$

$$P_{EC,total,min} \leq P_{EC,total}(t) \leq P_{EC,total,max} \quad (57)$$

$$P_{EC,total,min,b} \leq P_{EC,total,b}(t) \leq P_{EC,total,max,b}, \quad \forall b \in B \tag{58}$$

$$\sum_{b} P_{EC,total,b}(t) = P_{EC,total}(t) \tag{59}$$

$$P_{EC,z} = \frac{Q_{EC,z}}{COP}, \;\; P_{EC,total} = \frac{Q_{EC,total}}{COP} \tag{60}$$

If any of the technical limits of the HVAC consumption of a building is violated, the total power of this building is set equal to the technical limit violated ($P'(t)$), and then subtracted from the total cooling power consumed by all microgrid's buildings ($P_{new}(t) = P_{EC,total}(t) - P'(t)$). The dispatch of the total thermal power consumption is reapplied and the total power P_{new} is dispatched to each thermal zone of the other buildings.

- *Building Electrical Load Constraints*

$$n_{shift,min} \leq n_{shift} \leq n_{shift,max} \tag{61}$$

$$\sum_{t=T_{shift,0}}^{T_{shift,f}} P_{non_{cr}}(t) \cdot \Delta t = \sum_{t=T_{shift,0}}^{T_{shift,f}} P^*_{non_{cr}}(t) \cdot \Delta t \tag{62}$$

$$\sum_{t=T_{shift,0}}^{T_{shift,f}} P_{el,non,b}(t) \cdot \Delta t = \sum_{t=T_{shift,0}}^{T_{shift,f}} P^*_{el,non,b}(t) \cdot \Delta t, \quad \forall b \in B \tag{63}$$

$$\sum_{b \in B} P^*_{el,non,b}(t) = P^*_{non_{cr}}(t) \tag{64}$$

with

$$P^*_{el,non,b}(t) = \begin{cases} n^*_{shift,b}(t) \cdot P_{el,non,b}(t), & \forall t \in [T_{shift,0} \; T_{shift,f}] \\ P_{el,non,b}(t), & otherwise \end{cases} \tag{65}$$

Where, $n^*_{shift,b}$ is the load shifting coefficient and $P^*_{el,non,b}$ is the optimal electric power consumption by the shiftable loads of bth building of the microgrid.

- *Plug-in Electric Vehicles Constraints*

$$SoC_{PB}(T_0) = SoC_{PB}(T_f) \tag{66}$$

$$SoC_{PB,min}(t) \leq SoC_{PB}(t) \leq SoC_{PB,max}(t) \quad \forall t \in [T_0 \; T_f] \tag{67}$$

$$P_{PB,min}(t) \leq P_{opt}(t) \leq P_{PB,max}(t) \quad \forall t \in [T_0 \; T_f] \tag{68}$$

$$P^*_{PEV}(i,t) \leq P_{max}(i), \quad \forall i \tag{69}$$

$$P^*_{PEV}(i,t) \geq P_{min}(i), \quad \forall i \tag{70}$$

$$SoC_{PEV}(i,t) - P^*_{PEV}(i,t) \cdot \Delta t < SoC_{high}(i, t + \Delta t), \quad \forall i \tag{71}$$

$$SoC_{PEV}(i,t) - P^*_{PEV}(i,t) \cdot \Delta t > SoC_{low}(i, t+\Delta t), \qquad \forall i \tag{72}$$

$$\sum_i P^*_{PEV}(i,t) = P_{opt}(t) \tag{73}$$

Constraints (71) and (72) ensure that $SoC(i,t)$ is maintained within permissible operation limits and allow each PEV reach the necessary level of charge at its disconnection time.

- *Diesel Generator Set Constraints*

$$st_g(t) \cdot P_{g,min} \le P_g(t) \le st_g(t) \cdot P_{g,max}, \ \ \forall t, g \tag{74}$$

$$t_{OFF,g} - t_{ON,g} \ \ge \ T_{ON\_min,g}\ , \ \ \forall g \tag{75}$$

$$t_{ON,g} - t_{OFF,g} \ \ge \ T_{OFF\_min,g}\ , \ \ \forall g \tag{76}$$

$$st_g(t) \cdot m_{em,g}(t) \le limEm_g\ , \ \ \forall g \tag{77}$$

Where, $limEm_g$ (in kg/h) denotes the emissions upper limit of the gth diesel generator. Minimum allowed duration of generator continuous operation or not ensured by (75) and (76), respectively.

6.2. Second Stage of Optimization Process

In the second optimization stage, the algorithm aims to minimize the total operational cost of the active distribution network by appropriately choosing the adjustment coefficient n_{DN_sh}. The optimal load shifting algorithm is permitted to transfer a certain percentage of the flexible load of one timeslot to a different one, provided that the energy that is consumed before and after the load shifting remains the same.

It is considered that the electrical power consumption of the flexible loads constitutes a percentage of the overall power that is consumed by the electrical loads of the distribution network ($P_{DN,load}$).

The objective function that is used in this optimization stage is formulated in (78). It aims to minimize the operational cost of the active distribution network by suitable load shifting. Network constraints are not considered in this stage.

$$TC_{DN} = \min_{n_{DN\_sh}} \left\{ \left(\sum_t P_{DN}(t) \cdot EP(t) \right) \cdot \Delta t \right\} \tag{78}$$

subject to

- *Flexible Electrical Load Constraints*

$$P^*_{DN,flex}(t) = \begin{cases} n_{DN\_sh}(t) \cdot P_{DN,flex}(t), & \forall t \ \in [T_{DN\_sh,0} \ T_{DN\_sh,f}] \\ P_{DN,flex}(t), & otherwise \end{cases} \tag{79}$$

$$n_{DN\_sh,min} \ \le n_{DN\_sh} \le n_{DN\_sh,max} \tag{80}$$

$$\sum_{t=T_{DN\_sh,0}}^{T_{DN\_sh,f}} P_{DN,flex}(t) \cdot \Delta\, t = \sum_{t=T_{DN\_sh,0}}^{T_{DN\_sh,f}} P^*_{DN,flex}(t) \cdot \Delta t \tag{81}$$

- *Power Balance Constraints*

$$P_{DN,load}(t) + st_{MG}(t) \cdot P_{MG}(t) = st_{DN}(t) \cdot P_{DN}(t) + P_{PV}(t) + P_{WT}(t) \ \ \forall\, t \in [T_0\ T_f] \tag{82}$$

with

$$P_{DN,flex}(t) = n_{flex} \cdot P_{DN,load}(t) \tag{83}$$

$$P_{DN,load}(t) = P_{DN,non\_flex}(t) + P^{*}_{DN,flex}(t) \tag{84}$$

$$P_{DN,min} \leq P_{DN}(t) \leq P_{DN,max} \tag{85}$$

6.3. Third Stage of Optimization Process

In this optimization stage, the deviations of the building's electric consumption $\Delta P_{buildings}$, diesel generator power ΔP_{diesel} and PEV parking lot power $\Delta P_{PEVs,aggr}$ from their optimal values are estimated. These optimal values are those that lead to the maximum deviations of the power that the microgrid exchanges with the active distribution network that contributes to all of the network constraint violation elimination processes and ensures satisfaction of all of the microgrid constraints. The objective function that is used in the third stage of optimization is provided in (86), followed by its respective constraints.

$$\underset{\substack{\Delta P_{buildings},\\ \Delta P_{diesel}\\ \Delta P_{PEVs,aggr}}}{max} \left\{ \sum_{t=\underline{T}_{reg,V\downarrow}}^{\overline{T}_{reg,V\downarrow}} |\Delta P_{MG}(t)| + \sum_{t=\underline{T}_{reg,V\uparrow}}^{\overline{T}_{reg,V\uparrow}} |\Delta P_{MG}(t)| \right\} \tag{86}$$

subject to (56)-(77) and

$$\Delta P_{buildings}(t) + \Delta P_{diesel}(t) + \Delta P_{PEVs,aggr} = \Delta P_{MG}(t) \tag{87}$$

$$\Delta P_{buildings,min} \leq \Delta P_{buildings}(t) \leq \Delta P_{buildings,max} \qquad t \notin \left[\underline{T}_{reg,V\downarrow}\ \overline{T}_{reg,V\downarrow}\right], \quad \left[\underline{T}_{reg,V\uparrow}\ \overline{T}_{reg,V\uparrow}\right] \tag{88}$$

$$\Delta P_{buildings,min} \leq \Delta P_{buildings}(t) \leq 0 \qquad t \in \left[\underline{T}_{reg,V\downarrow}\ \overline{T}_{reg,V\downarrow}\right] \tag{89}$$

$$0 \leq \Delta P_{buildings}(t) \leq \Delta P_{buildings,max} \quad t \in \left[\underline{T}_{reg,V\uparrow}\ \overline{T}_{reg,V\uparrow}\right] \tag{90}$$

$$\Delta P_{diesel,min} \leq \Delta P_{diesel}(t) \leq \Delta P_{diesel,max} \qquad t \notin \left[\underline{T}_{reg,V\downarrow}\ \overline{T}_{reg,V\downarrow}\right], \quad \left[\underline{T}_{reg,V\uparrow}\ \overline{T}_{reg,V\uparrow}\right] \tag{91}$$

$$0 \leq \Delta P_{diesel}(t) \leq \Delta P_{diesel,max} \qquad t \in \left[\underline{T}_{reg,V\downarrow}\ \overline{T}_{reg,V\downarrow}\right] \tag{92}$$

$$\Delta P_{diesel,min} \leq \Delta P_{diesel}(t) \leq 0 \quad t \in \left[\underline{T}_{reg,V\uparrow}\ \overline{T}_{reg,V\uparrow}\right] \tag{93}$$

$$\Delta P_{PEVs,aggr,min} \leq \Delta P_{PEVs,aggr}(t) \leq \Delta P_{PEVs,aggr,max} \qquad t \notin \left[\underline{T}_{reg,V\downarrow}\ \overline{T}_{reg,V\downarrow}\right], \quad \left[\underline{T}_{reg,V\uparrow}\ \overline{T}_{reg,V\uparrow}\right] \tag{94}$$

$$\Delta P_{PEVs,aggr,min} \leq \Delta P_{PEVs,aggr}(t) \leq 0 \qquad t \in \left[\underline{T}_{reg,V\downarrow}\ \overline{T}_{reg,V\downarrow}\right] \tag{95}$$

$$0 \leq \Delta P_{PEVs,aggr}(t) \leq \Delta P_{PEVs,aggr,max} \quad t \in \left[\underline{T}_{reg,V\uparrow}\ \overline{T}_{reg,V\uparrow}\right] \tag{96}$$

6.4. Fourth Stage of Optimization Process

The objective function of this optimization stage is formulated in (97).

$$TC_{DN} = \underset{\substack{n_{DN_{sh}},\\ P_{MG}}}{min} \left\{ \left(\sum_{t} P_{DN}(t) \cdot EP(t) \right) \cdot \Delta t \right\} \tag{97}$$

subject to (79)-(85) and

- *Active Distribution Network Constraints*

$$\boldsymbol{V} \cdot \overline{\boldsymbol{Y}} \cdot \overline{\boldsymbol{V}} = \boldsymbol{S}_{inj} = \boldsymbol{P}_{inj} + j \cdot \boldsymbol{Q}_{inj} \quad (98)$$

$$|\boldsymbol{V}(k,t)| \leq \boldsymbol{V}_{max}(k) \quad (99)$$

$$|\boldsymbol{V}(k,t)| \geq \boldsymbol{V}_{min}(k) \quad (100)$$

$$\boldsymbol{\theta}(k,t) \geq \boldsymbol{\theta}_{min}(k) \quad (101)$$

$$\boldsymbol{\theta}(k,t) \leq \boldsymbol{\theta}_{max}(k) \quad (102)$$

$$|\boldsymbol{Y}(k,l) \cdot (\boldsymbol{V}(k,t) - \boldsymbol{V}(l,t))| \leq \boldsymbol{I}_{max}(k,l) \quad (103)$$

where $\boldsymbol{V}$ and $\boldsymbol{\theta}$ are vectors representing the amplitudes and the angles of the distribution network voltages and $\boldsymbol{Y}$ is the network admittance matrix. The variable $|\boldsymbol{V}(k)|$ is the voltage amplitude at the k^{th} node, $\boldsymbol{\theta}(k)$ is voltage angle at the k^{th} node and $\boldsymbol{I}_{max}(k,l)$ is the maximum current flowing in the electric line connecting the k^{th} and l^{th} node. The $\boldsymbol{S}_{inj}$ vector comprises the apparent power injections at the nodes of the network while $\boldsymbol{P}_{inj}$ and $\boldsymbol{Q}_{inj}$ comprise the active and reactive power injections at all of the network nodes, respectively.

MatPower was used to solve the optimal power flow (OPF) problem with the constraints that are defined in (98)-(103) [69]. MatPower uses the solvers of non-linear constrained optimization problems that are provided in the Matlab Optimization Toolbox in order to solve the AC OPF problem and it can deal with the most constraints that are associated with the electrical network's operation.

6.5. Fifth Stage of Optimization Process

The decision variables in this stage are the first four that are described in the first optimization level. The objective function that is used in this optimization stage is provided in (104).

$$TC_{MG} = \min_{\substack{st_g, P_{opt}, \\ P_{EC,total}, n_{shift}}} \left\{ \left(\sum_t \sum_{g \in \mathcal{G}} st_g(t) \cdot FC_g\left(P_g(t)\right) \right) \cdot \Delta t \right\} \quad (104)$$

subject to (53)-(77).

The power that is exchanged by the microgrid and the active distribution network is required to be equal to that which was obtained in the fourth optimization level.

Chapter 7

Agents Modeling of Active Distribution Network Comprising Residential Buildings and PEVs

7.1. Local Agents

BTL/A calculates the internal temperature of each residential building it supervises over the optimization horizon according to the thermal model described in Chapter 7. The estimated indoor temperature of the building is used with its upper and lower limits to suitably define the flexibility of each building to increase or decrease its thermal power demand as in the following equations.

$$FL_b^{\uparrow}(t) = \frac{T_{in,b}(t) - T_{min,b}}{T_{max,b} - T_{min,b}} \tag{105}$$

$$FL_b^{\downarrow}(t) = \frac{T_{max,b} - T_{in,b}(t)}{T_{max,b} - T_{min,b}} \tag{106}$$

BEL/A is assigned to each building of the network and model electrical loads of the building. The modelling of the energy consumption profiles in residential buildings was developed taking into consideration the number, age and the activity level of occupants, as well as the number, type and the usage of electric household appliances [70],[71].

PEV/A calculates the bounds of each PEV's stored energy and active and reactive power it exchanges with the distribution network. According to these characteristics, the area the PEV is allowed to operate is derived, as described in detail in Chapter 5. Moreover, PEV/A estimates the flexibility of each individual PEV to change its power. These quantities are forwarded to the CPEV/A that supervises the cluster of PEVs.

7.2. Cluster Agents

7.2.1. Cluster of Building Thermal Loads Agent (CBTL/A), Cluster of Building Electrical Loads Agent (CBEL/A)

The primary goal of CBTL/As is to aggregate the responses they receive from the BTL/As being in their control areas. The flexibility of a cluster of buildings to increase or decrease its power is the respective weighted average of the flexibilities of the buildings it supervises, as it is described in following Equations.

$$FL_{CB}^{\uparrow}(t) = \frac{\sum_b FL_b^{\uparrow}(t) \cdot V_b}{\sum_b V_b} \tag{107}$$

$$FL_{CB}^{\downarrow}(t) = \frac{\sum_b FL_b^{\downarrow}(t) \cdot V_b}{\sum_b V_b} \tag{108}$$

Moreover, CBTL/As define suitable flexibilities ($FL_{CB,fz}$) exploiting fuzzy logic based on information regarding the respective node voltage and their primary flexibility to change their power, as shown in Figure 12. Initially, inputs and outputs are mapped into fuzzy sets using the respective membership functions. Both inputs are fuzzified using five sets with linguistic variables for the node voltage deviation from its upper or lower bound and the flexibility of the cluster of buildings to change its power. These variables are defined as very small (VS), small (S), medium (M), large (L) and very large (VL). The output of the fuzzy logic is determined by defining the rules indicated in Table I.

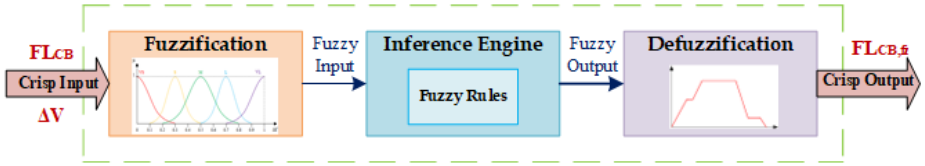

Fig. 12. Fuzzy inference system

TABLE I
FUZZY RULES FOR THE CALCULATION OF BUILDING CLUSTERS' FLEXIBILITY ($FL_{CB,fz}$)

Cluster of buildings flexibility (FL_{CB})	*ΔV*				
	VS	**S**	**M**	**L**	**VL**
VS	VS	VS	VS	VS	VS
S	VS	S	S	M	L
M	VS	S	M	L	L
L	VS	M	L	L	VL
VL	VS	L	L	VL	VL

CBEL/As aggregate the responses they receive from the BEL/As they control in order to model the electrical load profiles of clusters of residential buildings.

7.2.2. Cluster of Plug-in Electric Vehicles Agent (CPEV/A)

An innovative definition of the flexibility of a cluster PEVs to change its active power at time t, $flex_{CPEV}(c,t)$, is proposed in Chapter 6 and also followed in this case study as defined in Equation (109).

$$flex_{CPEV}(i,t) = t'(c,t) - t \tag{109}$$

Where, $t'(c,t)$ is the time point at which the SoC trajectory crosses SoC_{high} or SoC_{low} limits provided that the c^{th} cluster of PEVs (CPEV/A) absorbs or injects active power $P_{min}(CB)$ or $P_{max}(CB)$, respectively, as shown in Fig. 10.

Moreover, CPEV/As define suitable flexibilities ($FL_{CPEV,fz}$) exploiting fuzzy logic in a similar way with the flexibilities ($FL_{CB,fz}$) defined by CBTL/As. Both inputs and the output are fuzzified using five sets with linguistic variables. The inputs of the fuzzy logic system are the flexibility of a cluster of PEVs to change its active power at time t, $flex_{CPEV}(c,t)$ and the node voltage deviation from its upper or lower bound. The output of the fuzzy logic is determined by defining the rules indicated in Table I. The obtained flexibility $FL_{CPEV,fz}$ is used by ADNM/A to optimally dispatch the total active power of the aggregate battery of PEVs to each CPEV/A.

7.2.3. Active Distribution Network Management Agent (ADNM/A)

ADNM/A gathers the aggregated responses from the cluster agents and also information for the forecasted price of electricity, the node loads of the network and the power produced by RESs.

Equations (110)-(117) are used to estimate the time-varying maximum and minimum bounds of the buildings' electric power consumption.

$$P_{HVAC,total,max}(t) = \sum_{CB} P_{HVAC,CB,max}(t) \tag{110}$$

$$P_{HVAC,total,min}(t) = \sum_{CB} P_{HVAC,CB,min}(t) \tag{111}$$

$$P_{EL,total,max}(t) = \sum_{CB} P_{EL,CB,max}(t) \tag{112}$$

$$P_{EL,total,min}(t) = \sum_{CB} P_{EL,CB,min}(t) \tag{113}$$

with

$$P_{HVAC,CB,max}(t) = \sum_{b} P_{HVAC,b,max}(t) \quad (114)$$

$$P_{HVAC,CB,min}(t) = \sum_{b} P_{HVAC,b,min}(t) \quad (115)$$

$$P_{EL,CB,max}(t) = \sum_{b} P_{EL,b,max}(t) \quad (116)$$

$$P_{EL,CB,min}(t) = \sum_{b} P_{EL,b,min}(t) \quad (117)$$

Equations (118)-(125) are used to estimate the time-varying maximum and minimum bounds of the power and stored energy of the aggregate battery.

$$P_{PB,max}(t) = \sum_{CEV} P_{CEV,max}(t) \quad (118)$$

$$P_{PB,min}(t) = \sum_{CEV} P_{CEV,min}(t) \quad (119)$$

$$SoC_{PB,high}(t) = \sum_{CEV} SoC_{CEV,high}(t) - SoC_{PB,diff}(t) \quad (120)$$

$$SoC_{PB,low}(t) = \sum_{CEV} SoC_{CEV,low}(t) - SoC_{PB,diff}(t) \quad (121)$$

with

$$P_{CEV,max}(t) = \sum_{i} P_{max}(i,t) \quad (122)$$

$$P_{CEV,min}(t) = \sum_{i} P_{min}(i,t) \quad (123)$$

$$SoC_{CEV,high}(t) = \sum_{i} SoC_{high}(i,t) - SoC_{CEV,diff}(t) \quad (124)$$

$$SoC_{CEV,low}(t) = \sum_{i} SoC_{low}(i,t) - SoC_{CEV,diff}(t) \quad (125)$$

PEVs' plugging and unplugging over time affects the total stored energy of the dynamic equivalent aggregate battery. The resulting change of the aggregate SoC is indicated by $SoC_{PB,diff}$ and estimated in Equations (34)-(36) described in Chapter 5. Equation (37) in Chapter 5 indicates the total stored energy of the equivalent PEVs' battery at the next time interval, assuming that $P_{PB,total}(t)$ is the optimal total active power of the aggregate battery and adopting a generator convention.

Then, ADN exploits an optimization technique for the optimal operation scheduling of the ADN. Specifically, ADN uses Particle Swarm Optimization (PSO). ADN provides the optimal total electric power consumption of the HVAC systems of all hosted residential buildings and the optimal active power PEVs' aggregate battery. The structure of each particle of the swarm with its different parts comprising the respective decision variables of the optimization of the ADN is given in Fig. 13. Constrained OPF is exploited in order to maintain the voltages of the active distribution network and the currents of the power

lines within the permissible limits. Then the active and reactive power set-points resulted from the OPF exploitation are forwarded back to the respective cluster agents so as to be optimally dispatched to the local agents they supervise.

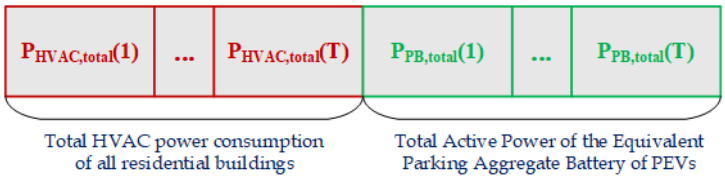

Fig. 13. Particle structure used by the ADNM/A.

The augmented cost function used by the PSO incorporating the imposed constraints, is provided in Equation (126). The objective of the optimization procedure is to minimize the ADN's overall daily operation cost in accordance with the cost of electricity, while also fully satisfying all ADN components' constraints incorporated into the term (Penalty) of the objective function.

$$TC_{ADN} = \min_{P_{PB,total}, P_{HVAC,total}} \left\{ \left(\sum_t P_{grid}(t) \cdot EP(t) \right) \cdot \Delta t + Penalty \right\} \quad (126)$$

Then ADNM/A optimally dispatches the total HVAC electric consumption of residential buildings ($P_{HVAC,total}$) to the CBTL/As it supervises according to Equation (126) and the obtained active and reactive power set-points are forwarded back to these clusters. Afterward, CBTLAs dispatch their power to the local agents BTL/As they supervise and control as formulated in (128).

$$P_{HVAC,CB}(t) = \frac{FL_{CB}(t) \cdot \sum_b V_b}{\sum_{CB}\{FL_{CB}(t) \cdot V_{CB}\}} \cdot P_{HVAC,total}(t) \quad (127)$$

$$P_{HVAC,b}(t) = \frac{FL_b(t) \cdot V_b}{\sum_b\{FL_b(t) \cdot V_b\}} \cdot P_{HVAC,CB}(t) \quad (128)$$

Where V_{CB} is the sum of the volumes of the buildings belonging to the respective cluster of buildings.

The process of the HVAC system's optimal power dispatch to the CBTL/As and then to the local agents BTL/As and more specifically to each hosted residential building is depicted in Fig. 14.

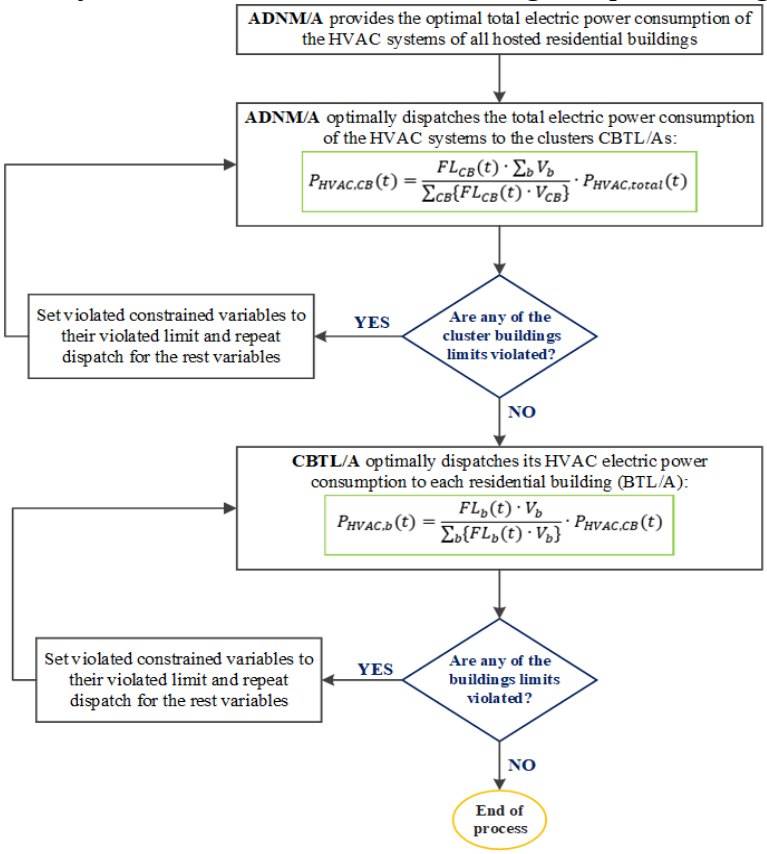

Fig. 14. Flowchart of the optimal power dispatch of the buildings' HVAC system.

A last optimization problem is solved to optimally dispatch the total power of the dynamic equivalent aggregate battery to CPEV/As and then to each PEV as formulated and described in detail in [72].

The exploitation of the optimization process for the optimal operation scheduling of examined ADN is subject to the following constraints.

- *Building Constraints*

$$P_{HVAC,total,min}(t) \le P_{HVAC,total}(t) \le P_{HVAC,total,max} \quad (129)$$

$$P_{EL,total,min}(t) \le P_{EL,total}(t) \le P_{EL,total,max} \quad (130)$$

$$P_{HVAC,CB,min}(t) \le P_{HVAC,CB}(t) \le P_{HVAC,CB,max} \quad (131)$$

$$P_{EL,CB,min}(t) \le P_{EL,CB}(t) \le P_{EL,CB,max} \quad (132)$$

$$P_{HVAC,b,min}(t) \le P_{HVAC,b}(t) \le P_{HVAC,b,max} \quad (133)$$

$$P_{EL,b,min}(t) \le P_{EL,b}(t) \le P_{EL,b,max} \quad (134)$$

$$\sum_{b} P_{HVAC,b}(t) = P_{HVAC,CB}(t) \quad (135)$$

$$\sum_{CB} P_{HVAC,CB}(t) = P_{HVAC,total}(t) \quad (136)$$

$$P_{HVAC,B} = \frac{Q_{HVAC,b}}{COP}, \;\; P_{HVAC,CB} = \frac{Q_{HVAC,CB}}{COP}, P_{HVAC,total} = \frac{Q_{HVAC,total}}{COP} \quad (137)$$

$$T_{min,b} \le T_{in,b}(t) \le T_{max,b} \quad (138)$$

- *Plug-In Electric Vehicles Constraints*

$$SoC_{PB}(T_0) = SoC_{PB}(T_f) \quad (139)$$

$$SoC_{PB,low}(t) \le SoC_{PB}(t) \le SoC_{PB,high}(t) \quad \forall\, t \in [T_0\ T_f] \quad (140)$$

$$P_{PB,min}(t) \le P_{PB,total}(t) \le P_{PB,max}(t) \quad \forall\, t \in [T_0\ T_f] \quad (141)$$

$$SoC_{CEV,low}(t) \le SoC_{CEV}(t) \le SoC_{CEV,high}(t) \quad \forall\, t \in [T_0\ T_f] \quad (142)$$

$$P_{CEV,min}(t) \le P_{CEV}(t) \le P_{CEV,max}(t) \quad \forall\, t \in [T_0\ T_f] \quad (143)$$

$$SoC_{low}(i,t) \le SoC(i,t) \le SoC_{high}(i,t) \quad \forall\, t \in [T_0\ T_f] \quad (144)$$

$$P_{min}(i,t) \le P(i,t) \le P_{max}(i,t) \quad \forall\, t \in [T_0\ T_f] \quad (145)$$

- *Power Balance Constraints*

$$P_{HVAC,total}(t) + P_{EL,total}(t) + P_{DNload}(t) = P_{PB,total}(t) + P_{PV}(t) + P_{WT}(t) + P_{grid}(t) \quad \forall\, t \in [T_0\ T_f] \quad (146)$$

$$P_{grid,min}(t) \leq P_{grid}(t) \leq P_{grid,max}(t) \quad \forall\, t \in \left[T_0\ T_f\right] \tag{147}$$

- *Active Distribution Network Constraints*

  The constraints described in Equations (98)-(103) in Chapter 6.

Chapter 8

Microgrid Frequency Support Modelling

A detailed model for the simulation of microgrid frequency deviation due to occurred load changes is shown in Fig. 15. The examined system comprises primary (proportional term $1/R$) and secondary (integral term K_I/s) frequency control. G_D, G_T and G_M are transfer functions representing the mechanical speed–governing system, the diesel turbine and the inertial response of the microgrid, respectively. Moreover, it is assumed that the building prosumers and the plug-in electric vehicles hosted by the microgrid are able to support microgrid frequency by adjusting their power demand with respect to the measured frequency deviation Δf.

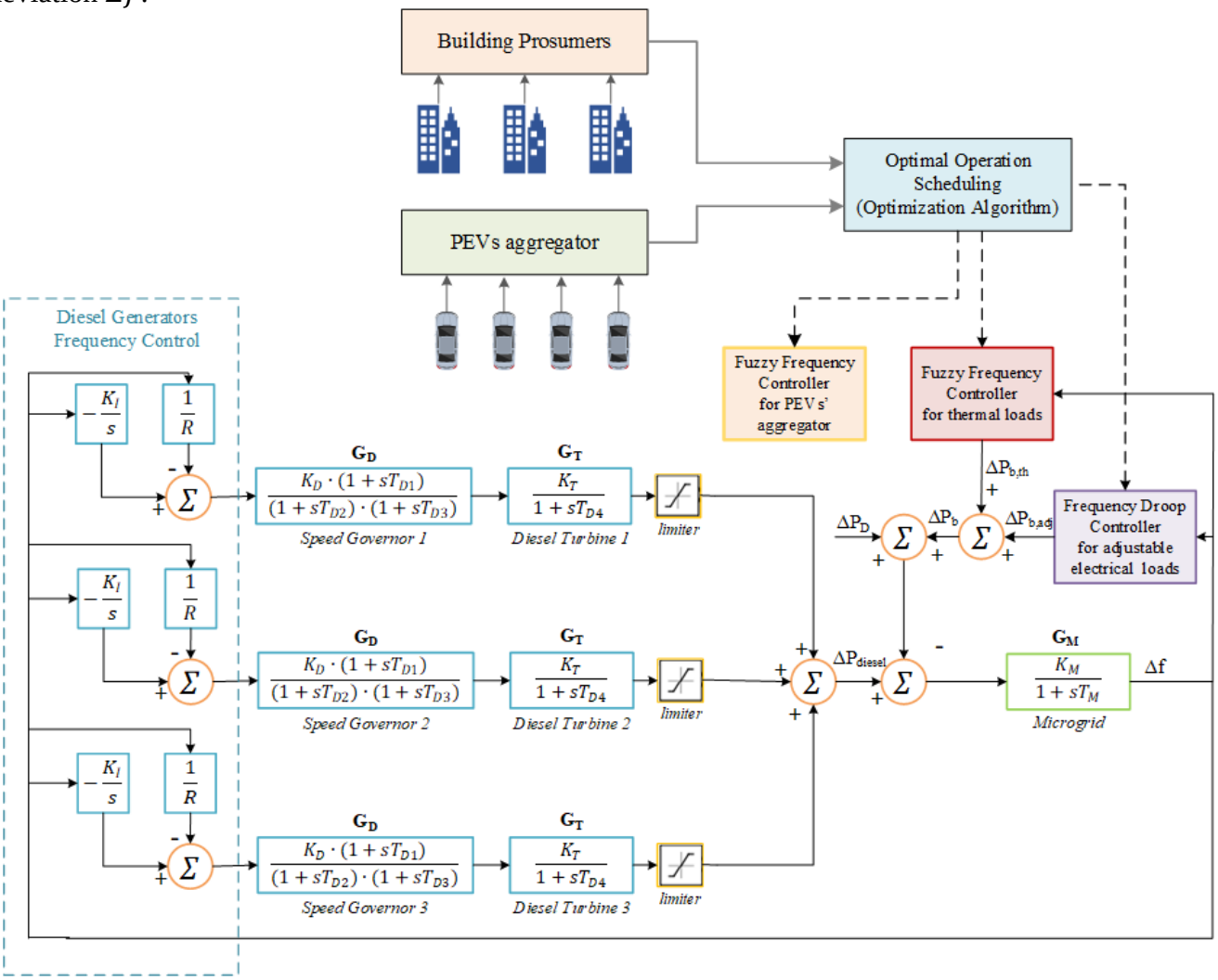

Fig. 15. Microgrid automatic generation control integrated with frequency support provided by the real-time building prosumers and PEVs power demand control.

8.1. Frequency Support by Buildings' Thermal Loads

The system frequency provides information about a power system's power balance and can be used as a regulating parameter to achieve overall system power balance. In case the balance is not maintained, the grid will suffer from power outages. Power outage in a power system leads system frequency to deviate from its nominal value. This frequency deviation has to be regulated under a permissible band. For instance, when the system is heavily loaded (high demand or low supply), the frequency drops, and the fuzzy

controller aims to decrease buildings' power consumption. Correspondingly, when the frequency increases, the goal of the fuzzy controller is to increase the power consumption.

In this work, a fuzzy-logic-based controller is proposed to estimate the appropriate power deviation of each building thermal load, ΔP_b, from its optimal set-point at the beginning of frequency deviation,t_d, in order to support system frequency. Fuzzy logic is a flexible and easy-to-implement method and has the aptitude to deal with uncertainty and non-linearity. Robust control can be attained using fuzzy logic controller rather than the conventional droop control method.

The first step of the design of a fuzzy logic system is the fuzzification stage, where inputs and outputs are mapped into fuzzy sets using the membership functions shown in Fig. 16. The output of the fuzzy logic controller depends on two inputs. Both inputs and the output are fuzzified using five linguistic variables for the frequency deviation from the nominal value (50 Hz) Δf, the flexibility of the building to increase ($FL_b^{\uparrow}$) or decrease ($FL_b^{\downarrow}$) its power demand and the power change coefficient p. These variables are defined as very small (VS), small (S), medium (M), large (L) and very large (VL) and they are normalized in the range of [0,1]. The normalization of the input Δf is given in the following equation.

$$\Delta f_{normalized} = \begin{cases} 1 - \dfrac{\Delta f_{min} - \Delta f}{\Delta f_{min}}, & \Delta f \leq -0.1 \\ 1 - \dfrac{\Delta f_{max} - \Delta f}{\Delta f_{max}}, & \Delta f > 0.1 \end{cases} \tag{148}$$

The estimated internal temperature of the zth thermal zone of each building of the microgrid is used together with its upper and lower limits to obtain the flexibility of each thermal zone to increase ($FL_z^{\uparrow}$) or decrease ($FL_z^{\downarrow}$) its power demand as in the following equations:

$$FL_z^{\uparrow}(t) = \frac{T_{in,z}(t) - T_{min,z}}{T_{max,z} - T_{min,z}} \tag{149}$$

$$FL_z^{\downarrow}(t) = \frac{T_{max,z} - T_{in,z}(t)}{T_{max,z} - T_{min,z}} \tag{150}$$

The flexibility of the building to increase ($FL_b^{\uparrow}$) or decrease ($FL_b^{\downarrow}$) its power demand is the respective weighted average of the flexibilities of the thermal zones. They are defined as it follows:

$$FL_b^{\uparrow}(t) = \frac{\sum_z FL_z^{\uparrow}(t) \cdot V_z}{\sum_z V_z} \tag{151}$$

$$FL_b^{\downarrow}(t) = \frac{\sum_z FL_z^{\downarrow}(t) \cdot V_z}{\sum_z V_z} \tag{152}$$

A typical dead-band of 0.2 Hz is defined symmetrically around the nominal frequency. Within this range, the buildings follow the optimal set-point value of cooling power, so the they are unaffected by small frequency fluctuations. The appropriate power deviation for each building, ΔP_b, depending on the frequency deviation, is calculated in Equation (153).

$$\Delta P_b(t) = \begin{cases} \Delta P_{b,min}(t) \cdot p, & \Delta f \leq -0.1 \\ \Delta P_{b,max}(t) \cdot p, & \Delta f > 0.1 \end{cases} \tag{153}$$

$\Delta P_{b,max}$ and $\Delta P_{b,min}$ correspond to the maximum and minimum power deviation from the optimal set-point after the frequency support operation mode starts.

$$\Delta P_{b,max} = P_{EC,total,max}(t) - P_{EC,total,b}(t_d) - \Delta P_b(t) \tag{154}$$

$$\Delta P_{b,min} = P_{EC,total,b}(t_d) + \Delta P_b(t) - P_{EC,total,min}(t) \quad (155)$$

The output of the fuzzy logic system is determined by defining the rules indicated in Table II. Defuzzification is the final stage of the fuzzy logic system that leads to the estimation of a single crisp value for the output variable, p. The defuzzification technique used in this work is the centroid calculation, which returns the center of the area under the aggregate fuzzy set.

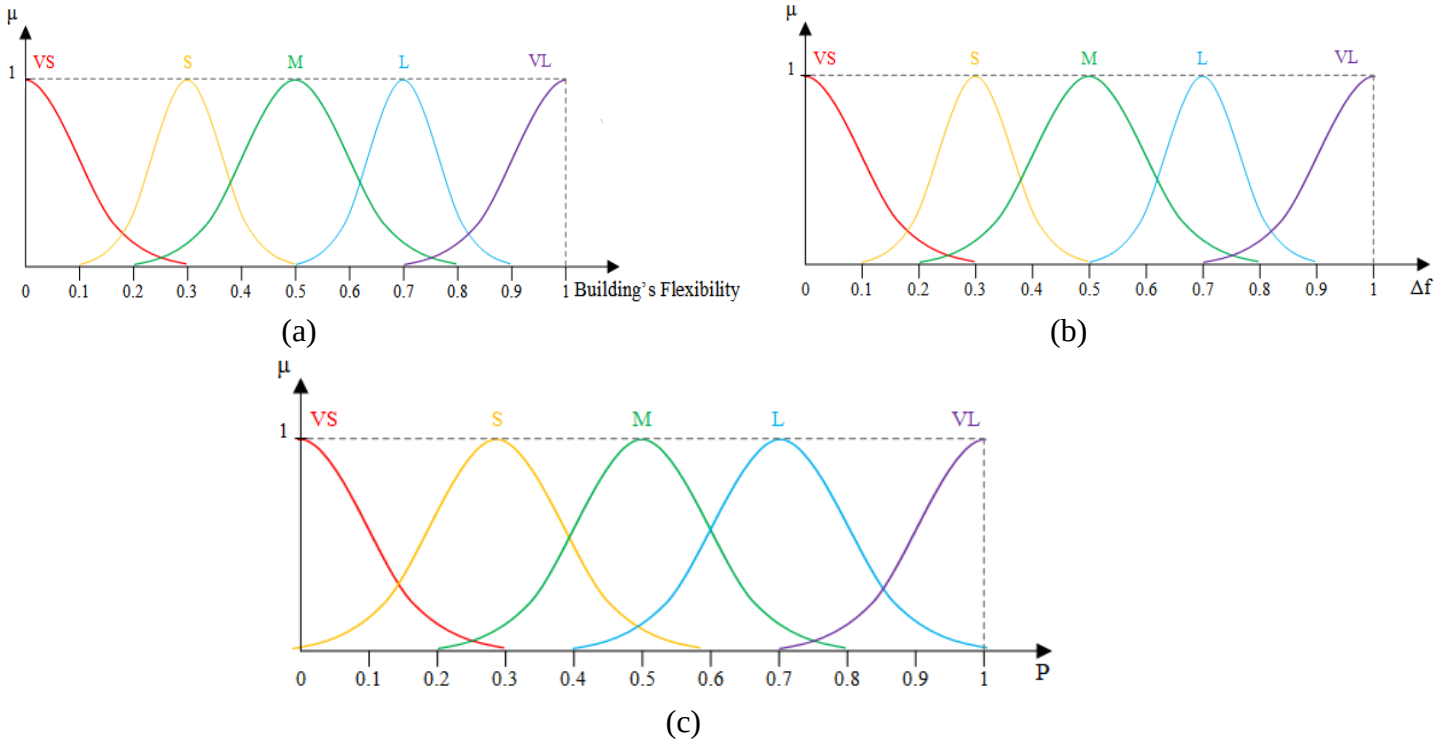

Fig. 16. Membership functions of the fuzzy variables: (a) the building's flexibility (b) frequency deviation from the nominal value (50 Hz), Δf (c) power change coefficient, p

TABLE II
FUZZY RULES FOR POWER CHANGE FACTOR *p*

Building's Flexibility	Δf				
	VS	S	M	L	VL
VS	VS	VS	VS	VS	VS
S	VS	S	S	M	L
M	VS	S	M	L	L
L	VS	M	L	L	VL
VL	VS	L	L	VL	VL

8.2. Frequency Support by Buildings' Adjustable Electrical Loads

Adjustable loads are electrical loads that can be partially curtailed or increased following suitable control signals. These loads can be involved in the demand response program on condition that the user's comfort conditions are maintained within the permissible levels. Adjustable loads can operate at lower power levels than their nominal power. Hence, they can reduce/increase their power consumption during peak/low load or high/low electricity price periods.

In case of significant frequency deviation, adjustable loads will be able to increase or decrease their active power to support system frequency. A frequency droop control strategy is adopted in this study due to its simplicity, as shown in Fig. 17. The frequency – power change characteristic is given in (156).

$$\Delta P_{b,adj} = \begin{cases} \Delta P_{b,adj,min} & , \quad \Delta f < \Delta f_{min} \\ \Delta P_{b,adj,min} - \dfrac{\Delta f - \Delta f_{min}}{-f_0 - \Delta f_{min}} \cdot \Delta P_{b,adj,min}, & \Delta f_{min} \le \Delta f < -f_0 \\ 0 & , \quad -f_0 \le \Delta f \le f_0 \\ \dfrac{\Delta f - f_0}{\Delta f_{max} - f_0} \cdot \Delta P_{b,adj,max} & , \quad f_0 < \Delta f \le \Delta f_{max} \\ \Delta P_{b,adj,max} & , \quad \Delta f > \Delta f_{max} \end{cases} \tag{156}$$

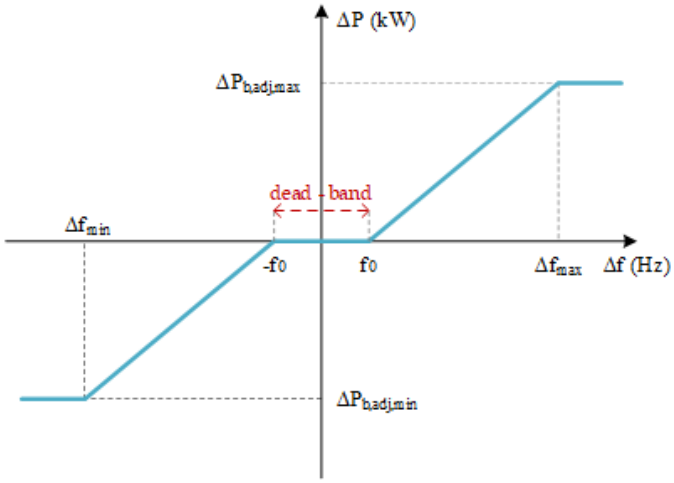

Fig. 17. Droop frequency control characterictic of adjustable electrical loads

8.3. Frequency Support by Plug-In Electric Vehicles

Initially, a fuzzy-logic-based controller is proposed to estimate the appropriate power deviation from its optimal set-point in order to support system frequency. The SoC of the equivalent aggregate battery will deviate from its optimal precalculated trajectory during frequency support implementation. For this purpose, another fuzzy-logic-based method was developed to estimate the power change coefficient in order to reach the precalculated SoC by appropriately increasing or decreasing the PEV power until the aggregated SoC coincides with the optimal precalculated one, when frequency support is no longer required.

The set-point of the power of the aggregate equivalent battery of the PEVs, P'_{opt}, that ensures frequency support and SoC restoration is estimated in the following equation.

$$P'_{opt}(t) = P_{opt}(t) + \Delta P_{PEV}(t) \tag{157}$$

Fuzzy-logic-based controller for frequency support by PEVs

A fuzzy-logic-based controller is proposed to estimate the appropriate power deviation, ΔP_{PEV}, from its optimal set-point in order to support system frequency. The first step of the design of a fuzzy logic system is the fuzzification stage, where inputs and outputs are mapped into fuzzy sets using the membership functions shown in Fig. 16. The output of the fuzzy logic controller depends on two inputs.

Both inputs and the output are fuzzified using five linguistic variables for the frequency deviation from the nominal value (50 Hz) Δf, the distance of the current SoC, $SoC_{distance}$, from its limits and the power change coefficient p. These variables are defined as very small (VS), small (S), medium (M), large (L) and very large (VL) and they are normalized in the range of [0,1]. In case of a negative frequency deviation, $SoC_{distance}$ represents the distance between current SoC and $SoC_{PB,min}$, as shown in Fig. 18. As SoC approaches its minimum value, $SoC_{distance}$ reduces and gets closer to zero. Less or even no power will be injected to the electric grid. The capability of the PEV aggregate battery to support frequency is reduced. Respectively, in case of a positive frequency deviation, SoC_{PB} increases and approaches the upper limit $SoC_{PB,max}$, while it deviates from the lower limit $SoC_{PB,min}$. $SoC_{distance}$ represents the distance between current SoC and $SoC_{PB,max}$, as shown in Fig. 19. As a result, an optimal tradeoff between the frequency deviation and the stored energy should be ensured by the fuzzy controller.

The normalization of the inputs, $SoC_{distance}$ and Δf, is given in the following equations.

$$SoC_{distance} = \begin{cases} \dfrac{SoC_{PB} - SoC_{PB,min}}{SoC_{PB,max} - SoC_{PB,min}}, & \Delta f \leq -0.1 \\ 1 - \dfrac{SoC_{PB} - SoC_{PB,min}}{SoC_{PB,max} - SoC_{PB,min}}, & \Delta f > 0.1 \end{cases} \quad (158)$$

$$\Delta f_{normalized} = \begin{cases} \dfrac{\Delta f}{\Delta f_{min}}, & \Delta f \leq -0.1 \\ \dfrac{\Delta f}{\Delta f_{max}}, & \Delta f > 0.1 \end{cases} \quad (159)$$

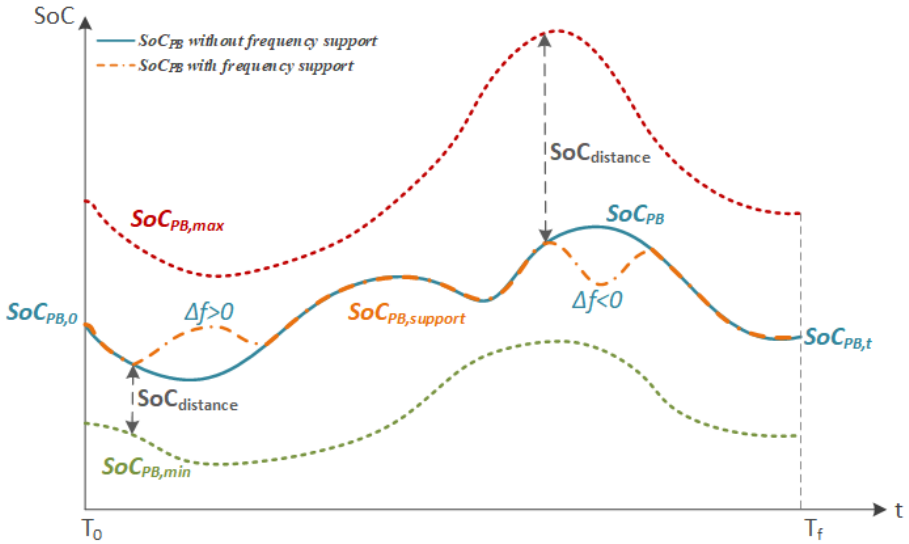

Fig. 18. Total energy stored in EVP aggregate battery with/without frequency support implementation.

A typical dead-band of 0.2 Hz is defined symmetrically around the nominal frequency in order to reduce excessive stress on PEVs' batteries. Within this range, the charging rate is equal to its optimal set-point value and the PEVs are unaffected to small power system frequency fluctuations. The appropriate power deviation, ΔP_{PEV}, depending on the frequency deviation, is calculated in equation (160).

$$\Delta P_{PEV}(t) = \begin{cases} \left(P_{PB,max}(t) - P'_{opt}(t)\right) \cdot p, & \Delta f \leq -0.1 \\ \left(P_{PB,min}(t) - P'_{opt}(t)\right) \cdot p, & \Delta f > 0.1 \end{cases} \quad (160)$$

When the system is heavily loaded (high demand or low supply), the frequency drops, and the fuzzy controller aims to decrease PEVs' power consumption or increase the power injection to the grid. Correspondingly, when the frequency increases, PEVs absorb more power from the power grid or inject less active power to it.

The output of the fuzzy logic system is determined by defining the rules of Table III. Defuzzification is the final stage of the fuzzy logic system. A graphical representation of the output of the fuzzy inference system, p parameter, is shown in Fig. 19.

TABLE III
FUZZY RULES FOR POWER CHANGE FACTOR p (red) and d (blue)

$SoC_{dist}/\Delta P$	$\Delta f/\Delta SoC$				
	VS	**S**	**M**	**L**	**VL**
VS	VS	VS	VS	VS	VS
S	VS	S	S	M	L
M	VS	S	M	L	L
L	VS	M	L	L	VL
VL	VS	L	L	VL	VL

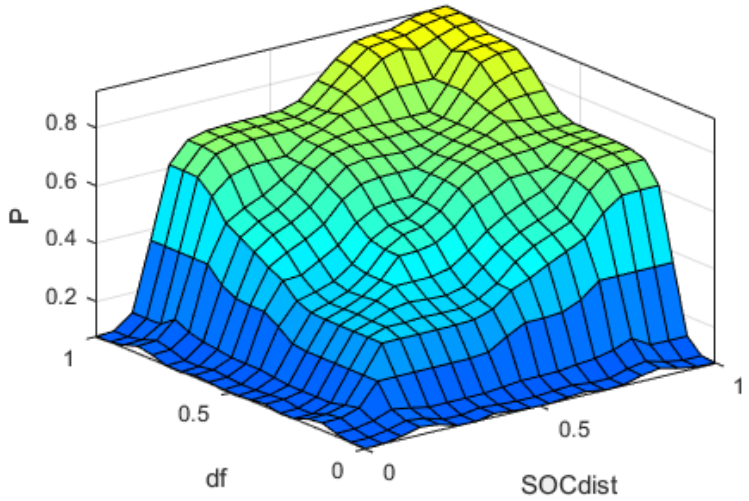

Fig. 19. A 3D graph of fuzzy system output p

Fuzzy-logic-based controller for PEVs' SoC restoration after frequency support

The SoC of the equivalent aggregate battery will deviate from its optimal precalculated trajectory during frequency support implementation. A fuzzy-logic-based method was developed to estimate the power change coefficient p' in order to reach the precalculated SoC by appropriately increasing or decreasing the PEV power until the aggregated SoC coincides with the optimal precalculated one, when frequency support is no longer required.

The output of the fuzzy logic controller, d, depends on two inputs, ΔSoC and ΔP. ΔSoC is the distance between the precalculated optimal trajectory of SoC and the trajectory of SoC after frequency support implementation and ΔP is the distance between the optimal trajectory of the active power of the aggregate battery from its limits. Each of the fuzzy sets corresponds to the linguistic variables: very small (VS), small (S), medium (M), large (L) and very large (VL) and they are normalized in the range of [0,1]. The membership functions used for the fuzzification stage are depicted in Fig 20. The rules used for the estimation of the power change factor, d, are given in Table III. A defuzzification strategy based on centroids is used to generate a crisp value for the power change factor.

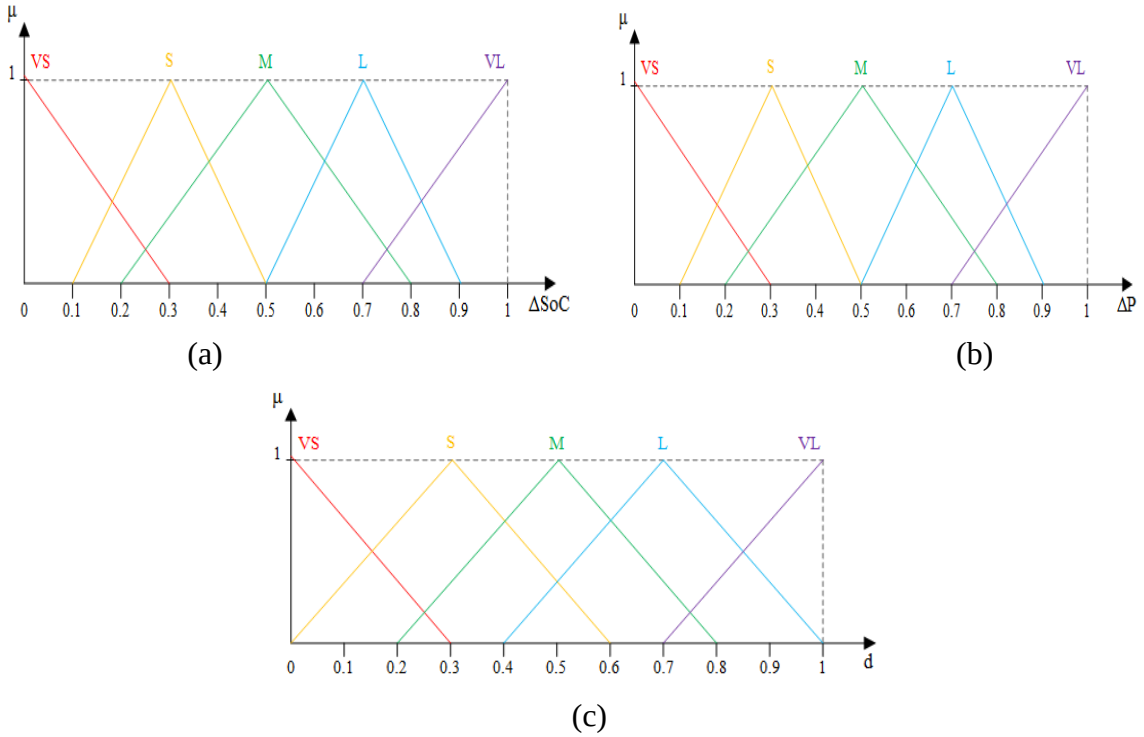

Fig. 20. Membership functions of the fuzzy variables: (a) ΔSoC (b) ΔP (c) power change coefficient, d

The normalization of the inputs, ΔSoC and ΔP, is given in the following equations.

$$\Delta SoC = \begin{cases} \dfrac{SoC_{PB} - SoC_{PB,fs}}{SoC_{PB,max} - SoC_{PB}}, & SoC_{PB} > SoC_{PB,fs} \\ \dfrac{SoC_{PB,fs} - SoC_{PB}}{SoC_{PB} - SoC_{PB,min}}, & SoC_{PB} < SoC_{PB,fs} \end{cases} \tag{161}$$

$$\Delta P = \begin{cases} \dfrac{P_{opt} - P_{PB,min}}{P_{PB,max} - P_{PB,min}}, & SoC_{PB} > SoC_{PB,fs} \\ \dfrac{P_{PB,max} - P_{opt}}{P_{PB,max} - P_{PB,min}}, & SoC_{PB} < SoC_{PB,fs} \end{cases} \tag{162}$$

The appropriate power deviation, ΔP_{PEV}, is calculated in Equation (163).

$$\Delta P_{PEV}(t) = |P_{PEV}(t)| \cdot d \tag{163}$$

8.4. Frequency Support by Diesel Generators

The mathematical model of a diesel engine comprises the transfer functions of the mechanical speed-governing system and the diesel turbine, as shown in Equations (164) and (165), respectively. The control gains and time constants are suitably set in order to simulate the fast response of diesel generators and the power generated by them.

$$G_D = \frac{K_D \cdot (1 + sT_{D1})}{(1 + sT_{D2}) \cdot (1 + sT_{D3})} \tag{164}$$

$$G_T = \frac{K_T}{1 + sT_{D4}} \tag{165}$$

The motion dynamics of the examined microgrid is modelled as a first-order transfer function as in the following equation.

$$G_M = \frac{K_M}{1 + sT_M} \tag{166}$$

Hence, the total power deviation of diesel generators required for frequency support is estimated by the following equation.

$$\Delta P_{diesel}(s) = -\sum_{g} \left(\frac{K_I}{s} + \frac{1}{R}\right) \cdot \frac{K_D \cdot (1 + sT_{D1})}{(1 + sT_{D2}) \cdot (1 + sT_{D3})} \cdot \frac{K_T}{1 + sT_{D4}} \cdot \Delta f(s)\,, \quad \forall g \in G \tag{167}$$

Chapter 9

Case Study – Coordinated Optimal Operation Scheduling of Active Distribution Network & Microgrid

The developed models and algorithms are verified through the simulation of realistic microgrid operation scenarios. A notable feature of this work is that the developed methods are fully parametric in order to ensure the application of the finally developed energy management to energy systems of various sizes and complexity. Particularly, the proposed energy system is able to include buildings scaling from simple residential ones up to mega office or commercial buildings, buildings with simple floor plans and a few thermal zones up to buildings with complex floor plans and large number of thermal zones. This is achieved by appropriately modifying model parameters such as the number of thermal zones and building floors, the buildings' dimensions and construction characteristics, the profiles of building thermal and electrical loads for each building thermal zone.

In this work we have chosen to examine large-scale office buildings which are more challenging to optimize due to their complexity. Moreover, in the examined case study, three kinds of floor plans are selected for demonstration purposes in order to examine and compare the thermal behavior of buildings with different characteristics and complexity, as shown in Figure 21. The examined microgrid also comprises one large EV parking lot, two auxiliary diesel generators, three PV parks and one wind turbine park. The IEEE 33-node radial distribution network has been used as the electric network of the microgrid. The single-line of the examined electric distribution network is shown in Fig. 22. The model parameters that are associated with the buildings of the microgrid are tabulated in Tables IV-VI. Four types of PEV batteries are considered in this article with their technical characteristics given in Table VII. All the necessary technical parameters of the diesel generators are presented in Table VIII.

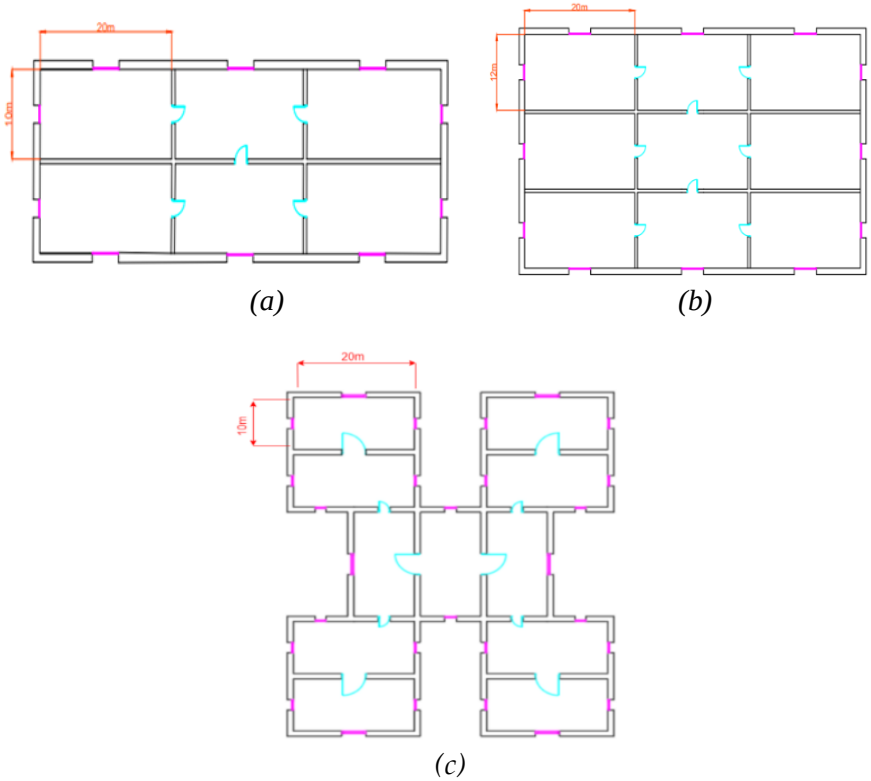

(a) *(b)*

(c)

Figure 21. Floor plans (a) Building 1 (15 floors, 90 thermal zones), (b) Building 2 (25 floors, 225 thermal zones), (c) Building 3 (35 floors, 385 thermal zones)

TABLE IV
BUILDING MODEL DATA

THERMAL ZONES MODELLING DATA

	Thermal zones			All thermal zones					
	B1	**B2**	**B3**						
Side_1 (m)	10	12	10	$p_z(kg/m^3)$	1.2	$\tau_{win,z}$	$1.1 \cdot 10^{-3}$	$\beta_z(°)$	90
Side_2 (m)	20	20	20	$C_z(kWh/(kg \cdot °C))$	1/3600	$a_{w,z}$	$18.6 \cdot 10^{-3}$	$\theta(°)$	11.9
Height (m)	3	3	3	$U_{wall,z}(kW/(m^2 \cdot °C))$	$2.04 \cdot 10^{-3}$	SC_z	0.54	$\theta_z(°)$	39.9
Tmin / Tmax (°C)	19/27.5	19/27.5	19/27.5	$U_{win,z}(kW/(m^2 \cdot °C))$	$5.6 \cdot 10^{-3}$	p_g	0.2	$R_{se,z}((m^2 \cdot °C)/kW)$	40

BUILDING PARAMETERS

	B1	**B2**	**B3**
Number of floors	15	25	35
Total number of thermal zones	90	225	385

TABLE V
BUILDING LOADS PARAMETERS

	Thermal Loads (W)	**Electrical Loads (W)**
PC	70	500
Printer	40	100
Display	60	100
Charger	20	100
Scanner	30	80
Lighting	35	120
Human Body	150	-

TABLE VI
NON-CRITICAL LOADS PARAMETERS

	Building 1	**Building 2**	**Building 3**
n_{non_cr}	0.25	0.25	0.25
$n_{shift,min}$	0.70	0.75	0.65
$n_{shift,max}$	1.3	1.25	1.35
$T_{shift,min}$	07:00	07:00	07:00
$T_{shift,max}$	17:00	17:00	17:00

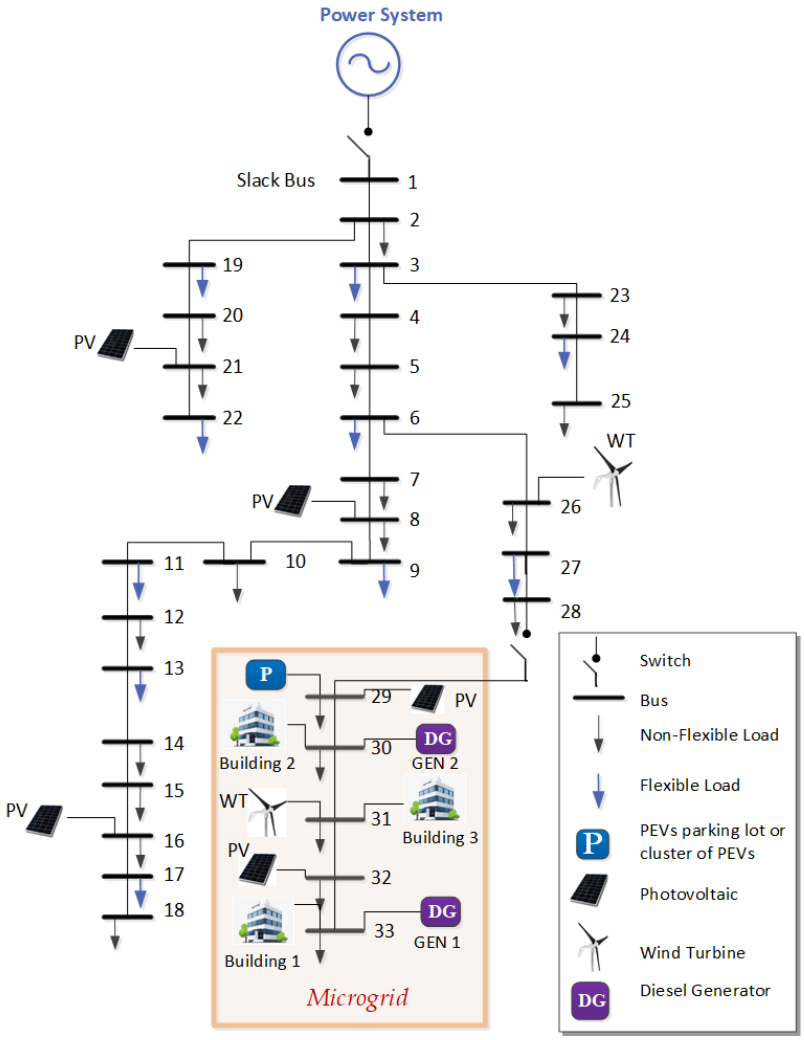

Fig. 22. Single-line diagram of the examined distribution network.

TABLE VII
PEV PARAMETERS

	PEV type			
	1	**2**	**3**	**4**
$Battery\ Capacity(kWh)$	77	45	26.8	66.5
SoC_{max} /SoC_{min} (kWh)	69.3/7.7	40.5/4.5	24.12/2.7	60/6.65
P_{max} /P_{min} (kW)	11/-11	7.2/-7.2	6.6/-6.6	11/-11

TABLE VIII
DIESEL GENERATORS MODEL DATA

	GEN1	**GEN2**
Technical Minimum (kW)	285	600
Technical Maximum (kW)	1000	2100
Minimum hours for generator being in operation/out of operation (h)	1/1	1/1
Cost of consumed fuel (m.u./h)	$62.8 - 0.1114 \cdot P + \ldots + 2 \cdot 10^{-4} \cdot P^2$	$137 - 0.122 \cdot P + \ldots + 8 \cdot 10^{-5} \cdot P^2$

The ambient temperature that was used in this case study is a typical daily temperature time series from late summer in Greece. In order to take into consideration, the stochastic behavior of the ambient temperature, various trajectories were generated and used. Fig. 23a displays the base trajectory of the data set selected for demonstration purposes together with its variation area. Similarly, different trajectories of the actual electricity price were randomly produced. It was assumed that the electricity price that was forecasted was carried out by the power system operator and provided to the microgrid and the active distribution network. Provided that the computation time that is required by the proposed method is small (of the scale of a few minutes), it was assumed that the electricity price forecast would be provided to the local electricity market participants after the day-ahead electricity market was carried out. The time series of the actual electricity price forecast that was used in the examined scenario and its respective variation area are shown in Fig. 23b.

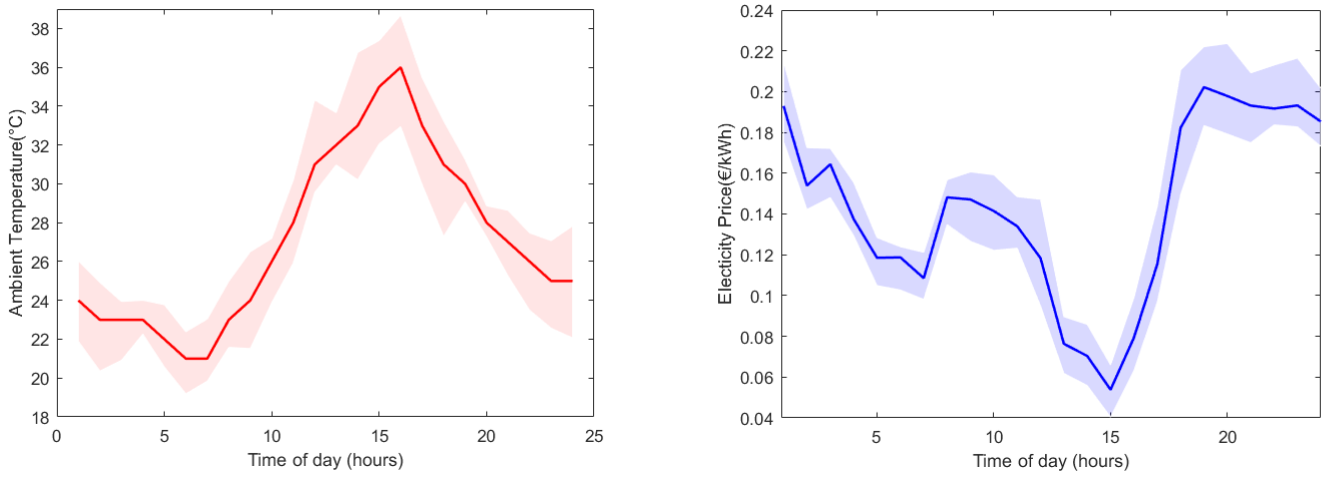

Fig. 23. (a) Ambient temperature and its variation area (b) Variable electricity price and its variation area

The number of people having activity in each building of the microgrid is shown in Fig. 24a. As seen in this figure, the maximum number of people for each building takes place during 13:00 – 14:00. The obtained total number of the connected EVs during the examined time period is shown in Fig. 24b. The connection and the dwell times of the PEVs depend on the different type of activities (home, work, shop, social) that their drivers have, and they are estimated using the respective probability density functions (PDFs), shown in Fig. 25.a and Fig. 25.b, respectively. For instance, as it can be observed, the connection rate for PEVs of citizens being at work peaks at the 450th min (7:30 a.m.), whereas their dwell time peaks approximately at 510 mins (8.5 h).

Various trajectories of the total AND load consumption, as well as of the total power generated by the wind park and the photovoltaics were randomly generated and the respective data are shown in Figs. 26a and 26b, respectively.

The internal temperatures of all of the buildings' thermal zones that are obtained in the first optimization level, with their upper and lower bounds, are given in Fig. 27. It was observed that the internal temperatures of all of the thermal zones of each building were consistently well-maintained between the comfortable temperature range of 19–27.5°C and they all tended to behave in the same way.

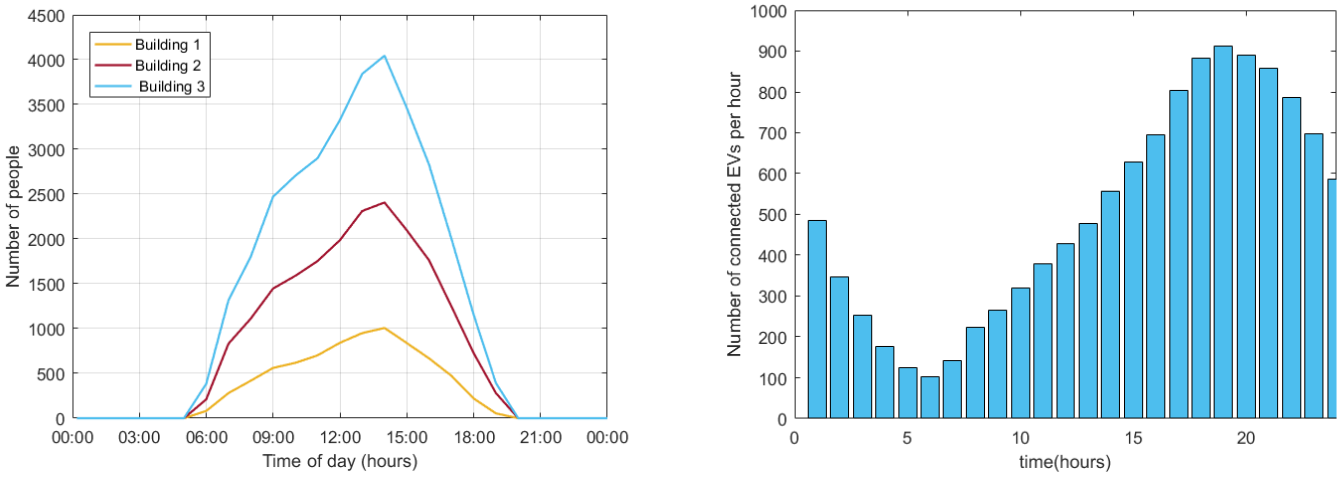

Fig. 24. (a) Forecasted number of active people in microgrid's building. (b) Number of connected EVs.

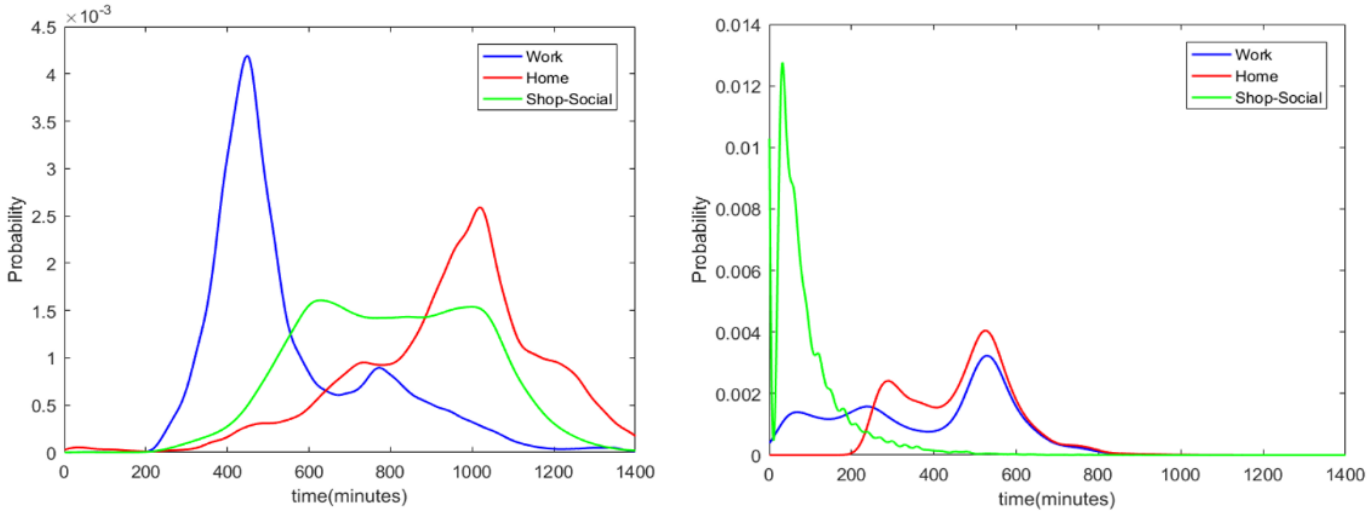

Fig. 25. a) PDF of PEV arrival time (b) PDF of PEV dwell time

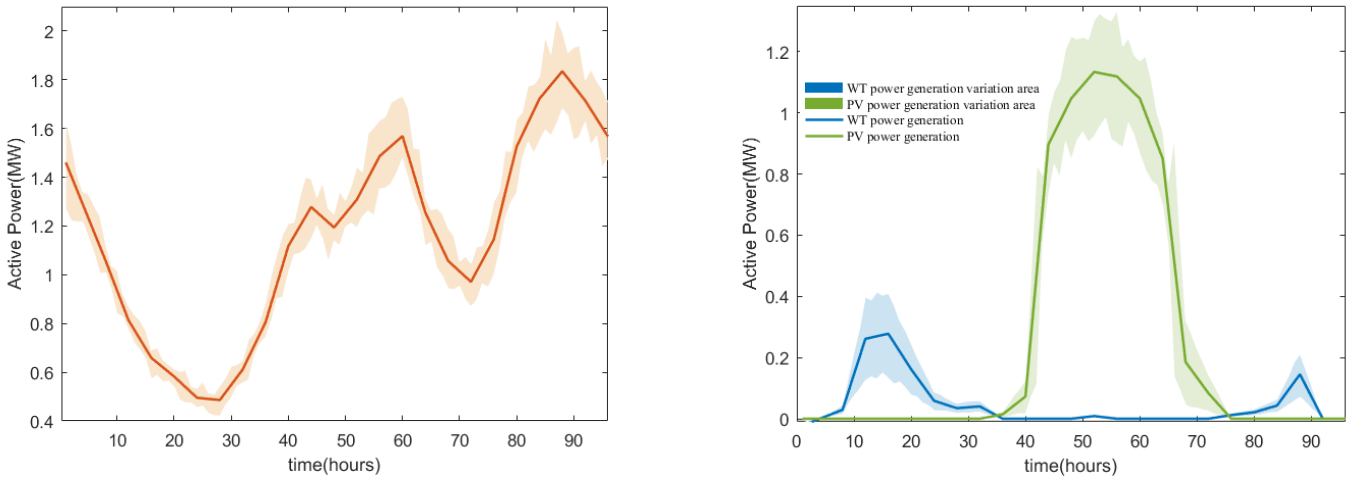

Fig. 26. a) Distribution Network Load (b) Wind turbine and photovoltaic power generation

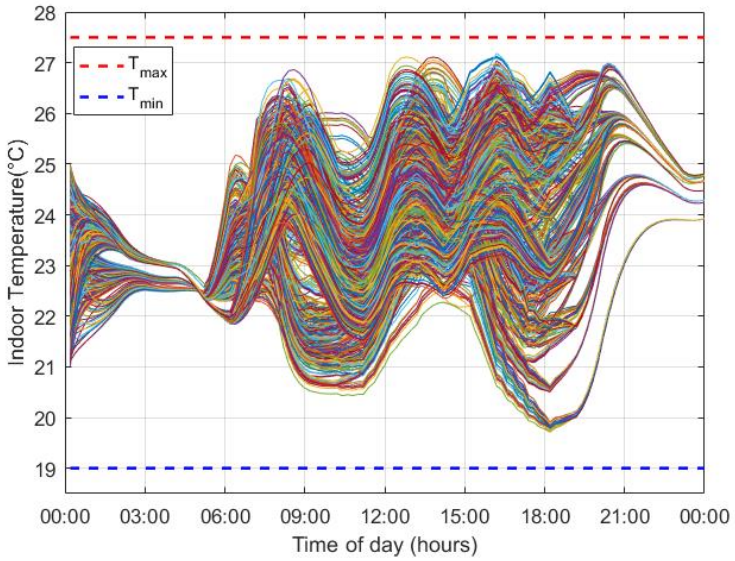

Fig. 27. Internal temperatures of all buildings' thermal zones (optimization level 1).

The electric power consumptions of the HVAC systems of each building of the microgrid obtained from the execution of the first level of optimization are shown in Fig. 28a, as resulted from the optimal dispatch of the total buildings' HVAC power. The total cooling power of each building follows the ambient temperature and the pattern of the forecasted number of people having activity in the buildings, as it was expected. Obviously, the largest building has the biggest cooling requirements. As it can be observed, in this case the algorithm tries to decrease the power consumption at time periods of relatively high electrical price. Fig. 28b depicts the electric power consumption of the HVAC systems of indicative building thermal zones. Their power consumption varies due to the fact that each building consists of a different number of floors and thermal zones with different building specifications.

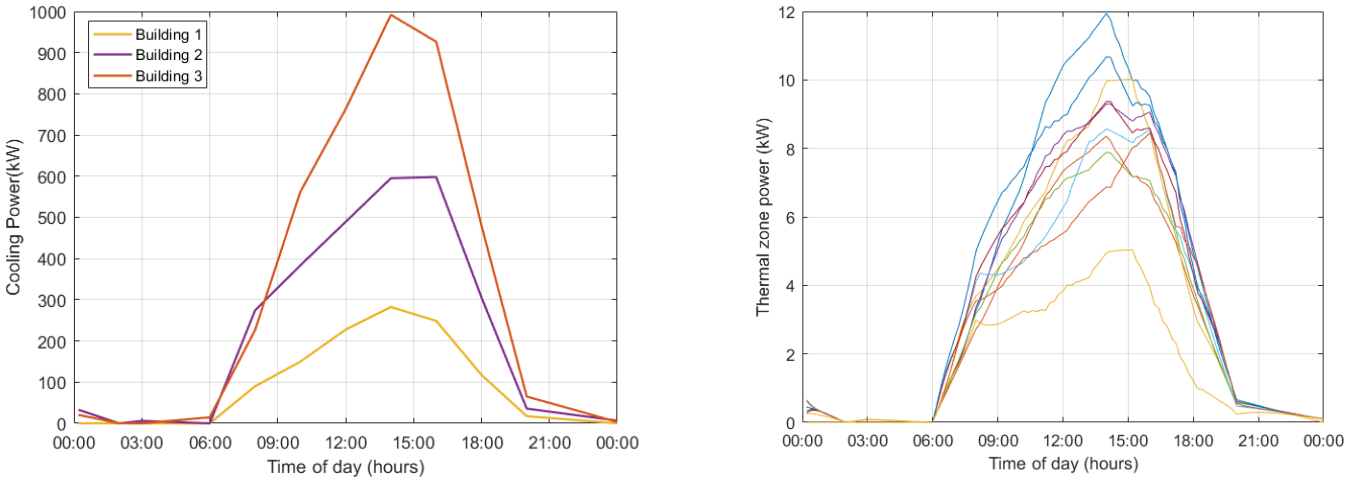

Fig. 28. Cooling power of a) each microgrid's building (optimization level 1) b) indicative thermal zones

The total non-critical electrical demand of the buildings of the microgrid is shown in Fig. 29a, before and after the first level of optimization was implemented. It is observed that non-critical electrical loads are shifted to time periods of low electricity price is low, in order to contribute to the minimization of microgrid's total operation cost while satisfying all the operational constraints, at the same time. Specifically, the algorithm shifts the electrical loads from the high electricity time period 07:00-09:00 to the low electricity price time period 13:00-15:00. Fig. 29b presents the non-critical loads of each building of the microgrid before and after the first level of optimization was implemented, as resulted from the optimal power dispatch of the total electric power demand.

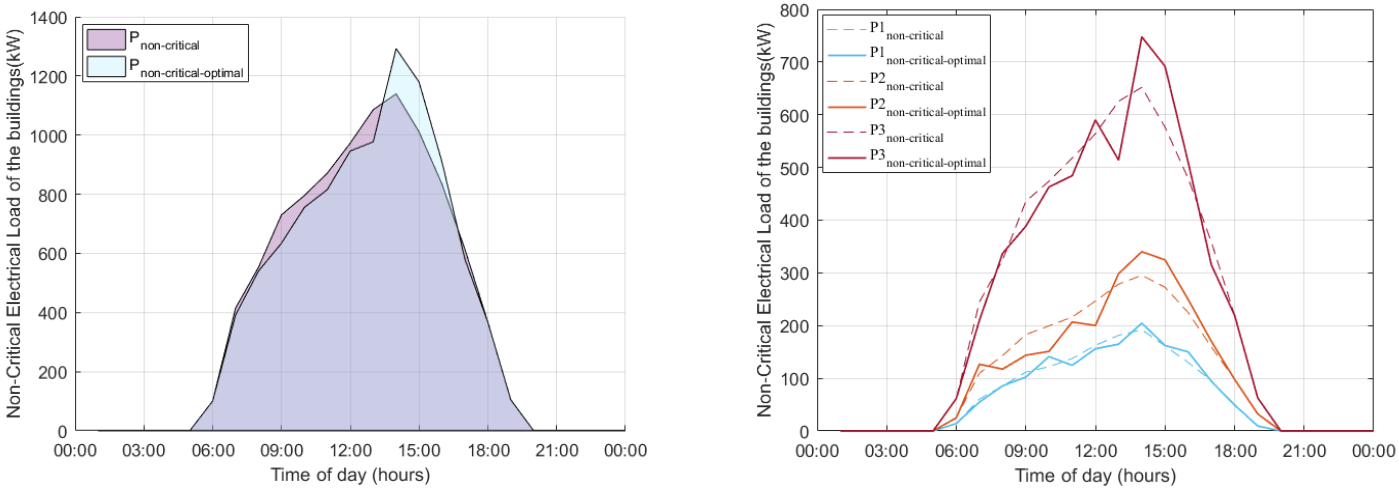

Fig. 29. Electric power of non-critical loads of a) all microgrid's building (optimization level 1) b) each building

The total active power of the PEV parking lot, together with its respective upper and lower limits, is shown in Fig. 30. Generator convention was used, hence the negative values indicate that the aggregate battery absorbed power from the grid (i.e., it was charging), while positive values indicate that the battery injected power to the grid (i.e., it was discharging).

The total energy that was stored in the equivalent aggregate battery of the microgrid's parking lot, as well as its respective upper and the lower limits, is shown in Fig. 31. These limits changed over time as a result of the fluctuating number of connected EVs and electricity price variations.

The algorithm effectively covered the microgrid's energy demand with internal power sources during its autonomous operation and, at the same time, it reduced its daily operational cost. It was observed that all of the PEVs managed to reach their energy targets while satisfying all of the operational and technical constraints. In order to guarantee that the necessary energy was stored during the microgrid's island operation, the PEVs were compelled to store extra energy from the electric grid before the grid's power supply was interrupted.

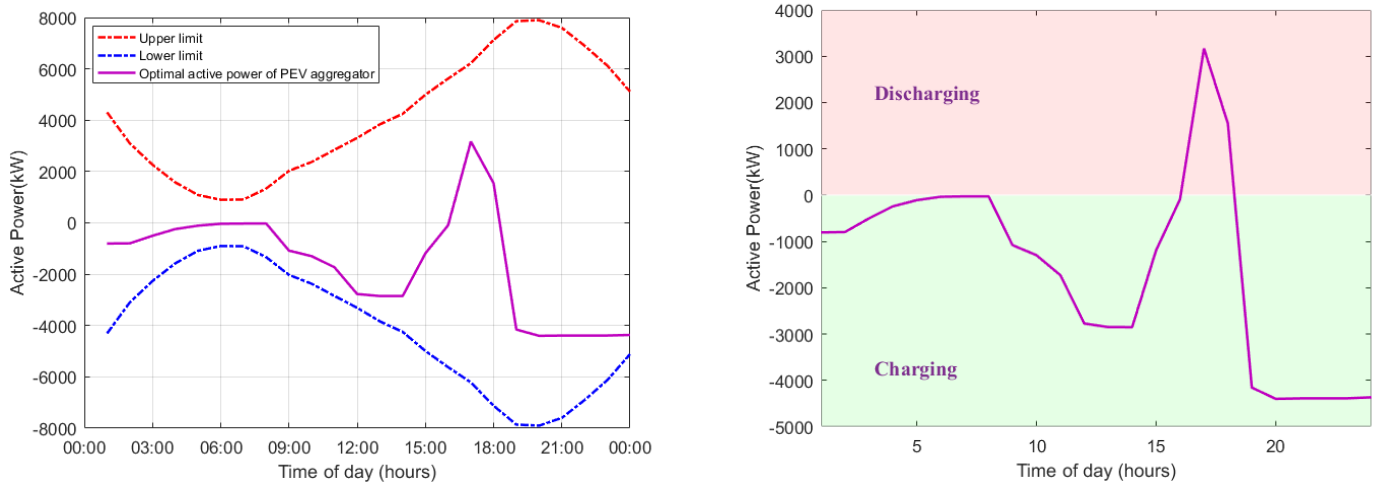

Fig. 30. Active power of PEV aggregator and its upper and lower bounds.

Fig. 32 exhibits the power that was produced by the diesel generators. The generators were scheduled to operate as close as possible to their optimal operation point.

The time series of all of the node voltages after the execution of optimization stage 2 are shown in Fig. 33. The upper and lower voltage limits were set to 1.1 and 0.9 p.u., respectively. According to Fig. 33, the voltages of the network buses were out of the predefined limits during the time period from 19:00–22:00.

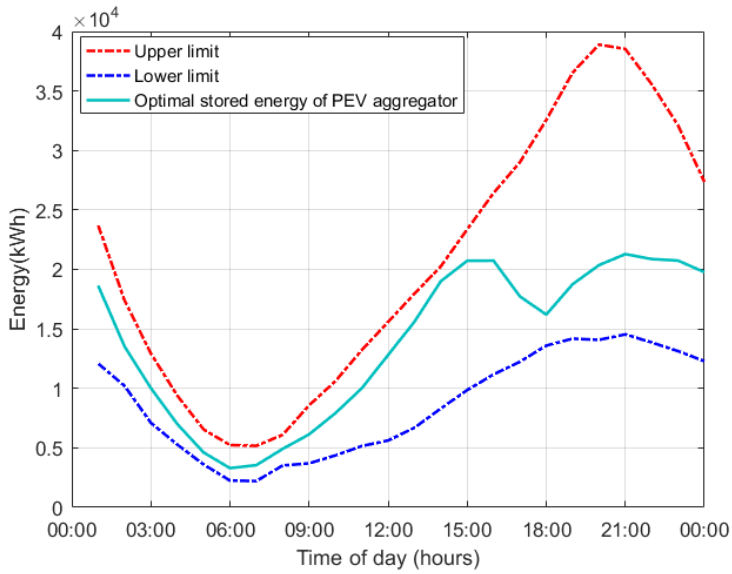

Fig. 31. Total stored energy of PEV aggregator and its upper and lower bound.

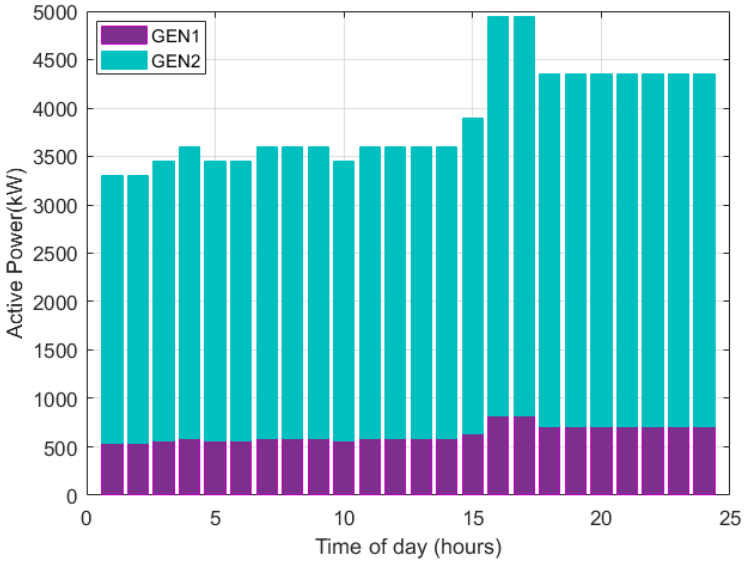

Fig. 32. Power produced by auxiliary diesel generators (optimization level 1).

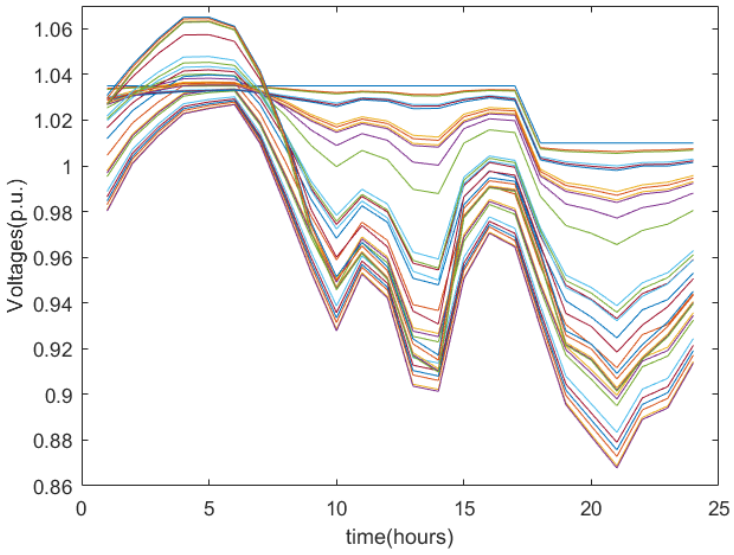

Fig. 33. Node voltages (optimization level 2).

Therefore, it was necessary to identify the time periods during which the network constraints were violated and provide them to the microgrid in order to evaluate the minimum and maximum possible deviations of its power exchange in optimization stage 3, as is shown in Fig. 34. It was considered that the maximum permitted fluctuations of the power of the buildings, parking lots' aggregate battery and diesel generators were up to 20% of their installed power capacity. In the time period from 19:00–22:00, when the voltages of the distribution network nodes dropped, the cooling power of the buildings was required to be reduced (as is shown in Fig 34) and, therefore, the indoor temperatures of the buildings increased.

Moreover, Fig. 34 exhibits the optimal deviation of the power that was exchanged between the microgrid and the active distribution network as was obtained from optimization stage 4. It is obvious that it was within its predefined bounds. Fig. 35 depicts the optimal power deviation of each building of the microgrid and of the optimal power deviation of the parking dynamic equivalent battery. At the same time, as can be observed in Fig. 36, the internal temperatures of all of the thermal zones of the buildings were well-maintained between their minimum and maximum limits.

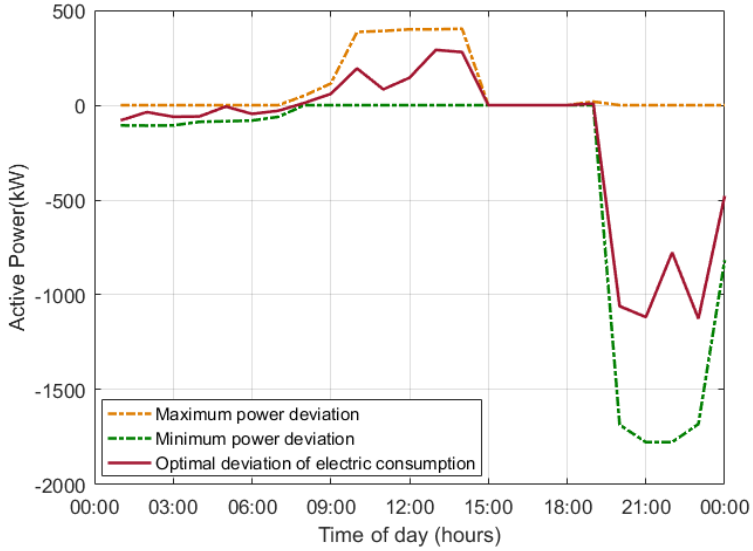

Fig. 34. Optimal deviation of the power transferred between the microgrid and the active distribution network.

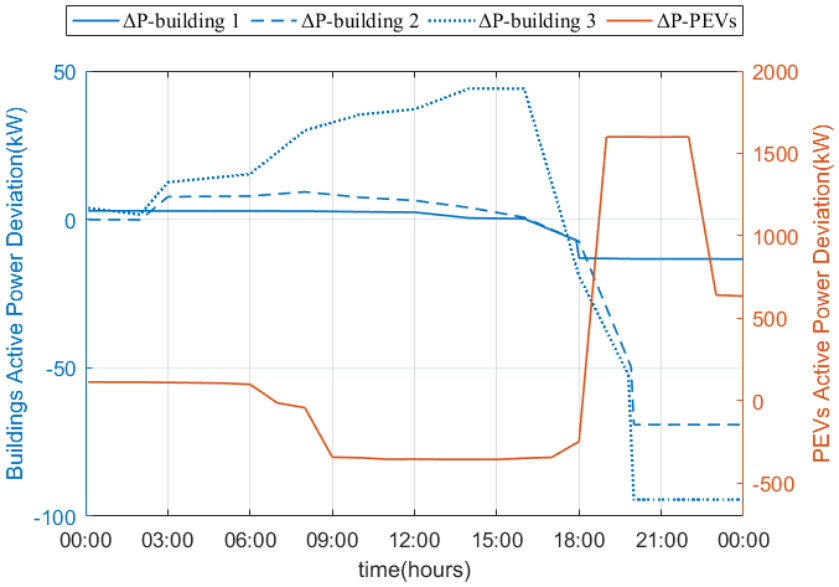

Fig. 35. Optimal deviation of each building and PEV parking lot of the microgrid.

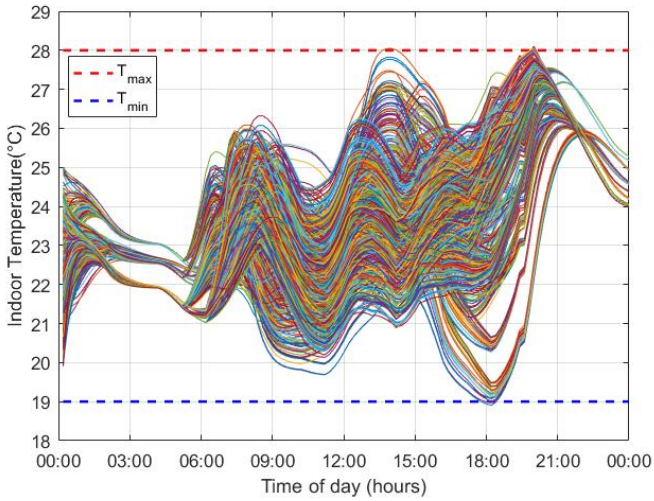

Fig. 36. Internal temperatures of all building thermal zones (optimization level 4).

Fig. 37 exhibits the active distribution network load before and after optimization stages 2 and 4 were implemented. In the second optimization stage, it was observed that the flexible electrical loads were shifted to time periods of low electricity price (13:00–15:00) in order to contribute to the minimization of the active distribution network's total operational cost while satisfying all of the operational constraints at the same time. The time series of all of the node voltages after the execution of optimization stage 2 are shown in Figure 38. It can be seen that the distribution network voltages were well-maintained within their permissible limits.

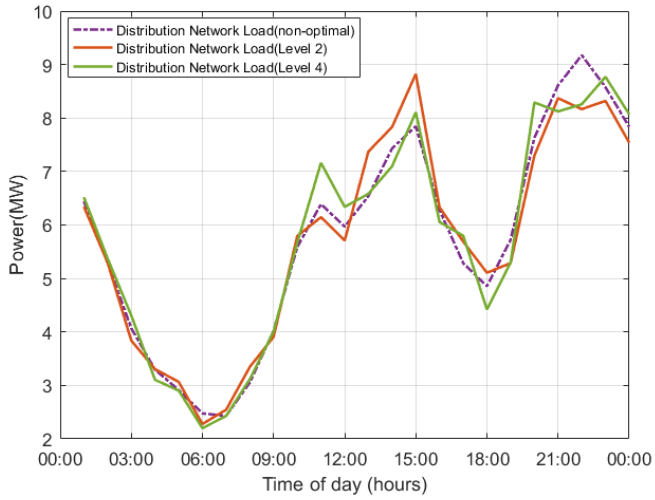

Fig. 37. Active distribution network load before and after the execution of the optimization levels 2 and 4.

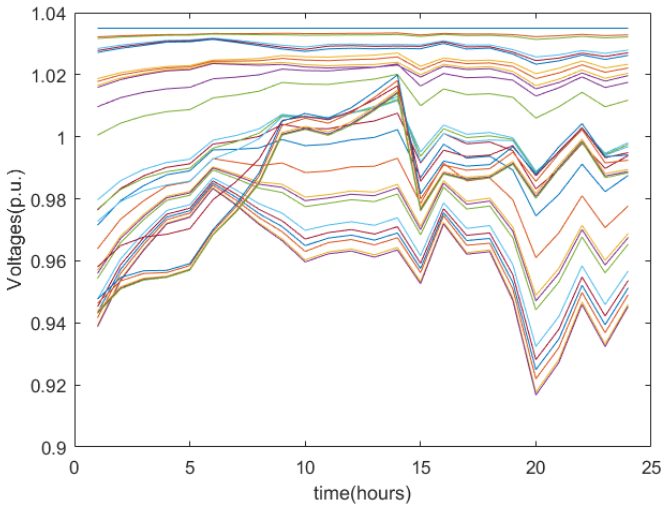

Fig. 38. Node voltages (optimization level 4).

Fig. 39 exhibits the power that was exchanged between the microgrid and the active distribution network after the execution of optimization levels 1 and 4.

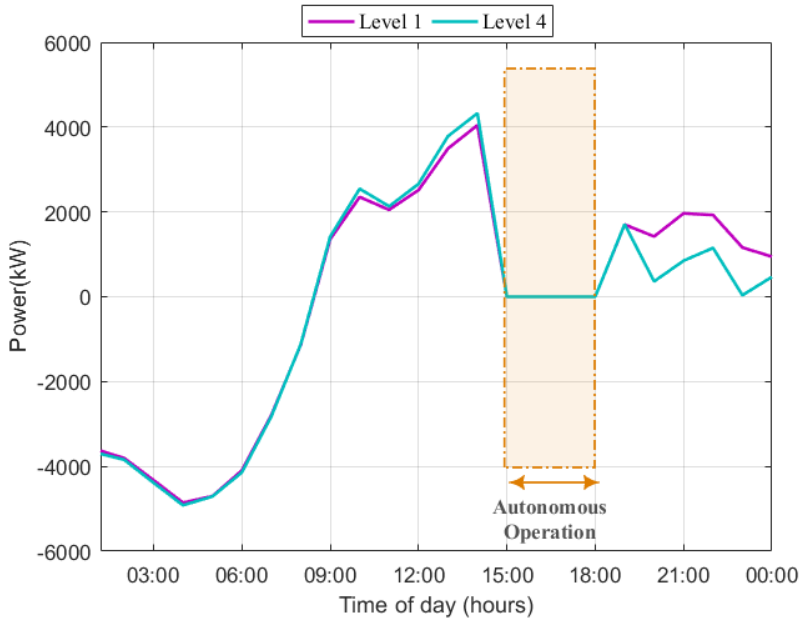

Fig. 39. Active power exchanged between microgrid and active distribution network (optimization levels 1 and 4).

CO_2 emissions of each diesel generator of the microgrid are depicted in Figure 40. The algorithm maintains the pollutant emissions of all auxiliary generators below their limits (the second diesel generator was forced to limit its emissions).

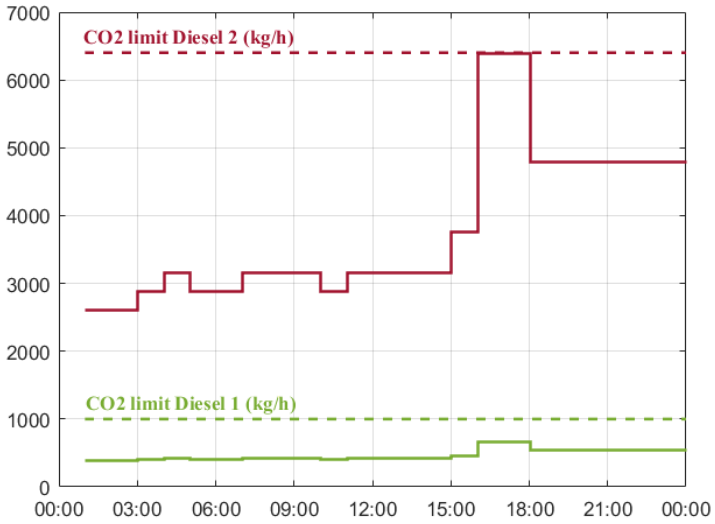

Fig. 40. Auxiliary diesel generators CO_2 emissions with their upper limits

The total daily operation cost of the microgrid as resulted from the first optimization stage is given in Table IX. It is acknowledged that the buildings and the Microgrid could have conflicted interests regarding the operation cost savings. To this end and for the sake of fairness, the total profit of the microgrid can be optimally and fairly allocated to the building prosumers and plug-in electric vehicles hosted by the microgrid by developing suitable optimization algorithms. Moreover, it was shown the considered uncertainties of electricity price and the ambient temperature slightly increases the operation cost by 0.9% according to Table IX.

TABLE IX
MICROGRID OPERATION COST

Daily Microgrid Operation Cost	Without uncertainties	With uncertainties
Total operation cost (m.u.)	10856	10953,7

Chapter 10

Case Study – Optimal Operation Scheduling of ADN Comprising Distributed Residential Buildings and PEVs

The suggested method is applied to the IEEE 33-bus radial distribution network comprising 1000 residential building prosumers, 32 clusters of PEVs, three photovoltaic parks and one wind park. The developed models are verified through detailed simulation results.

Four types of residential buildings and PEVs with different technical specifications are considered in this work. Probability density functions (PDFs) are used to obtain the arrival and dwell periods of the PEVs and they can be found in Table VI in previous case study. Fig. 41a shows the total number of connected PEVs to the distribution network, while Fig. 41b shows the number of connected PEVs to each node of the network. The ambient temperature, considering a summer scenario, the forecasted electricity price, as well as the total power generated by the wind park and the photovoltaics are the same with those used in previous case study.

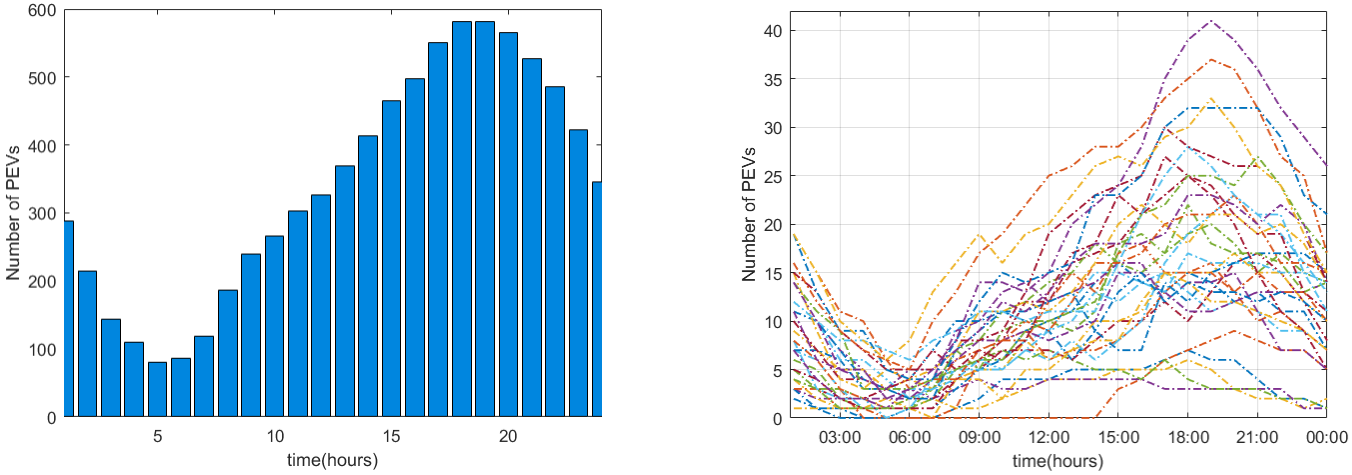

Fig. 41. (a) Total connected PEVs in the ADN; (b) Connected PEVs to each node of the ADN.

In addition to the proposed optimization approach, a typical ADN operation case study was considered, in which the residential building thermal loads, as well as the hosted electric vehicles are not subject to any optimization. In this case, the objective of the operation of HVAC systems is to maintain the internal temperature of buildings at a predetermined set point. Electric vehicles only absorb power in order to charge their batteries and attain the desired energy level and they have not the V2G operation ability. The examination of this case study is taken into account in order to compare its results with the respective results of the proposed strategy for the optimization of ADN's operation.

The total HVAC electrical power consumption and other building loads' electrical power consumption of all residential buildings hosted in the examined active distribution network are given in Fig. 42a. As it can be observed, the residential buildings absorb the largest amount of thermal power around 15:00 p.m. where the electricity price is very low, as the proposed algorithm aims to minimize the total operation cost of the examined system. Moreover, in this time period the ambient temperature is high enough and obviously the cooling requirements of the residences are increased. Figure 42b provides the comparison of the total buildings' HVAC power consumption between the proposed optimization examined case study and the typical scenario of the ADN's operation. It is observed that when the suggested optimization algorithm is implemented, a significant reduction in HVAC systems' required power is achieved. Fig. 43

depicts the HVAC power consumption of the clusters of the buildings connected to the distribution network nodes as resulted from the optimal dispatch of the total HVAC power them. Their power consumption varies due to the fact that each node consists of a different number of residential buildings with different building specifications.

Figs. 44a and 44b present the indoor temperatures of all buildings hosted by the ADN obtained by the proposed ADN optimal operation scheduling technique and the execution of the typical ADN operation, respectively. All temperatures are maintained within the considered permissible comfort range of 21 – 26℃. Fig. 45 indicatively shows the power consumed by the non-flexible electrical loads of two buildings of the distribution network.

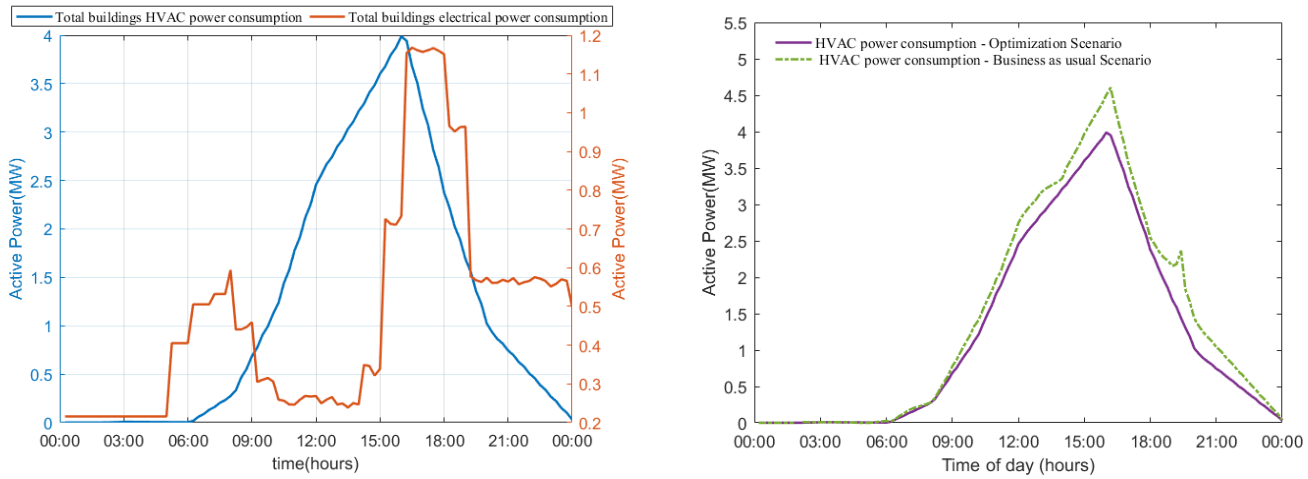

Fig. 42. Total buildings HVAC and electrical power consumption (a) Optimal Operation (b) Typical Operation.

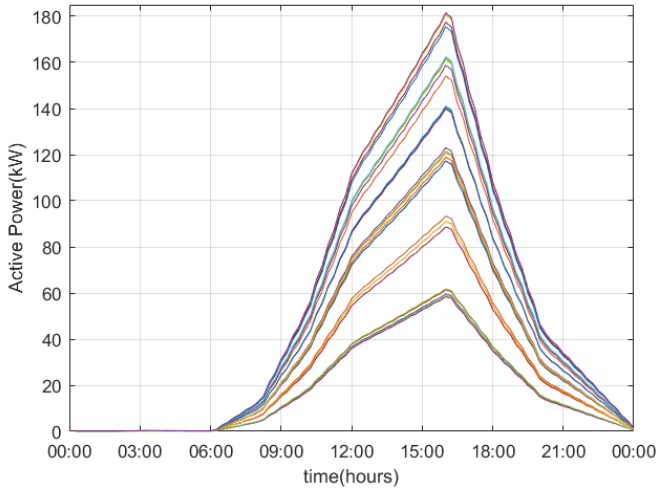

Fig. 43. Building clusters HVAC power consumption in each distribution network node.

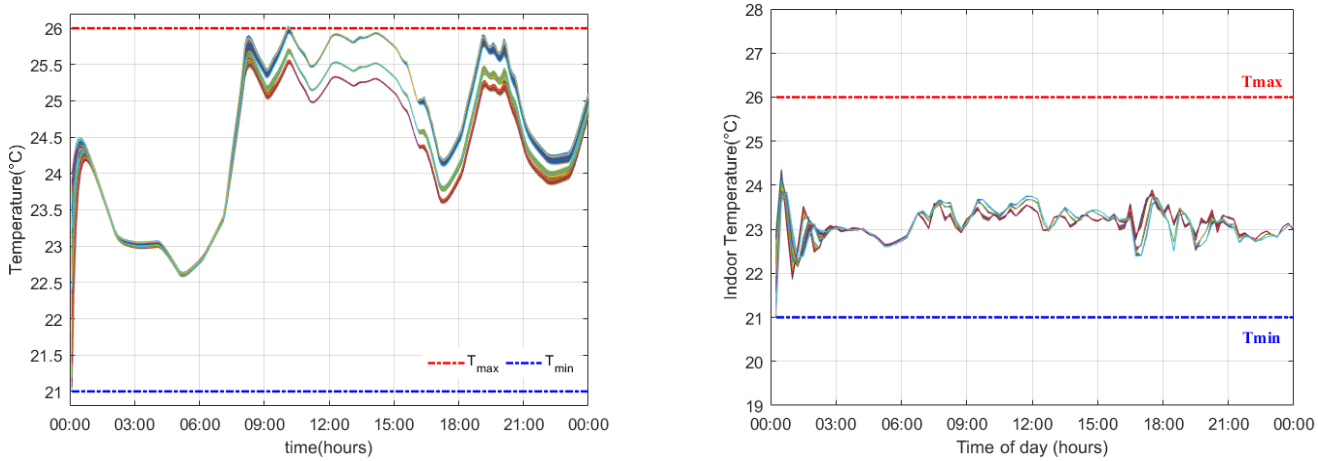

Fig. 44. Indoor temperatures of the buildings hosted in the distribution network (a)Optimization (b)Typical Case.

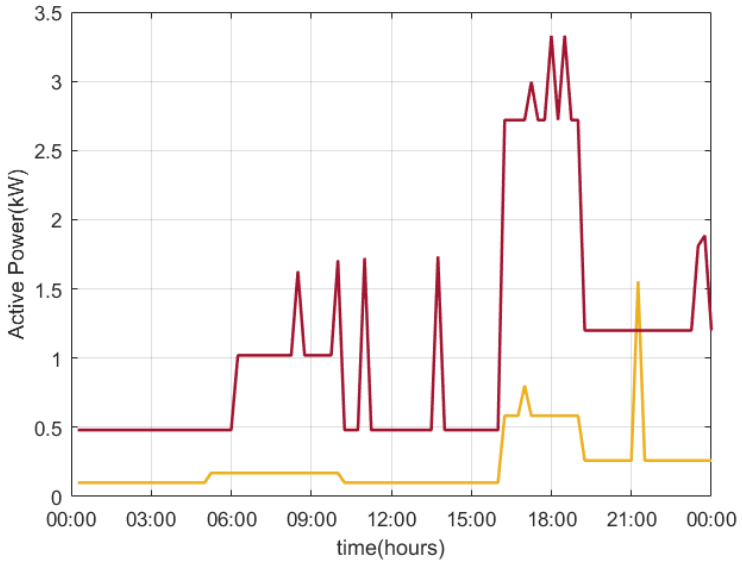

Fig. 45. Electrical power consumption of 2 indicative buildings of the network.

Figs. 46a and 46b depict the total optimal active power and the stored energy of the aggregated batteries of the clusters of PEVs obtained by the proposed ADN optimal operation scheduling technique and the execution of the typical ADN operation. Figs. 47a and 48a depict the active power of two indicative clusters of PEVs located at nodes 21 and 31 of the examined ADN, while Figs. 47b and 48b depict their stored energy, respectively. Moreover, their respective upper and lower bounds are given in the same figures. It is noticed that both the active power that clusters of PEVs exchange with the network and the energy stored in their batteries are kept within their limits. These quantities have been obtained by the implementation of the optimal dispatch of the total active power of the network's equivalent aggregate PEV battery according to the proposed flexibilities of PEV clusters to change their power.

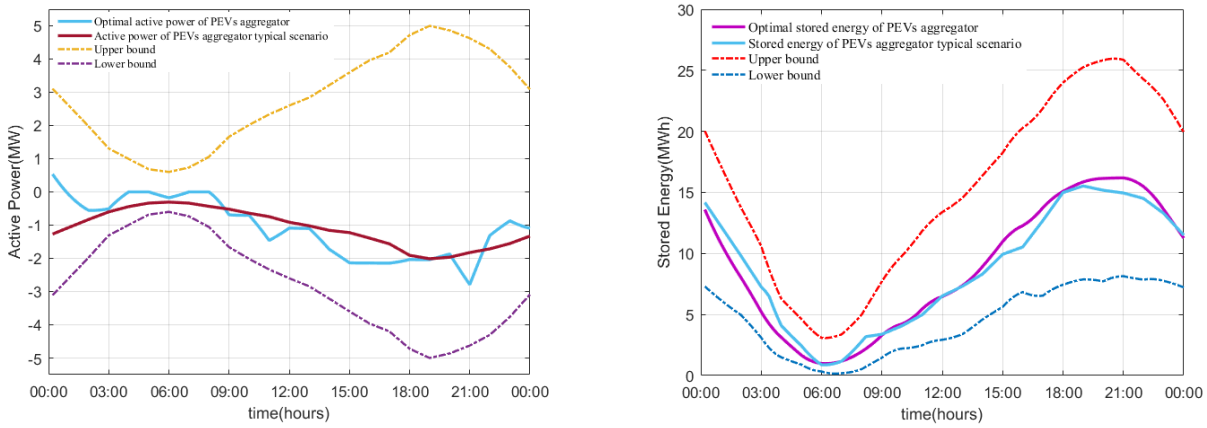

Fig. 46. (a) Total active power; (b) total stored energy of the PEVs aggregate battery

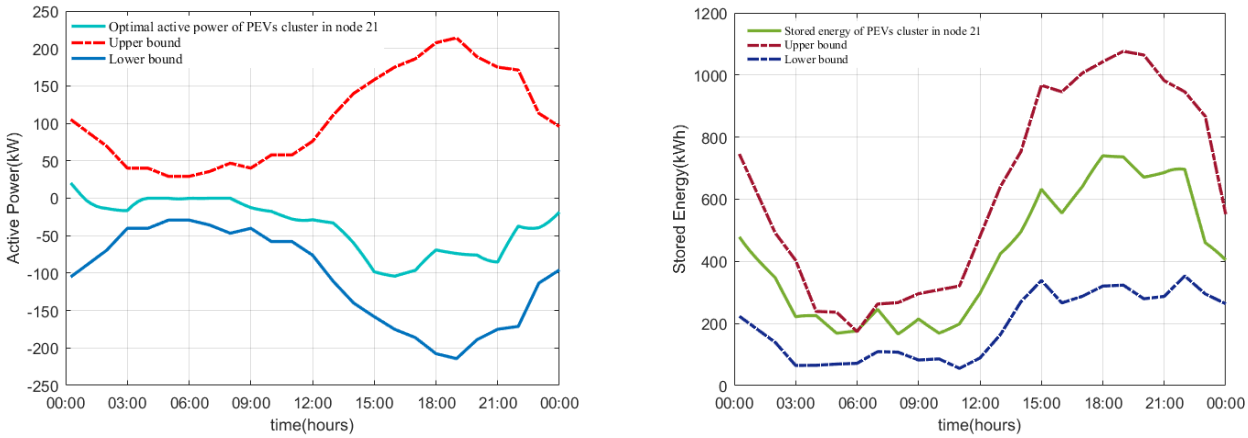

Fig. 47. (a) Active power; (b) Stored energy of the cluster of PEVs in node 21 with their limits

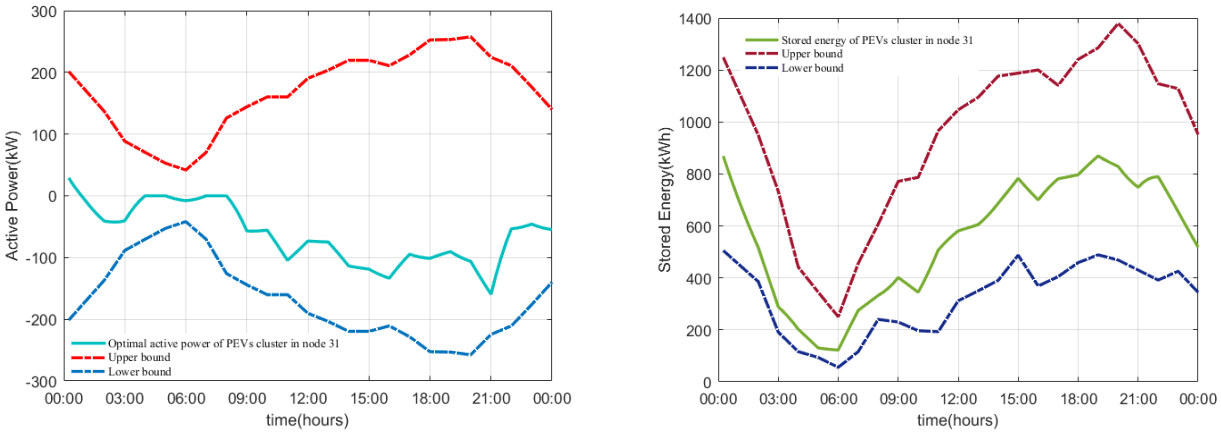

Fig. 48. (a) Active power; (b) Stored energy of the cluster of PEVs in node 31 with their limits

The total power consumptions of the buildings and PEVs together with the ADN's load, the active power the ADN exchanges with the main electric grid and RES generation are shown in stacked form in Fig. 49.

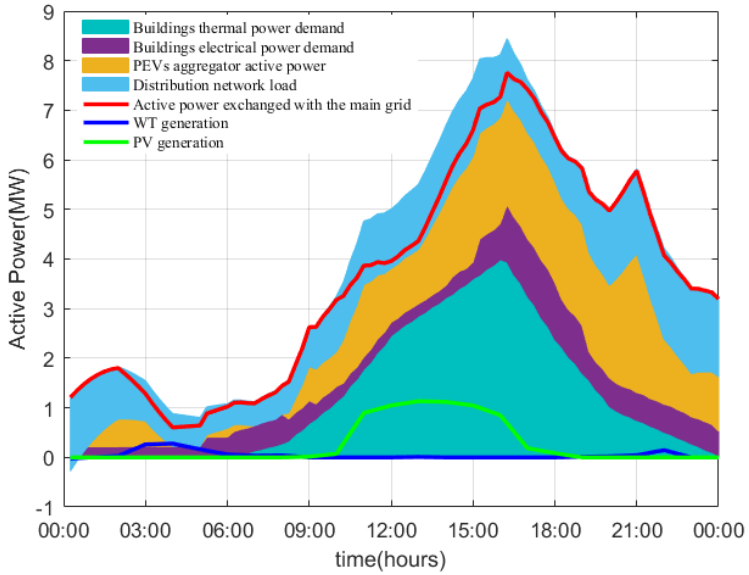

Fig. 49. Buildings and PEVs total power demand, ADN load, RES generation, main grid power.

The clusters of PEVs regulate optimally the reactive power exchanged with the network as depicted in Fig. 50a in order to keep the voltages of the distribution network busses within the permissible limits and satisfy the line power flow constraints. Specifically, the reactive power set-points resulted from the OPF exploitation are forwarded back to the PEVs' cluster agents so as to be optimally dispatched to each PEV they supervise. Maximum and minimum voltage bounds are set to 1.1 and 0.9 (p.u.), respectively while nominal voltage is considered 1 p.u. As shown in Fig. 50b, all node voltages do not violate their bounds.

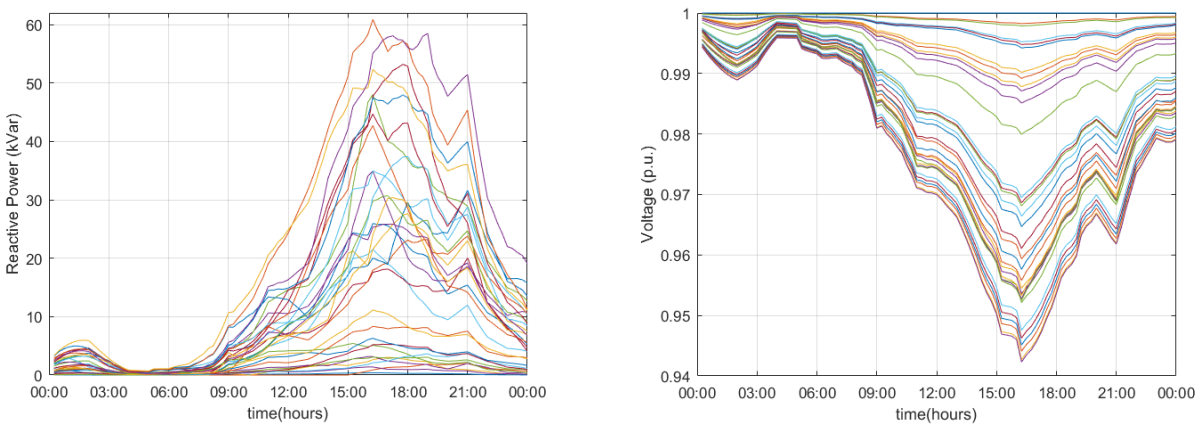

Fig. 50. (a) Reactive power of PEVs clusters; (b) Distribution network node voltages

The active power the distribution network exchanges with the main electric grid both in its optimal and typical operation is given in Figure 51.

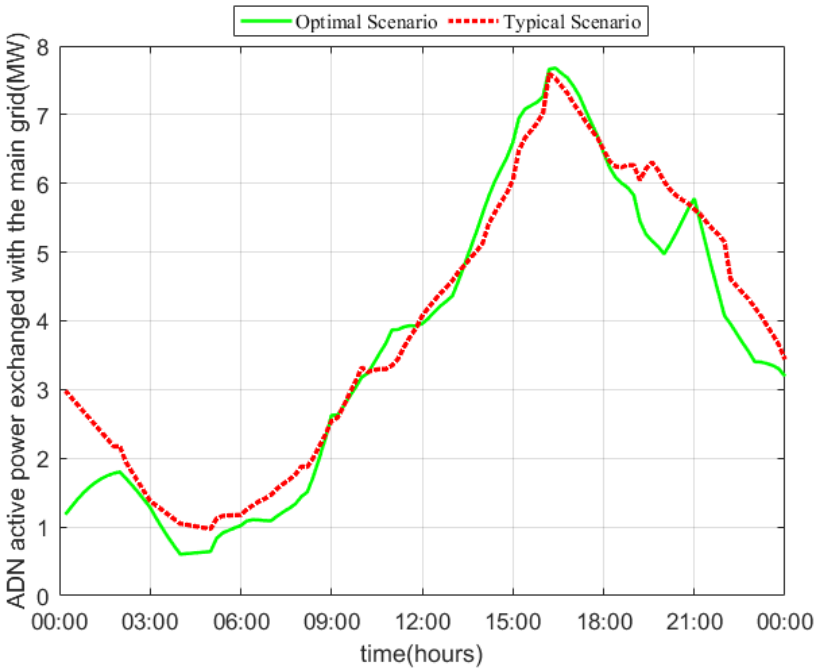

Fig. 51. Total AND's active power both in optimal and typical operation scenario.

The major information of the obtained cost resulted from the execution of the examined operation case studies is tabulated in Table X. A significant cost reduction of 2478 m.u./day (in the range of 17%) is achieved as a result of the implementation of the suggested optimization algorithm in comparison with a typical operation of the ADN. In addition, when the uncertainty of the ambient temperature and the electricity price is taken into consideration, a slight increase of 0,92% of the daily operation cost of the examined system is observed.

TABLE X
EXAMINED OPERATION CASE STUDIES

Operation Case Study	Optimal without uncertainty	Optimal with uncertainty	Typical
Total operation cost (m.u./day)	12333	12446,5	14812

Chapter 11

Case Study – Optimal Real-Time Operation of Microgrid's of Large Building Prosumers

In the examined case study large-scale office buildings are examined. Moreover, the three kinds of floor plans given in Figure 21 were selected for demonstration purposes. Theoretically the decision variables amount up to 57220. The single-line of the examined IEEE 33-node electric distribution network is shown in Figure 52. The necessary data of buildings' model parameters are included in Table XI. Table XII contains the technical specifications of building diesel generators.

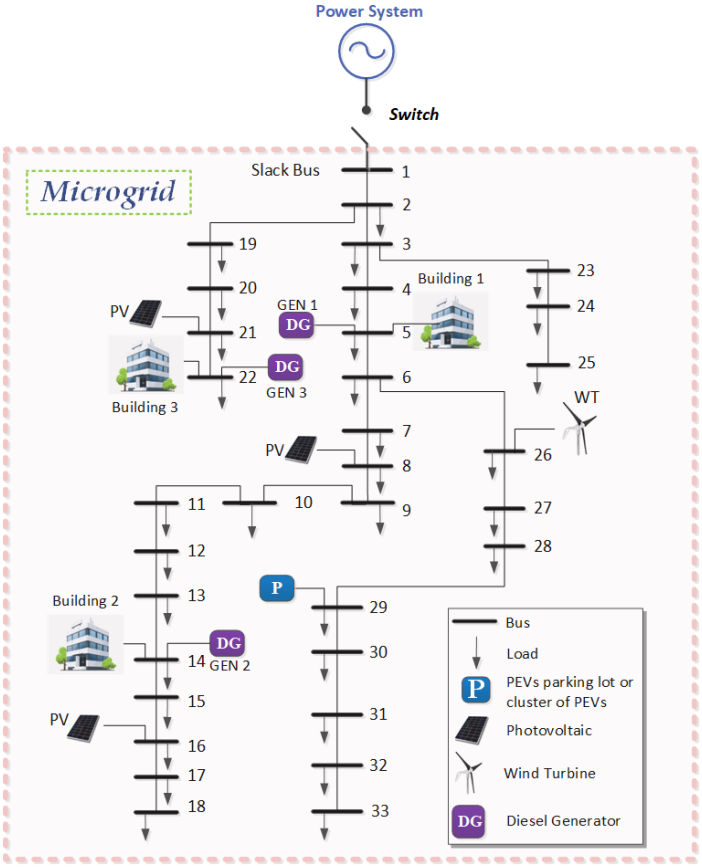

Figure 52. Single-line diagram of microgrid electric network

TABLE XI
BUILDING MODEL DATA

THERMAL ZONES MODELLING DATA									
	Thermal zones			All thermal zones					
	Building 1	Building 2	Building 3						
Side_1 (m)	10	12	10	$\rho_z(kg/m^3)$	1.2	$\tau_{win,z}$	$1.1 \cdot 10^{-3}$	$\beta_z(°)$	90
Side_2 (m)	20	20	20	$C_z(kWh/(kg \cdot °C))$	1/3600	$a_{w,z}$	$18.6 \cdot 10^{-3}$	$\theta(°)$	11.9
Height (m)	3	3	3	$U_{wall,z}(kW/(m^2 \cdot °C))$	$2.04 \cdot 10^{-3}$	SC_z	0.54	$\theta_z(°)$	39.9
Tmin / Tmax (°C)	19/27.5	19/27.5	19/27.5	$U_{win,z}(kW/(m^2 \cdot °C))$	$5.6 \cdot 10^{-3}$	ρ_g	0.2	$R_{se,z}((m^2 \cdot °C)/kW)$	40

BUILDING PARAMETERS			
	Building 1	Building 2	Building 3
Number of floors	20	40	70
Total number of thermal zones	120	360	770

TABLE XII
BUILDING AUXILIARY GENERATORS DATA

Diesel Generators Parameters			
	G1	**G2**	**G3**
Technical Minimum (kW)	285	620	1226
Technical Maximum (kW)	1000	2170	4300
Minimum hours for generator being in operation/out of operation (h)	1/1	1/1	1/1

The times series of ambient temperature, electricity price, total consumption of distribution network loads, PV and WT power generations and the probability density functions (PDFs) to estimate the arrival and dwell times of the electric vehicles used in the examined case study are the same with those used in previous case studies. Figure 53.a depicts the number of building occupants over time, while Figure 53.b shows the total number of hosted PEVs over time.

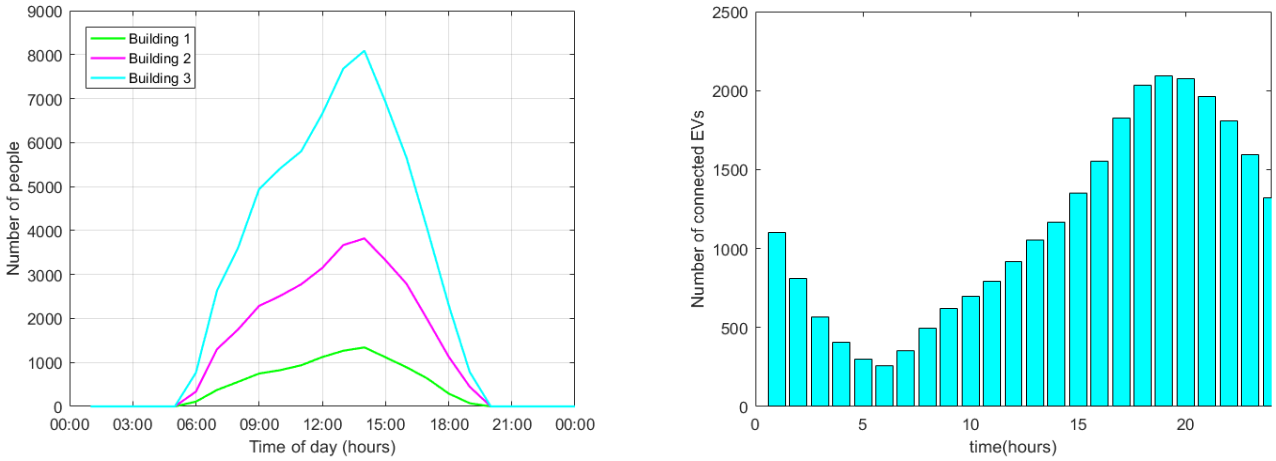

Figure 53. (a) Forecasted number of occupants (b) Number of connected PEVs

11.1. Case 1: Frequency Support by Building Prosumers and Diesel Generators

In the examined operation scenario, the building prosumers are able to support microgrid's frequency. In order to demonstrate more emphatically the capacity of the proposed frequency support method the examined microgrid is assumed to operate autonomously. In this way, variations of microgrid's demand can lead to considerable frequency deviations. A step increase of microgrid load is applied and the resulting frequency deviations with and without building frequency support ancillary service are simulated.

The parameters of microgrid automatic generation control method (shown in Fig. 15) are given in Table XIII. The values of all parameters are suitable for use in per-unit system.

TABLE XIII
MICROGRID PARAMETERS

Diesel turbine parameters	**Diesel Generator 1**	**Diesel Generator 2**	**Diesel Generator 3**	***Base Power*** $10MVA$
	$K_T = 0.5, T_{D4} = 3s$	$K_T = 1.0, T_{D4} = 3s$	$K_T = 2.0, T_{D4} = 3s$	
Parameters of speed governor	$K_D = 1, T_{D1} = 1s, T_{D2} = 2s, T_{D3} = 0.025s$			
Diesel generators frequency control parameters	$K_I = 1, R = 0.05$			***Base Frequency*** $50Hz$
Microgrid inertial response parameters	$K_P = 0.12, T_P = 0.2s$			

The internal temperatures of all building thermal zones obtained in the examined scenario together with their upper and lower limits are shown in Fig. 54. It can be observed that the internal temperatures of all thermal zones of each building are well-maintained within the comfort range of 20–27°C and they all tend to follow the same pattern.

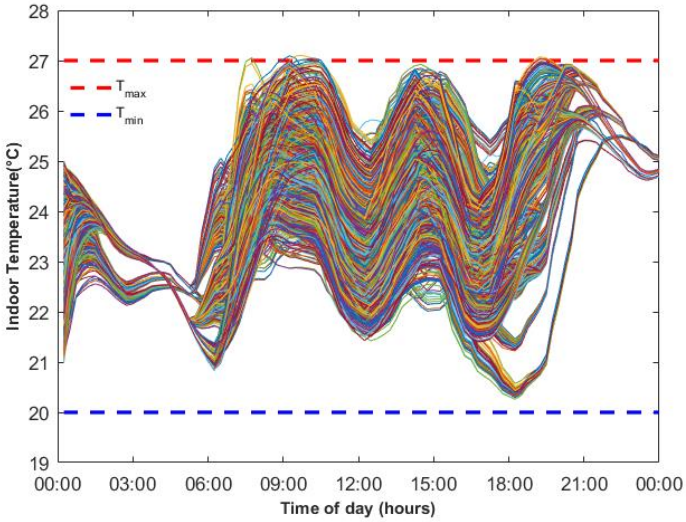

Fig. 54. Internal temperatures of all building thermal zones

The electric power consumptions of the HVAC systems of the buildings are shown in Fig. 55.a. The total cooling power of each building follows the outdoor temperature and the pattern of the forecasted number of people having activity in the buildings, as it was expected. Obviously, the largest building has the biggest cooling requirements. The total cooling power consumption for every building of the microgrid results from the execution of the first level of optimization. The algorithm aims to decrease the power consumption at time periods of relatively high electricity price. Fig. 55.b exhibits the total non-critical electrical loads of the buildings before and after the application of the optimization method. It is observed that non-critical electrical loads are shifted to time periods of low electricity price, in order to contribute to the minimization of microgrid's total operation cost while satisfying all the operational constraints, at the same time. Specifically, the algorithm shifts the electrical loads from the high electricity time period 07:00-09:00 to the low electricity price time period 13:00-15:00.

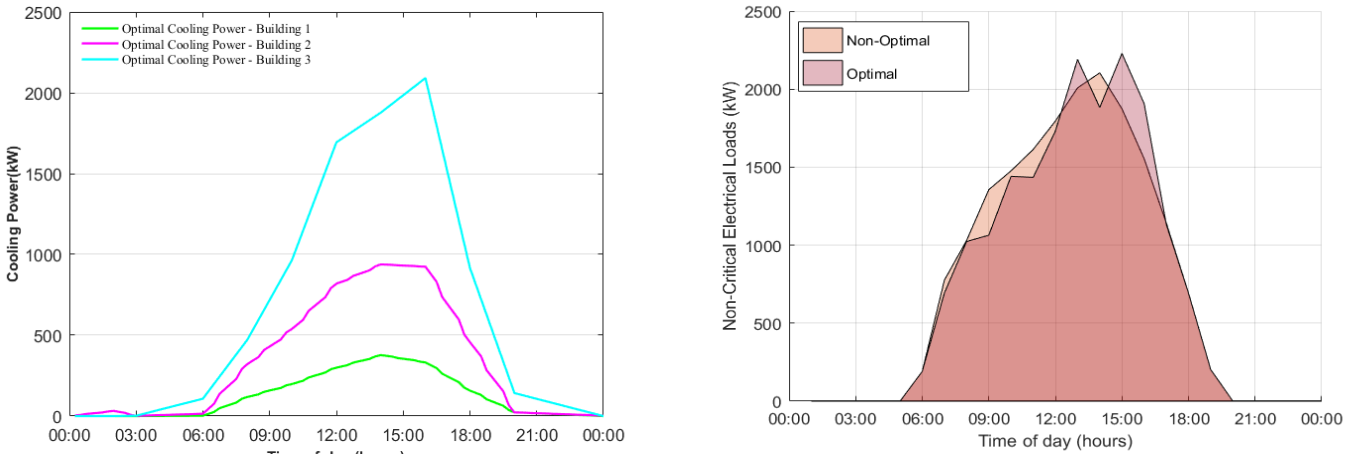

Figure 55. (a) Electric power demand for building cooling (b) Total non-critical electrical loads of the buildings before and after optimization

The power produced by diesel generators is shown in stack form in Fig. 56.a. Each generator is regulated to operate as close as possible to its optimal operation point during the examined time period. In Fig. 56.b, CO_2 emissions of each diesel generator of the microgrid are shown. The algorithm maintains CO_2 emissions of all auxiliary generators below their limits (only the third diesel generator was forced to limit its emissions).

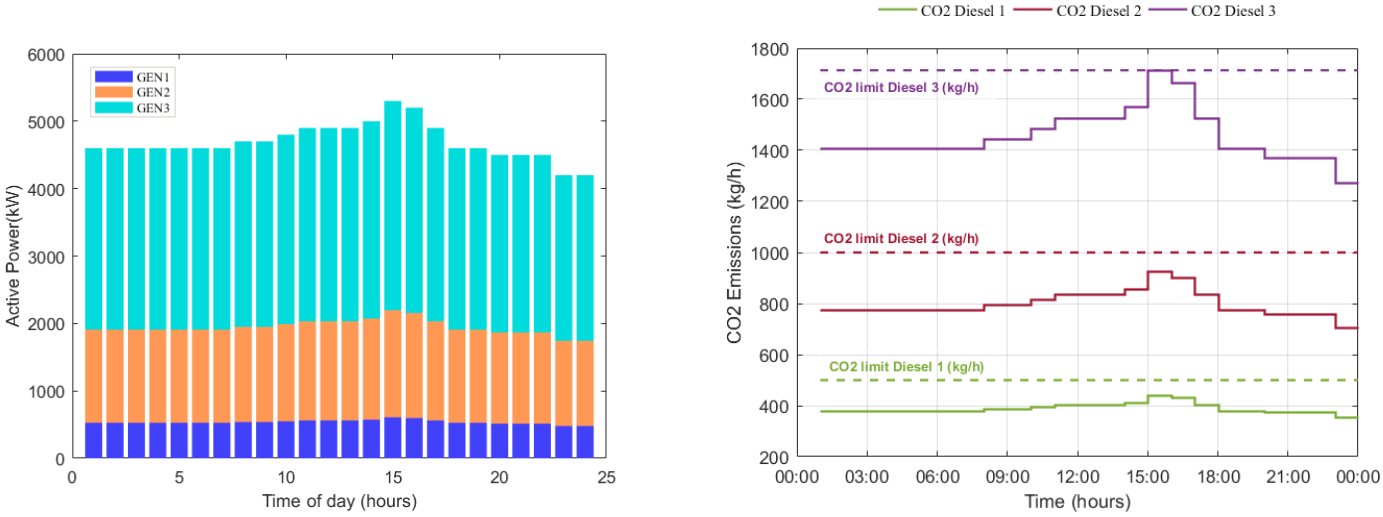

Figure 56. Auxiliary diesel generators (a) power produced & (b) CO_2 emissions with their upper limits

Node voltages are shown in Figure 57. Voltage upper and lower boundaries were set to 1.1 and 0.9 p.u., respectively. The voltages of all network buses are well maintained within the predefined limits.

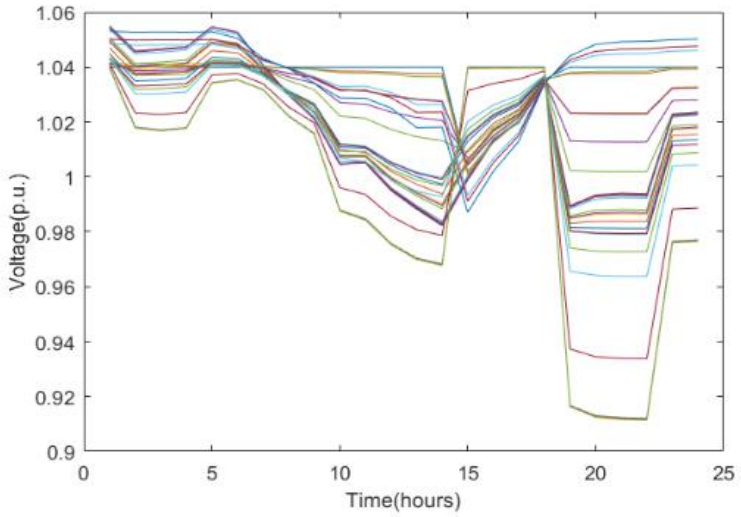

Figure 57. Node voltages

It is noted that the average time for the execution (load agents modelling, energy management level) of the proposed method was 3.5 min. This is a particularly low computation time since the method is applied to a highly complex optimization problem with hundreds of thousands of decision variables and constraints. Moreover, it allows its online application for power and energy management purposes as the proposed method deals with a day-ahead operation scheduling and power management problem; hence, the required computation time is absolutely satisfactory. The average time for the execution of a traditional optimization method (following the steepest gradient descent approach) was 1.2 min. However, classical optimization techniques do not ensure convergence to a global optimum, as they depend highly on the selected initial point. Moreover, it was shown that our method managed to reduce the operation cost by 12.7% more than the classical method, on average.

It is assumed that the microgrid is experiencing a step load increase of 2MW at $t = 57600s$. In Fig. 58, microgrid's frequency deviation obtained with and without building prosumers frequency support is shown. It is obvious that when exploiting buildings power demand flexibility, the maximum frequency deviation from 50Hz is smaller while frequency regulation is faster and smoother.

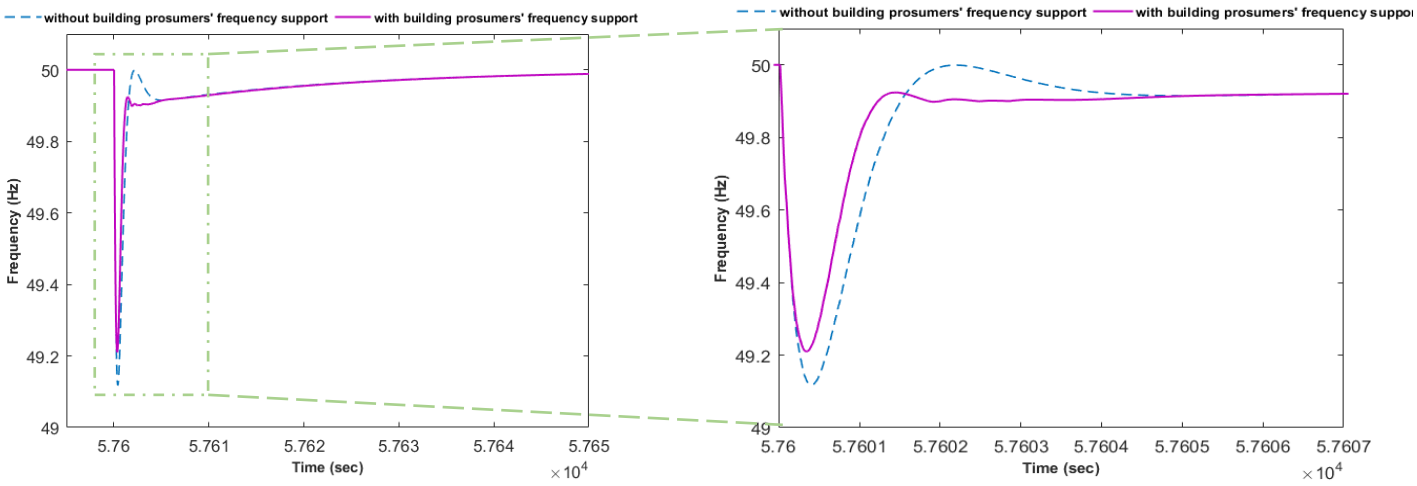

Fig. 58. Microgrid frequency evolution

In Fig. 59, microgrid load change, total change of the power of the diesel generators and the building prosumers' electric power demand are shown. It is observed that building prosumers' power demand is reduced fast after the step increase of the microgrid load to reduce the resulting imbalance between the power of the diesel generators and electric power demand of the microgrid. The above observations are also validated by Fig. 60 where the obtained deviations from the optimal operation of the diesel generators with and without frequency support being provided by building prosumers are compared.

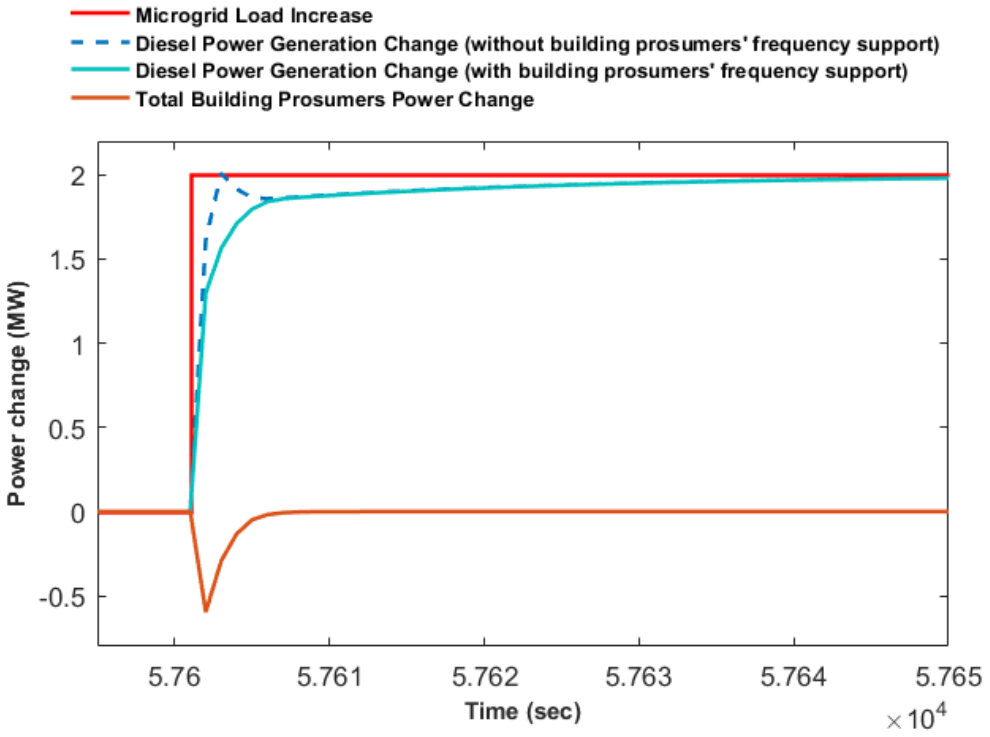

Fig. 59. Microgrid load change, change of the power of the diesel generators with and without buildings' frequency support and total buildings' power demand change

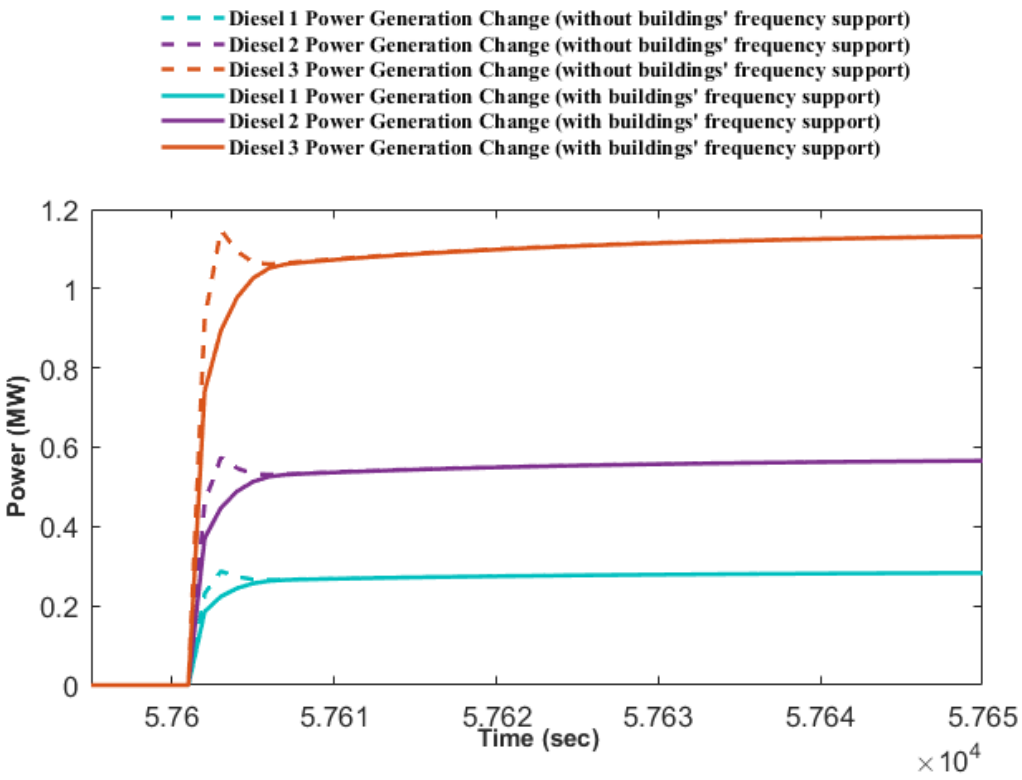

Fig. 60. Change of the power of each diesel generator of the microgrid with and without buildings' frequency support

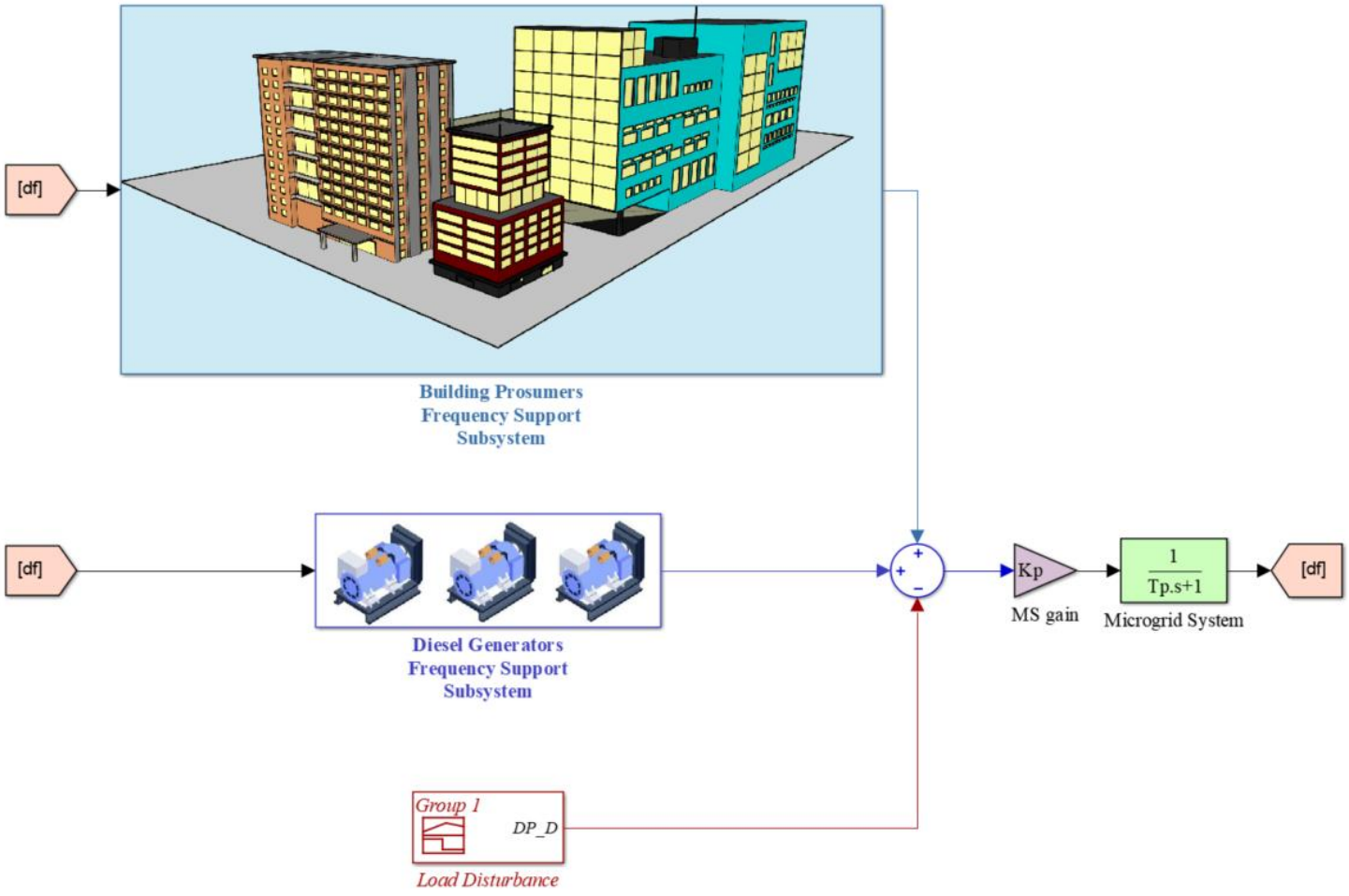

Fig. 61. Configuration of the examined system for microgrid's frequency support by building prosumers and diesel generators

Building Prosumers Frequency Support Subsystem

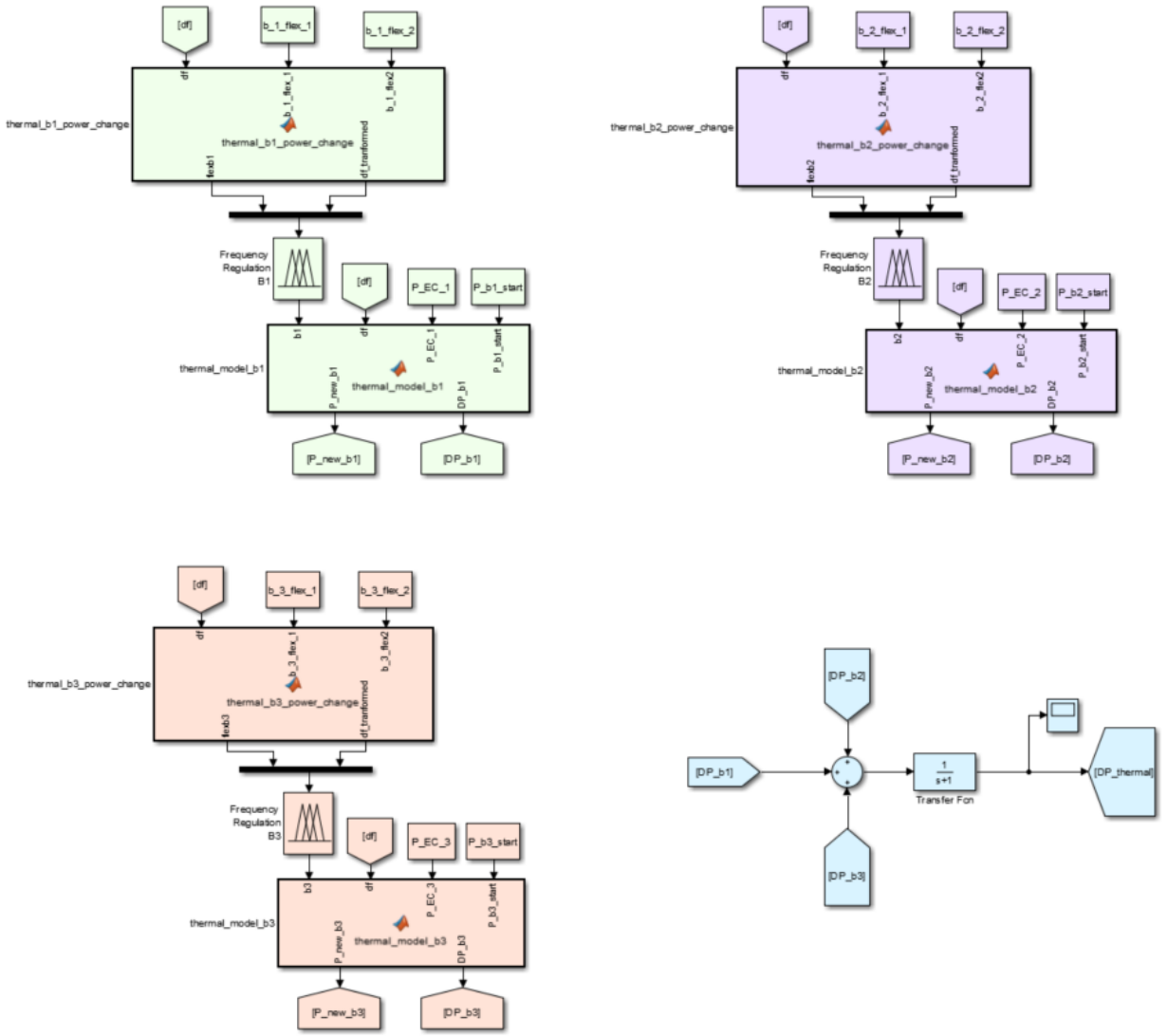

Fig. 62. Building prosumers frequency support subsystem

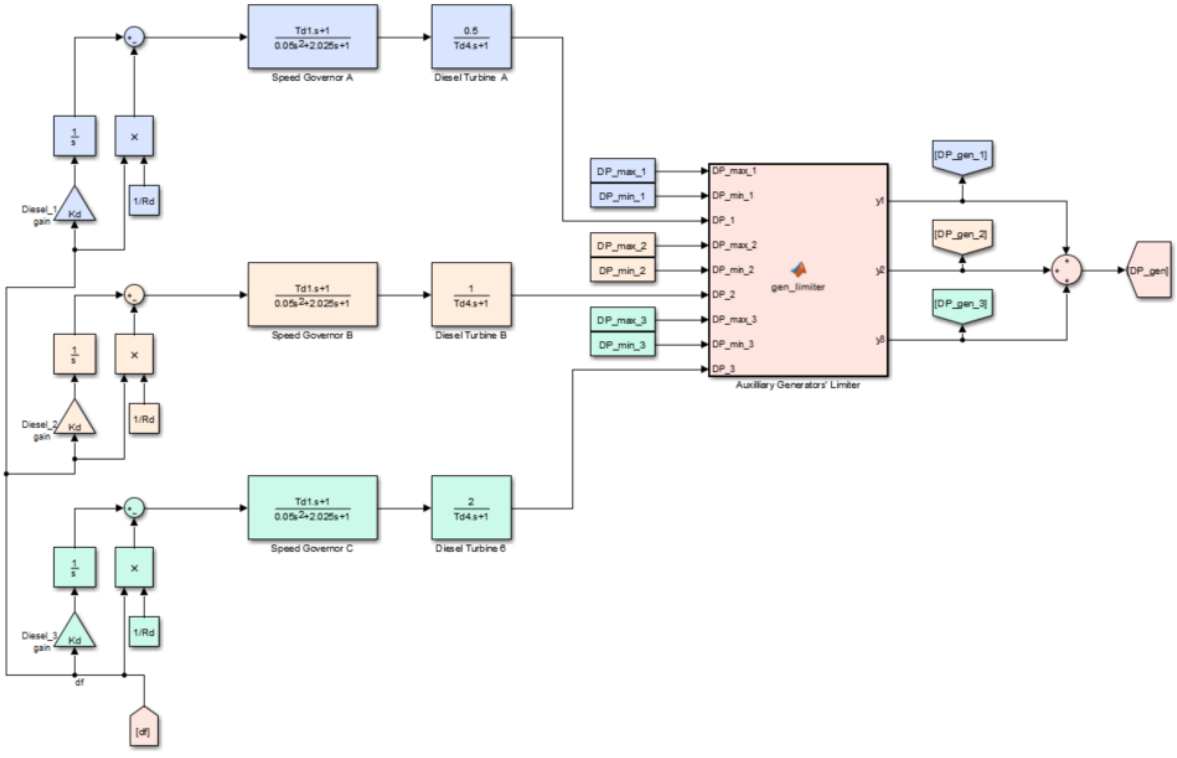

Fig. 63. Diesel generators frequency support subsystem

11.2. Case 2: Demand Response by Plug-In Electric Vehicles

Figures 64.a and 64.b depict the active power and the total stored energy of the aggregate battery of the PEVs together with their bounds in microgrid operation scenario including autonomous operation. The equivalent aggregate battery of the PEVs absorbs power from the utility grid or injects power according to the variable electricity price in order to contribute to the minimization of the microgrid's overall operation cost. During autonomous operation (15:00-18:00), the aggregate battery of the PEVs is mainly used to meet the energy needs of the microgrid providing the necessary amount of energy to it. It is noted that the obtained results showed that all PEVs managed to reach their energy target without violating any operation or technical constraint.

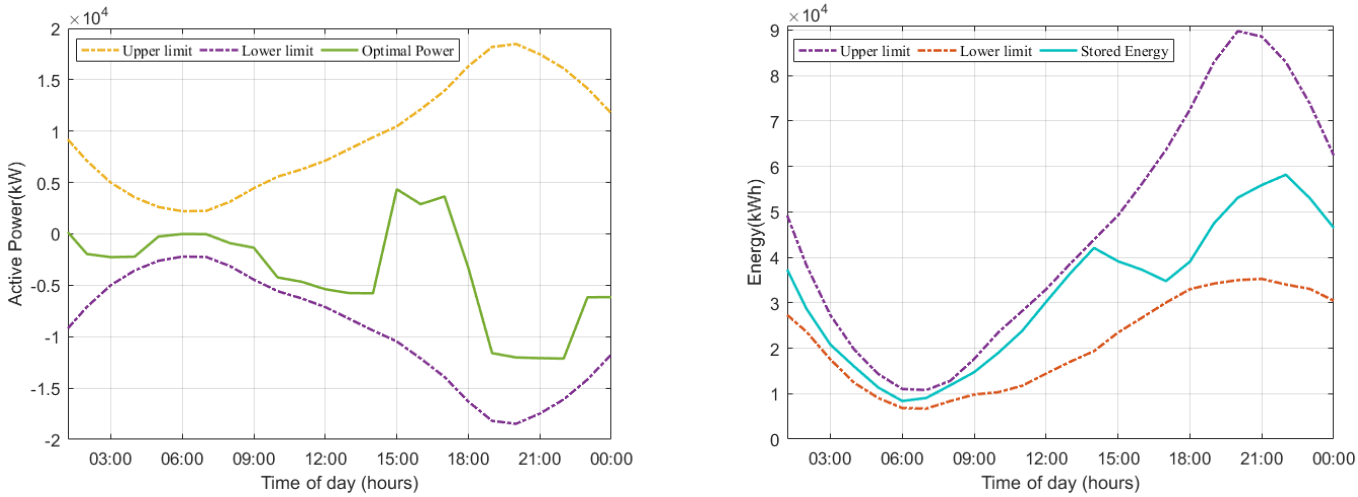

Figure 64. (a) Active power & (b) energy stored of EV aggregate battery with their respective limits.

In addition to the assessment of the accuracy of the electric vehicles' parking lot equivalent battery model, its demand response capability was assessed. Specifically, it is assumed that the power system automatic generation control system is integrated with a system for PEVs power demand response to frequency deviations. The nominal value of power system frequency is considered $50Hz$ and it is assumed that the power system is experiencing a step load increase that leads to the frequency deviation depicted in Fig. 65.

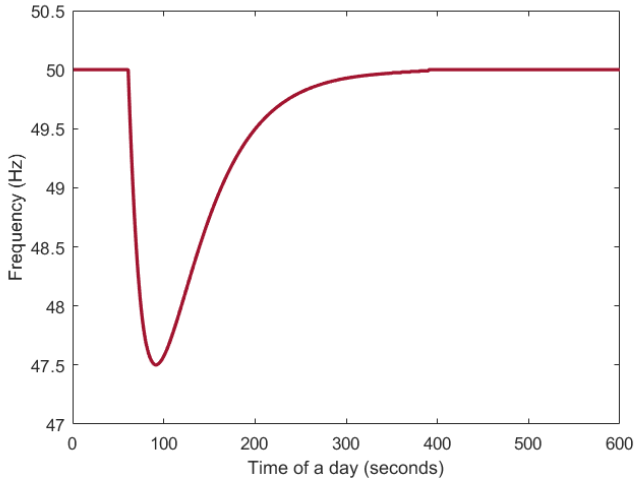

Figure 65. Power system frequency evolution.

Fig. 66 shows the obtained change of the power the PEVs exchange with the electric network. When the frequency drops the developed fuzzy controller aims to decrease PEVs' power consumption or increase the power injection to the grid. Fig. 67 illustrates the optimal SoC trajectory in the absence of demand response, as well as, the SoC trajectory when demand response is applied and during the SoC restoration (after frequency is restored and takes values inside its deadband).

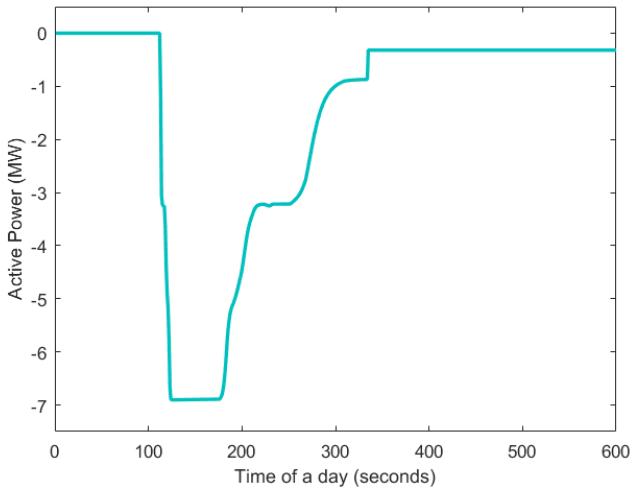

Figure 66. Aggregate equivalent battery of PEVs power change.

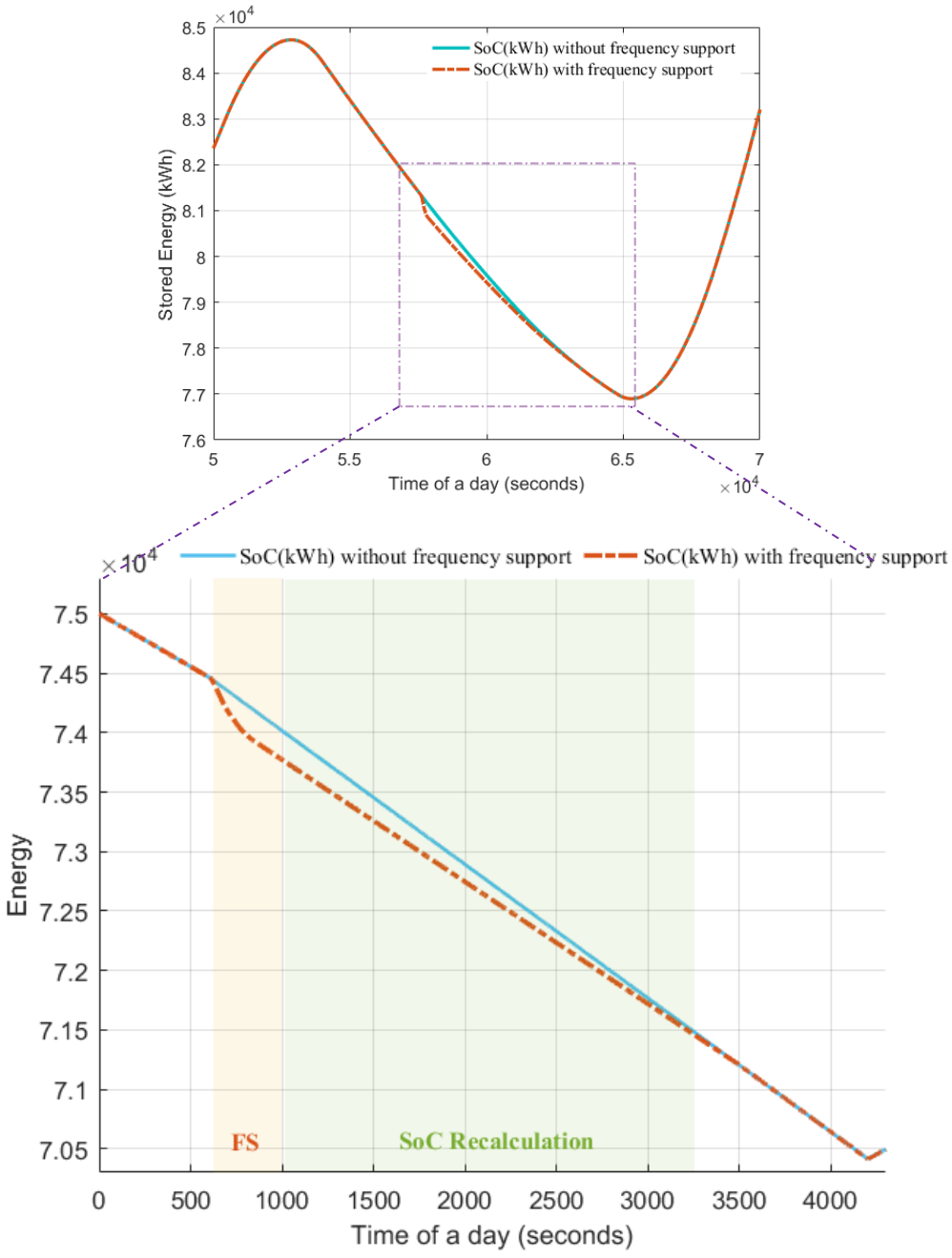

Figure 67. Total Stored Energy Aggregate equivalent battery of PEVs before and after demand response execution.

Chapter 12

Conclusion and Future Work

In this paper, a method for the coordinated optimal operation scheduling and real-time operation of active distribution networks hosting complex microgrids comprising buildings scaling from simple residential ones up to mega office or commercial buildings and plug-in electric vehicle aggregators is proposed. Despite the complexity and the large size of the examined building prosumers the proposed method can exploit detailed integrated models of their thermal-electrical power systems. Moreover, an aggregation technique is applied to the hosted PEVs without compromising the accuracy of the results while ensuring large reduction of the required computation time. The proposed method can be applied to extremely complex building prosumers without the expected increase of the required computation time. This is mainly achieved by the exploitation of an innovative method for the dispatch of total building thermal needs to the respective building thermal zones that has been developed in this work. Moreover, the proposed method can be applied to grid-connected or islanded operation of the microgrid of building prosumers ensuring operation cost minimization in both cases while PEVs are exploited as small power generation units during island operation. A modified IEEE 33-bus test case system was used to test the efficiency of the proposed method. Moreover, detailed control methods that ensure optimal frequency support for the microgrid and the electric network the microgrid is connected to are developed. To this end, suitable flexibility indices are defined for all associated components and exploited for the optimal provision of frequency support. The obtained simulation results show that the proposed method led to the optimization of the operational costs of both the active distribution network and the microgrid while it ensured adherence to a large set of operation constraints of the microgrid and the active distribution network.

To extend the scope of this thesis in the future, the real-time operation of the microgrid will be further enhanced by the exploitation of model parameter estimation techniques. It is well known that some of the parameters of the models are difficult to be measured e.g., zone thermal gains, while others vary with time e.g., thermal conductivity of wall, windows, solar irradiation etc. All these parameters will be estimated in real time with the use of suitable measurements. Moreover, expert systems for readjusting the operation of some microgrid components' parameters in real time can be developed to further reduce the required computation time and increase the robustness of the method. Expert systems will be continuously trained from appropriate collected operation data. In addition, the microgrid operation scheduling performed in MAS second level is susceptible to the uncertainties arising from the forecasts of stochastic variables like the price of electricity, renewable energy production, and the activity of people and electric vehicles. To this end, the setpoints of all microgrid components will be optimally readjusted in the real-time operation by executing the optimization process of MAS second level in relatively small-time windows and using updated values of all forecasted quantities. This is possible as all the developed subsystem models in MAS second level are run-time efficient allowing them to be executed in real-time. Therefore, the overall model will be able to be run repeatedly at regular time intervals throughout the optimization period in order to cancel out deviations resulting by forecast errors. Moreover, the code developed for the simulation of all the above-mentioned models and optimization processes may be suitably adapted and possibly modified or translated in order to be suitable for use in microprocessors of future commercial products.

References

[1] Features and Benefits About Microgrids. Available Online: https://www.districtenergy.org/microgrids/about-microgrids97/features.

[2] Challenges Faced during Microgrid Implementation. Available online: https://www.phoenixenergygroup.com/blog/challenges-faced-during-microgrid-implementation.

[3] Vera, Y.E.G., Dufo-López, R. & Bernal-Agustín, J.L. 2019, "Energy management in microgrids with renewable energy sources: A literature review", *Applied Sciences (Switzerland)*, vol. 9, no. 18.

[4] LITHIUM-ION BATTERY. Available online: https://www.cei.washington.edu/education/science-of-solar/battery-technology/.

[5] Lead Acid Batteries. Available Online: https://www.pveducation.org/pvcdrom/batteries/lead-acid-batteries.

[6] Flow Batteries. Available Online: https://flowbatteryforum.com/what-is-a-flow-battery.

[7] Hydrogen Fuel Cells. Available Online: https://www.energy.gov/eere/fuelcells/fuel-cells.

[8] High-power ultracapacitor energy storage solutions based on breakthrough graphene material. Available Online: https://www.skeletontech.com/ultracapacitor-technology

[9] Why the Future of Driving is Electric. Available online: https://evolveetfs.com/2018/11/why-the-future-of-driving-is-electric/.

[10] Advantages of electric cars – top benefits of EVs. Available Online: https://www.energysage.com/electric-vehicles/advantages-of-evs/.

[11] TYPES OF ELECTRIC VEHICLES. Available Online: https://www.acecwi.com/types-of-electric-vehicles/.

[12] Elmouatamid, A., Ouladsine, R., Bakhouya, M., Kamoun, N.E., Khaidar, M. & Zine-Dine, K. 2021, "Review of control and energy management approaches in micro-grid systems", *Energies*, vol. 14, no. 1.

[13] Thomas, D.; Deblecker, O.; Ioakimidis, C.S. Optimal operation of an energy management system for a grid-connected smart building considering photovoltaics' uncertainty and stochastic electric vehicles' driving schedule. Appl. Energy 2018, 210, 1188–1206.

[14] Sturzenegger, D.; Gyalistras, D.; Morari, M.; Smith, R.S. Model Predictive Climate Control of a Swiss Office Building: Implementation, Results, and Cost-Benefit Analysis. IEEE Trans. Control. Syst. Technol. 2016, 24, 1–12.

[15] Carli, R.; Dotoli, M. Decentralized control for residential energy management of a smart users' microgrid with renewable energy exchange. IEEE/CAA J. Autom. Sin. 2019, 6, 641–656.

[16] Alibabaei, N.; Fung, A.S.; Raahemifar, K.; Moghimi, A. Effects of intelligent strategy planning models on residential HVAC system energy demand and cost during the heating and cooling seasons. Appl. Energy 2017, 185, 29–43.

[17] Akter, M.N.; Mahmud, M.A.; Oo, A.M.T. A hierarchical transactive energy management system for energy sharing in residential microgrids. Energies 2017, 10, 12.

[18] Jiang, Q.; Xue, M.; Geng, G. Energy management of microgrid in grid-connected and stand-alone modes. IEEE Trans. Power Syst. 2013, 28, 3380–3389.

[19] Li, Z.; Xu, Y. Optimal coordinated energy dispatch of a multi-energy microgrid in grid-connected and islanded modes. Appl. Energy 2018, 210, 974–986.

[20] Worku, M.Y.; Hassan, M.A.; Abido, M.A. Real time energy management and control of renewable energy based microgrid in grid connected and Island modes. Energies 2019, 12, 276.

[21] Zheng, Y.; Li, S.; Tan, R. Distributed Model Predictive Control for On-Connected Microgrid Power Management. IEEE Trans. Control. Syst. Technol. 2018, 26, 1028–1039.

[22] Zhang, Y.; Gatsis, N.; Giannakis, G.B. Robust energy management for microgrids with high-penetration renewables. IEEE Trans. Sustain. Energy 2013, 4, 944–953.

[23] Pinzon, J.A.; Vergara, P.P.; Da Silva, L.C.P.; Rider, M.J. Optimal Management of Energy Consumption and Comfort for Smart Buildings Operating in a Microgrid. IEEE Trans. Smart Grid 2019, 10, 3236–3247.

[24] Pinzon, J.A.; Vergara, P.P.; Da Silva, L.C.P.; Rider, M.J. A MILP model for optimal management of energy consumption and comfort in smart buildings. In Proceedings of the 2017 IEEE Power and Energy Society Innovative Smart Grid Technologies Conference, ISGT, Arlington, VA, USA, 2017, 23–26 April 2017.

[25] Hao, H.; Corbin, C.D.; Kalsi, K.; Pratt, R.G. Transactive Control of Commercial Buildings for Demand Response. IEEE Trans. Power Syst. 2017, 32, 774–783.

[26] Bharati, G.R.; Razmara, M.; Paudyal, S.; Shahbakhti, M.; Robinett, R.D. Hierarchical optimization framework for demand dispatch in building-grid systems. In Proceedings of the IEEE Power and Energy Society General Meeting, Boston, MA, USA, 17–21 July 2016.
[27] Tavakoli, M.; Shokridehaki, F.; Marzband, M.; Godina, R.; Pouresmaeil, E. A two-stage hierarchical control approach for the optimal energy management in commercial building microgrids based on local wind power and PEVs. Sustain. Cities Soc. 2018, 41, 332–340.
[28] Sehar, F.; Pipattanasomporn, M.; Rahman, S. Coordinated control of building loads, PVs and ice storage to absorb PEV penetrations. Int. J. Electr. Power Energy Syst. 2018, 95, 394–404.
[29] Liang, Z.; Bian, D.; Zhang, X.; Shi, D.; Diao, R.; Wang, Z. Optimal energy management for commercial buildings considering comprehensive comfort levels in a retail electricity market. Appl. Energy 2019, 236, 916–926.
[30] Dakanalis, M.; Kanellos, F.D. Efficient model for accurate assessment of frequency support by large populations of plug-in electric vehicles. Inventions 2021, 6, 89.
[31] Liu, Z.; Chen, Y.; Zhuo, R.; Jia, H. Energy storage capacity optimization for autonomy microgrid considering CHP and EV scheduling. Appl. Energy 2018, 210, 1113–1125.
[32] Lan, T.; Jermsittiparsert, K.; Alrashood STRezaei MAl-Ghussain, L.; Mohamed, M.A. An advanced machine learning based energy management of renewable microgrids considering hybrid electric vehicles' charging demand. Energies 2021, 14, 569.
[33] Han, Y.; Chen, W.; Li, Q. Energy management strategy based on multiple operating states for a photovoltaic/fuel cell/energy storage DC microgrid. Energies 2017, 10, 1.
[34] Eseye, A.T.; Lehtonen, M.; Tukia, T.; Uimonen, S.; Millar, R.J. Optimal Energy Trading for Renewable Energy Integrated Building Microgrids Containing Electric Vehicles and Energy Storage Batteries. IEEE Access 2019, 7, 106092–106101.
[35] Anvari-Moghaddam, A.; Rahimi-Kian, A.; Mirian, M.S.; Guerrero, J.M. A multi-agent-based energy management solution for integrated buildings and microgrid system. Appl. Energy 2017, 203, 41–56.
[36] Li, Y.; Feng, B.; Li, G.; Qi, J.; Zhao, D.; Mu, Y. Optimal distributed generation planning in active distribution networks considering integration of energy storage. Appl. Energy 2018, 210, 1073–1081.
[37] Nick, M.; Cherkaoui, R.; Paolone, M. Optimal Planning of Distributed Energy Storage Systems in Active Distribution Networks Embedding Grid Reconfiguration. IEEE Trans. Power Syst. 2018, 33, 1577–1590.
[38] Nuchkrua, T.; Leephakpreeda, T. Novel Compliant Control of a Pneumatic Artificial Muscle Driven by Hydrogen Pressure Under a Varying Environment. IEEE Trans. Ind. Electron. 2022, 69, 7120–7129.
[39] Malik A. & Ravishankar J. 2018, "A hybrid control approach for regulating frequency through demand response", Applied Energy, vol. 210, pp. 1347-1362.
[40] J. A. Short, D. G. Infield and L. L. Freris, "Stabilization of Grid Frequency Through Dynamic Demand Control," in IEEE Transactions on Power Systems, vol. 22, no. 3, pp. 1284-1293.
[41] Zhao P., Henze G.P., Brandemuehl M.J., Cushing V.J. & Plamp S. 2015, "Dynamic frequency regulation resources of commercial buildings through combined building system resources using a supervisory control methodology", Energy and Buildings, vol. 86, pp. 137-150.
[42] Cai J. & Braun J.E. 2019, "A regulation capacity reset strategy for HVAC frequency regulation control", Energy and Buildings, vol. 185, pp. 272-286.
[43] Pavlak G.S., Henze G.P. & Cushing, V.J. 2014, "Optimizing commercial building participation in energy and ancillary service markets", Energy and Buildings, vol. 81, pp. 115-126.
[44] E. Vrettos, F. Oldewurtel and G. Andersson, "Robust Energy-Constrained Frequency Reserves from Aggregations of Commercial Buildings," in IEEE Transactions on Power Systems, vol. 31, no. 6, pp. 4272-4285.
[45] O. Ma et al., "Demand Response for Ancillary Services," in IEEE Transactions on Smart Grid, vol. 4, no. 4, pp. 1988-1995.
[46] H. Hao, Y. Lin, A. S. Kowli, P. Barooah and S. Meyn, "Ancillary Service to the Grid Through Control of Fans in Commercial Building HVAC Systems," in IEEE Transactions on Smart Grid, vol. 5, no. 4, pp. 2066-2074.
[47] Y. Lin, P. Barooah, S. Meyn and T. Middelkoop, "Experimental Evaluation of Frequency Regulation from Commercial Building HVAC Systems," in IEEE Transactions on Smart Grid, vol. 6, no. 2, pp. 776-783.
[48] H. Hao, D. Wu, J. Lian and T. Yang, "Optimal Coordination of Building Loads and Energy Storage for Power Grid and End User Services," in IEEE Transactions on Smart Grid, vol. 9, no. 5, pp. 4335-4345.
[49] B. Lundstrom, S. Patel, S. Attree and M. V. Salapaka, "Fast Primary Frequency Response using Coordinated DER and Flexible Loads: Framework and Residential-scale Demonstration," 2018 IEEE Power & Energy Society General Meeting (PESGM), 2018, pp. 1-5.
[50] Worku M.Y., Hassan M.A. & Abido M.A. 2019, "Real time energy management and control of renewable energy based microgrid in grid connected and Island modes", Energies, vol. 12, no. 2.
[51] F. Nejabatkhah and Y. W. Li, "Overview of Power Management Strategies of Hybrid AC/DC Microgrid," in IEEE Transactions on Power Electronics, vol. 30, no. 12, pp. 7072-7089.

[52] N. Eghtedarpour and E. Farjah, "Power Control and Management in a Hybrid AC/DC Microgrid," in IEEE Transactions on Smart Grid, vol. 5, no. 3, pp. 1494-1505.
[53] M. Bayat, K. Sheshyekani, M. Hamzeh and A. Rezazadeh, "Coordination of Distributed Energy Resources and Demand Response for Voltage and Frequency Support of MV Microgrids," in IEEE Transactions on Power Systems, vol. 31, no. 2, pp. 1506-1516.
[54] W. Liu, G. Geng, Q. Jiang, H. Fan and J. Yu, "Model-Free Fast Frequency Control Support With Energy Storage System," in IEEE Transactions on Power Systems, vol. 35, no. 4, pp. 3078-3086.
[55] Serban I. & Marinescu C. 2014, "Battery energy storage system for frequency support in microgrids and with enhanced control features for uninterruptible supply of local loads", International Journal of Electrical Power and Energy Systems, vol. 54, pp. 432-441.
[56] H. Liu, J. Qi, J. Wang, P. Li, C. Li and H. Wei, "EV Dispatch Control for Supplementary Frequency Regulation Considering the Expectation of EV Owners," in IEEE Transactions on Smart Grid, vol. 9, no. 4, pp. 3763-3772.
[57] Almeida, P.M.R., Soares, F.J. & Lopes, J.A.P. 2015, "Electric vehicles contribution for frequency control with inertial emulation", Electric Power Systems Research, vol. 127, pp. 141-150.
[58] H. Liu, Z. Hu, Y. Song and J. Lin, "Decentralized Vehicle-to-Grid Control for Primary Frequency Regulation Considering Charging Demands," in IEEE Transactions on Power Systems, vol. 28, no. 3, pp. 3480-3489.
[59] H. Liu, Z. Hu, Y. Song, J. Wang and X. Xie, "Vehicle-to-Grid Control for Supplementary Frequency Regulation Considering Charging Demands," in IEEE Transactions on Power Systems, vol. 30, no. 6, pp. 3110-3119.
[60] S. Han, S. Han and K. Sezaki, "Development of an Optimal Vehicle-to-Grid Aggregator for Frequency Regulation," in IEEE Transactions on Smart Grid, vol. 1, no. 1, pp. 65-72.
[61] S. Izadkhast, P. Garcia-Gonzalez and P. Frías, "An Aggregate Model of Plug-In Electric Vehicles for Primary Frequency Control," in IEEE Transactions on Power Systems, vol. 30, no. 3, pp. 1475-1482.
[62] Falahati, S., Taher, S.A. & Shahidehpour, M. 2016, "Grid frequency control with electric vehicles by using of an optimized fuzzy controller", Applied Energy, vol. 178, pp. 918-928.
[63] F. D. Kanellos, "Real-Time Control Based on Multi-Agent Systems for the Operation of Large Ports as Prosumer Microgrids," in IEEE Access, vol. 5, pp. 9439-9452.
[64] Jin X., Wu J., Mu Y., Wang M., Xu X. & Jia H., "Hierarchical microgrid energy management in an office building", Applied Energy, vol. 208, pp. 480-494, 2017.
[65] Kyriakou D.G., Kanellos F.D., "Optimal Operation of Microgrids Comprising Large Building Prosumers and Plug-in Electric Vehicles Integrated into Active Distribution Networks," Energies, vol. 15, no. 17, pp. 6182, 2022.
[66] Farinis G.K., Kanellos F.D., "Integrated energy management system for Microgrids of building prosumers", Electric Power Systems Research, vol. 198, 2021.
[67] Kanellos F.D., Optimal Scheduling and Real-Time Operation of Distribution Networks with High Penetration of Plug-In Electric Vehicles", IEEE Systems Journal, vol. 15, no. 3, pp. 3938 – 3947, 2021.
[68] Kanellos F.D., "Optimal power management with GHG emissions limitation in all-electric ship power systems comprising energy storage systems", IEEE Transactions on Power Systems, vol. 29, no. 1, pp. 330-339, 2014.
[69] Zimmerman, R.D.; Murillo-Sanchez, C.E.; Thomas, R.J. MATPOWER: Steady-State Operations, Planning, and Analysis Tools for Power Systems Research and Education. IEEE Trans. Power Syst. 2011, 26, 12–19.
[70] H. Estiri and E. Zagheni, "Age matters: Ageing and household energy demand in the United States", Energy Research & Social Science, vol. 55, pp. 62-70, 2019.
[71] Csoknyai, J. Legardeur, A. A. Akle and M. Horváth, "Analysis of energy consumption profiles in residential buildings and impact assessment of a serious game on occupants' behavior", Energy and Buildings, vol. 196, pp. 1-20, 2019.
[72] Kanellos F. D., Kalaitzakis K., Psarras I., Katsigiannis Y., "Efficient and robust power and energy management for large clusters of plug-in electric vehicles and distribution networks", IET Energy Systems Integration, vol. 4, no. 3, pp. 393-408, 2022.

Publications

1) **Kyriakou D.G., Kanellos F.D**., "Optimal Operation of Microgrids Comprising Large Building Prosumers and Plug-in Electric Vehicles Integrated into Active Distribution Networks," *Energies*, vol. 15, no. 17, pp. 6182, 2022.

2) **Kyriakou D.G., Kanellos F.D.**, "Energy and Power Management System for Microgrids of Large-Scale Building Prosumers" (To be published).

3) **Kyriakou D.G., Kanellos F.D**., "Sustainable Operation of Active Distribution Networks" (To be published).

4) **Kyriakou D.G., Kanellos F.D**., "Optimal Frequency Support Method for Microgrids of Building Prosumers" (To be published).